

Trond Nordvik

**Geovisualization, Geometric
Modelling and Displacement
Analysis
- Applications to Rockslide
Investigations**

Thesis for the degree of Philosophiae Doctor

Trondheim, October 2010

Norwegian University of Science and Technology
Faculty of Engineering Science and Technology
Department of Civil and Transport Engineering



NTNU – Trondheim
Norwegian University of
Science and Technology

NTNU

Norwegian University of Science and Technology

Thesis for the degree of Philosophiae Doctor

Faculty of Engineering Science and Technology
Department of Civil and Transport Engineering

© Trond Nordvik

ISBN 978-82-471-2385-0 (printed ver.)
ISBN 978-82-471-2387-4 (electronic ver.)
ISSN 1503-8181

Doctoral theses at NTNU, 2010:203

Printed by NTNU-trykk

Abstract

This thesis addresses different aspects of spatial data handling in connection with investigations of large rockslides. As such, most of the research was carried out in a cross disciplinary and highly applied context. The focus of the thesis is on spatial data handling methodology which directly or indirectly can be used to support in rockslide investigations. *Rockslide investigation* is a comprehensive term covering all aspects of the evaluation process; from the initial planning of field investigations to data analysis and communication of final results.

Central topics addressed in this thesis are; a) How data reduction affect the geometrical accuracy of digital terrain models b) How interactive geometric modelling and geovisualization can be used in complex rockslide investigations and c) How statistical analyses can be used to evaluate displacement measurements of unstable rock slopes.

Digital terrain modelling forms an important component of the methodology used for rockslide investigations. The first subtopic addressed in this thesis is related to the construction of Triangulated Irregular Networks (TINs) from Light Detection and Ranging (LIDAR) data. As the LIDAR technology tends to generate large data volumes, the resulting terrain models are generally too large to be efficiently handled by ordinary workstations. Therefore, comparisons of various data reduction (decimation) methods were conducted. Their performances were evaluated by means of deviations from terrain models constructed from full datasets. Evaluation criteria included deviations in volume, surface area and elevation. The results showed that the method using a vertical point selection threshold combined with a data dependent triangulation had the overall best performance when tested on 30 different test datasets.

The main objective of the geovisualization part of this thesis was to determine the geometric shapes and locations of potential basal sliding surfaces, for the Åknes rockslide in western Norway, along with the volumes of unstable rock associated with different sliding scenarios. The Åknes rockslide is one of the world's most investigated rockslides due to its potentially catastrophic consequences. A custom written geovisualization application for the Åknes investigation provided the visual context needed for data interpretation and interactive geometric modelling of sliding surfaces. This geovisualization approach enabled geoscientists to develop different sliding scenarios. A scenario putting the basal sliding surface at a depth of 105m to 115m below the topographic surface, delineating an unstable rock volume of 43 million m³, was considered as the most realistic.

Statistical approaches for analyzing displacement measurements were also addressed in this thesis. Several methods including regression analysis, spectral analysis and hypothesis testing were demonstrated to measurements obtained from Global Positioning System (GPS), total stations and extensometers at the Åknes rockslide. Displacement measurements obtained from lasers and crackmeters at the Nordnes rockslide in Northern Norway were also analysed. As with the Åknes rockslide, the Nordnes rockslide has the potential for devastating consequences in terms tsunami generation. Consequently, thorough statistical analyses of the available displacement data are crucial in order to obtain accurate estimates for the displacement rates as well as for gaining insight into the sliding processes. Displacement data from both sites clearly showed seasonal variations but the overall long term displacements were regarded constant. Prediction intervals were derived from the current monitoring data from the Nordnes site. These prediction intervals are considered useful for evaluation of future displacement measurements.

Key words: rockslide investigations, geometric modelling, geovisualization, statistical analysis, displacement data

Preface

This thesis is submitted to Norwegian University of Science and Technology (NTNU), Trondheim, for the partial fulfilment of the requirements for the degree of philosophiae doctor.

The work reported in this thesis has mainly been carried out at Division of Geomatics at Department of Civil and Transport Engineering, NTNU, from 2006 to 2009 with Professor Terje Midtbø, Department of Civil and Transport Engineering, NTNU, as main supervisor and Professor Richard Sinding-Larsen, Department of Geology and Mineral Resources Engineering, NTNU, as co-supervisor. This doctoral work has been connected to International Centre for Geohazards, research theme “Application of Geographical Information Technology to Geohazards”.

The funding for this work was mainly provided by Faculty of Engineering Science and Technology, NTNU. Geological Survey of Norway (NGU) provided funding for the last three months.

Acknowledgement

First of all I wish to thank my main supervisor Professor Terje Midtbø, Norwegian University of Science and Technology (NTNU) for his help, guidance and encouragement throughout my PhD studies. I also thank my co-supervisor Professor Richard Sinding-Larsen, NTNU, for his useful advice and corrections during my doctoral work.

Special thanks are given to Dr. Chris Harding at Iowa State University for his invaluable help and professional advice on visualization.

I am also grateful for the support and professional advice on statistical analysis from Dr. Erik Nyrrnes at Statoil Research Centre.

All co-authors of the papers are acknowledged for their contributions. I also owe thanks to a large number of people affiliated with International Centre for Geohazards, NTNU or Geological Survey of Norway, particularly Dr. Guro Grøneng and Professor Lars Harald Blikra, for helping me with both geo-scientific and practical problems. Dr. Marc-Henri Derron is acknowledged for his useful advice and suggestions.

Gratitude is given to the faculty and staff at Division of Geomatics, NTNU; Professor Hossein Nahavandchi, Professor Ingolf Hådem, Assistant Professor Terje Skogseth, Professor Knut Ragnar Holm, Mrs Wenche Waal and Mr Svein Tore Dahl, for help, advice, discussions and social company during these years. I appreciate the assistance from my fellow PhD students at the early stage of my PhD studies; Dr. Trond Arve Haakonsen, Dr. Ali Soltanpour and Dr. Kouros Ghazavi.

I acknowledge the generous financial support from NTNU, Norges Tekniske Høgskoles Fond, Arnfinn og Lise Hejes Fond and Geoforum in connection with my stay at Iowa State University and conference participation.

I am indebted to my parents for their ever-present support. I am also grateful to my other family members and friends for their support and encouragement.

Finally, but in no sense least, I thank Therese for her understanding and constant support.

Table of contents

Abstract	2
Preface.....	4
Acknowledgement	5
Table of contents.....	6
1 Introduction.....	7
1.1 Background	7
1.2 Structure of the thesis and presentation of papers	8
1.3 Comments on scope and author’s contributions	14
2 Theoretical foundations	16
2.1 Spatial data and their digital representations	16
2.2 Digital terrain modelling.....	17
2.3 Geovisualization	23
2.3.1 Introduction.....	23
2.3.2 Foundation for geovisualization - interactive 3D computer graphics.....	24
2.4 Statistical methods	30
3 Discussion and some suggestions for future work.....	35
3.1 Digital terrain modelling and data reduction	35
3.2 Statistical analysis of rock slope deformation	35
3.2.1 Change detection using temporal LiDAR based DTMs	36
3.3 Geovisualization in rockslide investigations	39
4 Summary and conclusions	41
References.....	43
Appendix: Papers	50

1 Introduction

1.1 Background

Large rockslides pose threats to human lives, infrastructure, buildings and properties. In Norway, during the last century, the three large rockslides in Tafjord (1934) and in Loen (1905 and 1936) required 175 human lives in total (Skrednett 2009). The main contributing factors to large rockslides are steep rock slopes and weak zones in the bedrock. Investigations of large rockslides are essential in order to determine the extent and volume involved as well to gain insight into the sliding processes. This in turn enables appropriate remediation measures, such as stabilization measures or early warning systems, to be implemented.

Currently there are several ongoing investigations of large rockslides in Norway. This thesis considers some aspects of the investigation of two such rockslides; the Åknes rockslide in western Norway (see Kveldsvik (2008) and Grøneng (2010) for thorough geological evaluations) and the Nordnes rockslide in northern Norway (Henderson et al., in preparation).

The Åknes rockslide has particular interest due to the potential for catastrophic consequences if the rockslide accelerates into a rock avalanche into the fjord below. This would generate a tsunami in the adjacent fjord system and pose a threat to local settlements and infrastructure as well as to the many tourists visiting nearby areas in summer. Therefore a comprehensive mapping and monitoring program was initiated in 2004. The main objectives of this still ongoing program were to determine the extent and volume of the unstable rock mass and to implement an early warning system. Since 2004 substantial amounts of diverse geoscientific data, including both surface and subsurface data, have been collected at the Åknes site. The Nordnes rockslide shows similarities to the Åknes rockslide in terms of the potential for tsunami generation in the fjord located below and the resulting catastrophic consequences for local settlements.

Obviously, investigations of large rockslides involve geoscience disciplines such as geology, engineering geology and geophysics, but also spatial data handling through surveying, mapping, terrain modelling, geovisualization and data analysis. The work reported in this thesis is carried out in the intersection between geosciences and spatial data handling but the main focus is on the methodological part. Some central problems addressed in this thesis are:

i) How geometrical properties of digital terrain models (DTMs) are affected by data reduction (simplification). Terrain models form an essential component in rockslide assessments. However, if the data volume becomes too large, with respect to the available computing resources, this prevents successful DTM creation and use. This problem is frequently encountered when generating DTMs from high density Light Detection and Ranging (LiDAR) data. In this thesis the approximation performance of several data reduction methods associated with Triangulated Irregular Networks (TINs) are compared.

ii) How interactive geovisualization can be utilized to improve geometric models of potential sliding surfaces. Geometrical modelling of sliding surfaces is crucial to determine the extent and volume of the unstable rock mass. The determination of the sliding surfaces is also a prerequisite for stability analyses. Stability analyses are however outside the scope of this thesis. Stability analyses for the Åknes rockslide are reported in Kveldsvik (2008) and Grøneng (2010).

iii) How statistical methods can be used to obtain reliable estimates of rock slope displacement rates and thus serve as a mean to gain insight into the sliding processes including prediction of future displacement. Various statistical methods are employed to analyse time series from the two rockslides at Åknes and Nordnes. Adequate methodology for modelling seasonal variations in displacement rates as well as for analysing impacts from potential controlling factors is presented.

Chapter 2 outlines the theoretical foundations for this thesis and provides references to the existing body of literature.

1.2 Structure of the thesis and presentation of papers

This thesis consists of six components; five papers and a super structure (Fig. 1).

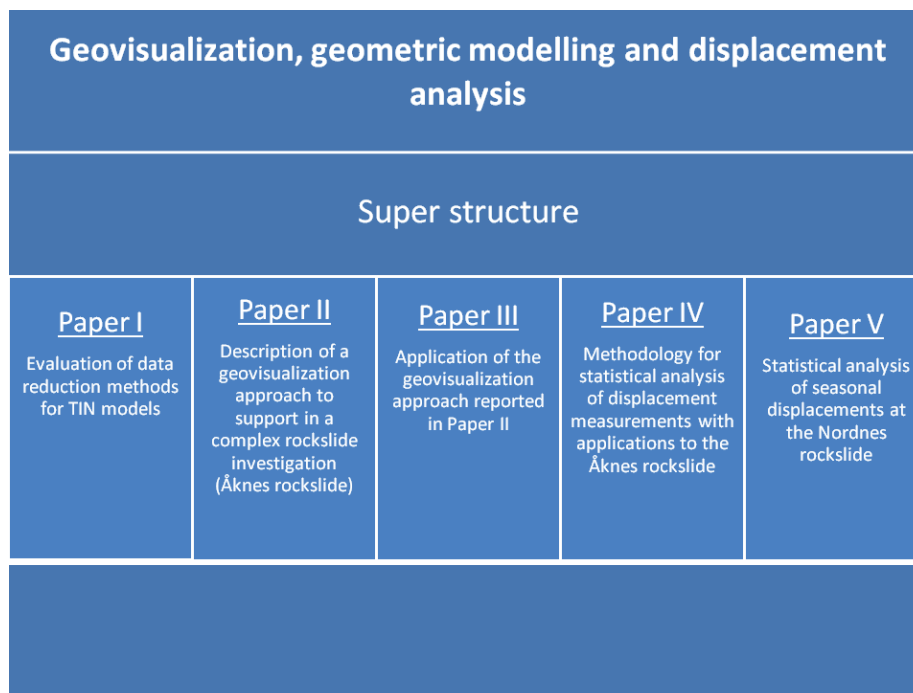


Figure 1. Structure of the thesis

The core of this thesis is reported in Paper I to Paper V. A brief presentation of the papers is given below.

Paper I

Nordvik T. and Midtbø T. (2007). Application of Data Reduction Methods in Dynamic TIN Models to Topographic LIDAR Data. In: Bjørke and Tveite (eds.): Proceedings of the 11th Scandinavian Research Conference on Geographical Information Science, Print: Rotator SiÅs, ISBN 978-82-7636-020-2, p. 111-128.

Reprint with Norwegian title; “Anvendelse av metoder for datareduksjon på topografiske LIDAR data”, in Kart og Plan, Vol. 100 (3), 2007, p. 155-167.

Paper I addresses data reduction methods associated with the construction of Triangular Irregular Networks (TINs) from topographic Light Detection and Ranging (LIDAR) data and emphasizes on the evaluation of the performance of these methods. The resulting surface models are intended both for visual and numerical analysis. Data reduction is regarded as an important pre-requisite for the construction of surface models from high density LIDAR data and thus crucial for the geovisualization approach reported in Paper II and Paper III.

Paper II

Nordvik T. and Harding C. (2008). Interactive geovisualization and geometric modelling of 3D data – a case study from the Åknes rockslide site, Norway. In: Ruas and Gold (eds), *Headway in Spatial Data Handling*, 13th International Symposium on Spatial Data Handling Series: Lecture Notes in Geoinformation and Cartography, Springer, ISBN 978-3-540-68565-4, p. 367-384.

Paper II describes the design and implementation of a software application prototype designed to meet specific requirements for the Åknes project in terms of geovisualization, geometric modelling of sliding surfaces and volume estimation of the unstable rock mass. This software application (Fig. 2) was based on the open source application programming interface (API) OpenSceneGraph (OSG) and utilizes principles from interactive 3D geovisualization by integrating a number of datasets that were considered relevant for analyses regarding the geometry of potential basal sliding surfaces. This geovisualization application comprises functionality for interactive modelling of the sliding surfaces' geometry using constrained Delaunay networks.

Paper III

Nordvik T., Grøneng G., Ganerød G.V., Nilsen B., Harding C. and Blikra L.H. (2009). Geovisualization, geometric modelling and volume estimation of the Åknes rockslide, Western Norway, *Bulletin of Engineering Geology and the Environment*, 68 (2), 245-256, DOI: 10.1007/s10064-009-0198-x.

Paper III demonstrates the application and benefits from using a custom written geovisualization application (Paper II) as an integral part of the overall investigation of the Åknes rockslide. The results obtained from a joint effort of several geoscientists, on interpretation of data and geometrical modelling of potential basal sliding surfaces, as well as estimation of corresponding volumes of unstable rock, are reported. An illustration of the three possible sliding scenarios proposed in this paper is shown in Fig. 3.

Paper IV

Nordvik T. and Nyrnes E. (2009). Statistical analysis of surface displacements – an example from the Åknes rockslide, western Norway. *Natural Hazards and Earth System Sciences*, 9, 713-724, DOI: 10.5194/nhess-9-713-2009.

Paper IV addresses statistical methods for analyzing surface displacement measurements. Measurements collected with GPS, total stations and extensometers at the Åknes rockslide were analyzed. Special attention was given to the time series

obtained from continuous measured GPS control points. In order to establish periodic components, such as seasonal variations, these time series were analyzed using spectral analysis.

Paper V

Nordvik T., Blikra L.H., Nyrnes E. and Derron M.H. (2010). Statistical analysis of seasonal displacements at the Nordnes rockslide, northern Norway, *Engineering Geology*, 114, 228-237, DOI:10.1016/j.enggeo.2010.04.019.

Paper V reports on the results from statistical analysis of monitoring data obtained from lasers and crackmeters at the Nordnes rockslide. Regression analysis was used for estimation of annual displacement rates and seasonal variations. Based on the fitted regression models, intervals for future observations were derived. These prediction intervals are assumed to be useful for the evaluation of future observations as they can serve as alert thresholds with respect to critical changes in displacement rates.

Other secondary papers not forming part of the thesis

Midtbø T. and Nordvik T. (2007). Effects of Animations in Zooming and Panning Operations on Web maps: A Web-based Experiment, *The Cartographic Journal*, Vol. 44, Number 4, pp. 292-303(12).

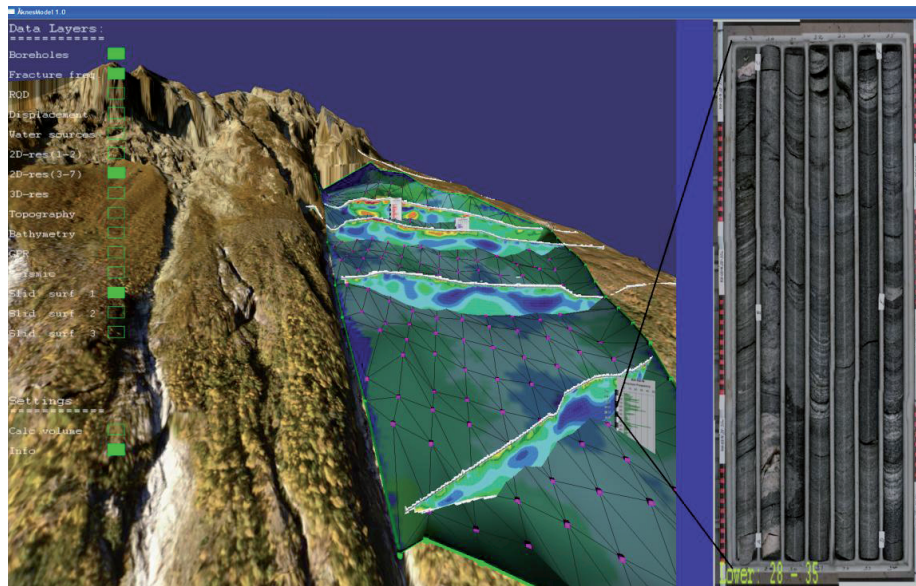


Figure 2. A screen dump from the geovisualization application described in Paper II. This application combines a wide range of spatial data collected at the Åknes rockslide site. A potential sliding surface is embedded into the surrounding terrain. The purple coloured points (vertices of a TIN model) were used as editable control points to adjust the location and shape of the sliding surface in accordance with the available datasets. The panel to the right shows a drill core image from a borehole.

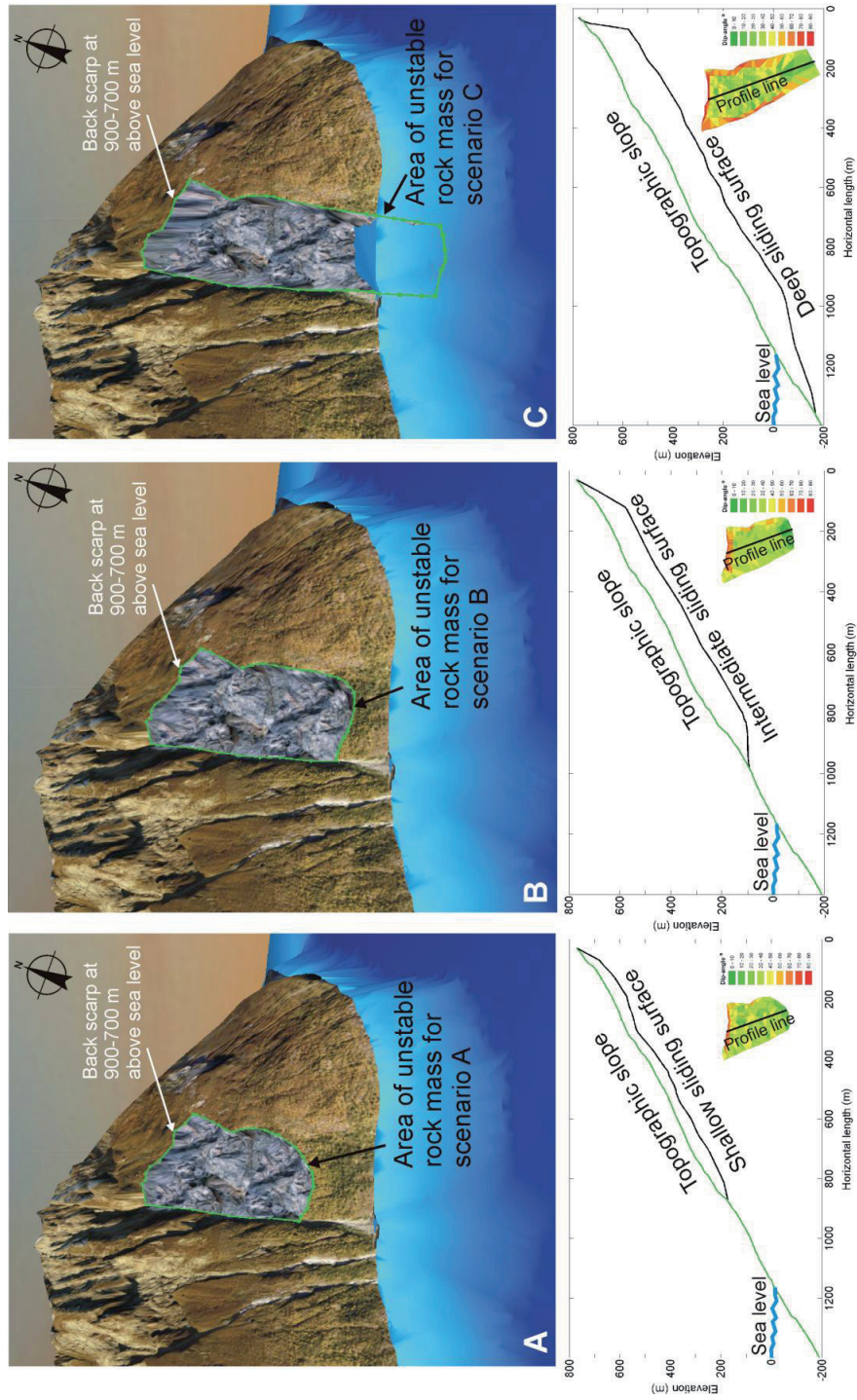


Figure 3. An illustration of the three scenarios proposed in Paper III.

1.3 Comments on scope and author's contributions

This PhD project has been connected to International Centre for Geohazards' (ICG) research theme; "Application of Geographical Information Technology to Geohazards". Although Geographical Information Technology (GIT) is closely connected to Geographical Information Systems (GIS), GIT is certainly not limited to using mainstream GIS software packages for addressing geohazards problems. The term geohazards includes a wide range of hazards related to geological and environmental conditions. However, this thesis only addresses investigations of large rockslides. The modifier *large* in the context of this thesis does not imply a specific minimum volume or extent, but refers to non trivial rockslide investigations where the investigations typically are motivated by potential devastating consequences.

The objective of this thesis is not to give a comprehensive evaluation of the Åknes rockslide, which has been used extensively as case study (Papers II, III and IV), or the Nordnes rockslide (Paper V), but rather to focus on approaches and methodology which can provide useful contributions to rockslide investigations in general.

Most of the work reported in this thesis was carried out in a highly applied context involving geoscientists from different geosciences disciplines.

Even though some of the subtopics addressed in this thesis have a dynamic nature, such as the algorithms for construction of TINs (Paper I) as well as the interactive geometrical modelling of sliding surfaces (Paper II and Paper III), the general framework used for the geovisualization part of this thesis is considered as static as it does not include any functionality for physical simulation or visualization of motion and deformation. As the reported geovisualization approach relies on interactive 3D visualization, only rendering methods suitable for real time visualization of large 3D models were considered. Except from 3D texturing, used for visualization of geophysical subsurface data (Paper II), boundary representations (b-rep) have been used for volume objects. Triangulated Irregular Networks were mainly used for surface modelling within this thesis (Papers I, II and III).

Statistical analysis, including quantification of uncertainty, may be important to many aspects of rockslide investigations. This thesis addresses statistical analysis of displacement measurements (Paper IV and Paper V). These measurements were obtained from lasers, GPS, total stations, extensometers and crackmeters which provided repeated measurements in time. The main focus for this part of the thesis is therefore on time series analysis.

A significant amount of time has been spent on C++ programming during this PhD project. The major portion was spent on geovisualization and geometrical modelling, as reported in Paper II and Paper III, using the C++ API to OSG. It took some time

both to get familiar with OSG as well as to explore the potential of OSG with respect to the geoscientific problems addressed in the thesis. Also the investigations reported in Paper I required some C++ programming. The basic incremental Delaunay triangulation algorithm used for Paper I was initially implemented by Professor Terje Midtbø as part of his doctoral work in the early 90s. In order to compare the performance of various data reduction methods, several extensions to this initial algorithm were required. Paper IV and Paper V only required a limited amount of scripting in MATLAB to perform statistical analysis of displacement data.

The remaining part of this section outlines the candidate's contribution to the individual papers.

Paper I: This paper was written by the candidate and all analyses were carried out by the candidate. The basic triangulation algorithm, provided by the co-author, was extended by the candidate in order to compare the various data reduction methods.

Paper II: This paper was drafted by the candidate and all implementations were performed by the candidate. The co-author provided advice on methods and the writing of the final paper was a joint effort of both authors

Paper III: All implementations were carried out by the candidate. However, the geoscientific interpretations and evaluations were carried out by co-authors. The writing of this paper was a joint effort.

Paper IV: The paper was written by the candidate and all analyses were performed by the candidate. The co-author provided advice on methods and review of final paper.

Paper V: All analyses were carried out by the candidate and most of the paper was written by the candidate. The co-authors provided geological evaluations of the results and some adjustments to the final paper.

2 Theoretical foundations

2.1 Spatial data and their digital representations

Geospatial or *spatial data* are usually referenced in the 2D or 3D Euclidean space either using Cartesian coordinate systems or spherical coordinate systems. In addition, usually one or more data *attributes* are associated with each spatial reference (location). Attributes refer to other properties besides the spatial location, such as the type of soil, the snow depth or the temperature. For some applications also the time component is crucial and therefore included. Spatial data which are also referenced in the time domain are commonly referred to as spatio-temporal data.

Real world geospatial objects tend to be quite complex and, depending on the scale, the level of details of such objects may be unbounded. Moreover, the vague nature of many geospatial objects makes it impossible to exactly determine their extent and attribute values. Therefore, their digital representations rely on abstractions, generalizations and discretizations of real world objects.

A variety of models for representing spatial data exists. Within Geographical Information Science (GIScience) two main approaches are recognized; namely *vector* and *raster* representations. In 2D, the raster representation is based on regular subdivisions of a plane such that each grid cell represents a data value or the absence of a data value. A generalization of the raster approach into 3D is the voxel representation which uses 3D regular grid cells as the fundamental unit. The vector approach uses different geometrical primitives such as points, lines and polygons to represent spatial data. The vector approach in 3D is similar to the one in 2D. In 3D, volume objects are represented by their boundaries such that a set of connected surface polygons make up their boundaries. This is often referred to as Boundary representation or B-rep in short. Both the raster and vector approach have their advantages and disadvantages. Thus, depending on the application one approach may be favourable compared to the other. For example, the vector representation is generally considered as the most suitable for performing network computations. In other applications the raster representation may be the most favourable due to its simpler structure and often more straightforward computations.

Spatial data structures are commonly employed to make efficiently use of the available computing resources. For example, when using raster or voxel representations of real world data, there will usually be a number of contiguous sub-areas or sub-volumes containing void or homogeneous values. The straightforward approach, using simple arrays to store the entire grids, will introduce repetitions and

therefore be inefficient. Instead, suitable spatial data structures can be utilized such that no subdivision is needed for contiguous homogenous regions. Common examples of such data structures include quad-trees, in 2D, and oct-trees in the 3D case. See e.g. Samet (1990) for a presentation of spatial data structures.

In addition to the (geo)metric properties of spatial data, the topology, i.e. the connectivity of a spatial model, may become a major consideration once spatial analyses or spatial queries come into play. Topological information may be explicitly given by the data structures being used. For example, references (pointers) to adjacent polygons can be embedded into the data structure of a polygonal mesh. The topological relations may alternatively be given implicitly in the data structure; this is the case if a regular grid is represented by an array. In this case the spatial neighbours of a specific cell are also neighbours in the array. On the other hand, if, for example, visualization is the only concern, topological relations may be less important.

2.2 Digital terrain modelling

Digital terrain models

In rockslide investigations, digital terrain models (DTMs) are essential. Not only for the determination of slope angles or volume calculations but also for the identification of geomorphologic features such as fault lines which can help delineating fault planes into the subsurface. As such, terrain models can also serve as a basis for identifying susceptible areas which may require field investigations or monitoring.

One of the first descriptions of the DTM concept is found in Miller and LaFlamme (1958). They defined DTM as “a statistical representation of the continuous surface of the ground by a large number of selected points with known x, y, z coordinates in an arbitrary coordinate field”. However, as pointed out by for example Podobnikar et al. (2000), defining the terms “DTM” and “DEM” is not an easy task since no uniform, generally accepted, definitions exists. Some authors seem to use DTM synonymously with *digital elevation model* (DEM) whereas others reserve the term DEM for a particular subset of DTMs, that is, regular grid models. For example, Li et al. (2005) define DEM as “elevation data organized in the form of a matrix”. Another possible distinction between DTMs and DEMs is that DTMs may include terrain features as well as additional non topographic surface information whereas DEMs only contain terrain elevation values (Li et al. 2005). This discussion is not concluded here, but in this thesis the term DTM refers to plain elevation surface models not including man-made objects such as buildings. In general, two main categories of DTMs can be identified; regular and irregular, typically materialized by regular grid DEMs and Triangular Irregular Networks (TINs), respectively. A brief description of TINs is

presented below. A detailed comparison of TINs and DEMs are found in Kumler (1994). Combinations of these approaches, called hybrid models, are also well documented (e.g. Bóo et al. 2007). Hybrid models aim to take the best from different approaches, typically by enhancing regular grid models with structural features.

Digital terrain models are usually represented as 2.5D surfaces. The advantage of this so-called 2.5D approach is that it is simpler than a fully 3D approach in that each height value is considered as an attribute to the corresponding x,y coordinates. On the other hand, as only one height value is allowed for each x,y location, this approach implies some limitations. For example, complete vertical sections or overhangs in a terrain surface cannot be adequately modelled by the 2.5D approach. However, in many real world applications these limitations are outweighed by the simplicity of a 2.5D approach compare to a fully 3D approach. For example, with respect to geometric modelling of basal sliding surfaces in this thesis, a 2.5D approach was found suitable as there were no need for overhangs in these surfaces (Papers II and III).

Triangulated irregular networks

Although triangle-based approaches to contouring were used as early as the mid 60's, the first known Triangulated Irregular Network (TIN) as a topologically-integrated triangulation, thought of as the upper surface of a three-dimensional solid, was described by Thomas K. Poiker (then spelled 'Peucker') in 1973 (Mark 1997). A TIN model consists of a set of contiguous non overlapping planar triangle facets. The Delaunay criterion (from Delaunay 1934) is commonly applied for TIN construction. A thorough description of Delaunay networks is found in Midtbø (1993). The Delaunay triangulation criterion uses the relative point configuration, in the x,y plane, as a basis for triangle generation. Given a point dataset, the resulting triangles become as close to equilateral as possible which generally provides an overall good approximation of the underlying height field. Besides the ability to cope with irregularly sampled data, the main advantage of TIN models is the ability to adapt the "resolution" to the underlying height field. These two properties were the main reasons for using TIN models for surface representations in this thesis (Papers I, II and III). The TIN model is, however, not limited to terrain modelling but can also be used for general 3D scientific modelling and visualization purposes, for example for representing iso-surfaces.

Terrain descriptors

Various terrain descriptors can be derived from the primary information of a DTM, i.e., the elevation values. According to Li et al. (2005) two basic types of terrain descriptors can be distinguished; qualitative descriptors and quantitative descriptors.

The first group is also referred to as general descriptors as they comprise descriptive statements regarding surface properties. This group is considered less important with respect to digital terrain modelling. Quantitative descriptors or numeric descriptors on the other hand are highly relevant with respect to digital terrain modelling. Some examples of numeric terrain descriptors include: slope, frequency spectrum and surface roughness.

Slope has two components; the first vertical derivative of the elevation surface (sometimes referred to as the gradient) and aspect which is the first horizontal derivative. If a terrain surface representation is transformed from the space domain into the frequency domain (typically by means of a Fourier transform), the major structural features of the surface correspond to long wavelengths, whereas the finer topographic undulations correspond to shorter wavelengths and measurement noise (even shorter wavelengths). Thus, spectral analysis may also be used to filter out specific frequency content, for example to smoothen the surface by removing the finer topographic features as well as measurement noise. Surface roughness may be computed in various manners. A simple measure of roughness is the ratio between the surface area and its projection onto the horizontal plane (Li et al. 2005). However, Mark (1975) found that roughness cannot be completely defined by a single parameter but should include a set of parameters; relief, wavelength and slope. In addition to the terrain descriptors mentioned above, volume and surface (or projection) area are also key descriptors in many applications. In general, the choice of suitable terrain descriptors are highly application dependent. Suggested literature addressing terrain descriptors include Wilson and Gallant (2000) and Li et al. (2005).

Sampling of terrain data

In a DTM context, sampling is the process of selecting discrete points to represent a continuous terrain surface. Traditionally, sampling has often been performed before the actual measurement. This is for example the case when tachymetry or RTK GPS is used for data acquisition; first the sample location is decided, typically along a break line or other characteristic terrain point, then this point is measured. However, sampling can take place both before and after measurement (Li et al. 2005). The adaptive triangulation approach applied in Paper I is an example of sampling *after* measurement since a subset of important points (in terms of describing the shape of the surface) is selected from an initial high density set of surface points. The initial point set were obtained from airborne LiDAR scanning which provided high density (semi random) point sets.

An important foundation for the sampling theory is the Nyquist theorem. In essence this theorem states that if a function $g(x)$ is sampled at an interval of d , then the frequencies higher than $1/(2d)$ cannot be reconstructed from the sampled data (Li et al. 2005). With respect to digital terrain modelling this means that the spacing

between the sample points determines the high frequency content (i.e. the degree of finer topographic details) that can be reconstructed from the sample points.

Data acquisition

A multitude of techniques can be used for DTM data collection. Some examples are tachymetry, GPS, remote sensing, photogrammetry, airborne Light Detection and Ranging (LiDAR), also referred to as Airborne Laser Scanning (ALS), as well as multi beam echo sounding for seabed mapping. Traditionally, photogrammetry has been the most widely used technique for high quality DTM data collection (Li et al. 2005). However, ALS has become very popular and is now a leading technique for the acquisition of DTM data (Maas 2002). Terrain models used in Paper I – III in this thesis were generated from ALS data.

The ALS technique is based on laser distance measurements combined with a scanning mirror mechanism (Maas 2002). Position and orientation parameters of the sensor system are mostly determined by an integrated GPS/INS system (Maas 2002). Thus, ALS provides polar measurements as distances and directional angles are measured from a known origin and known orientation. For each measured point, the outcome is x, y and z coordinates along with the intensity of the reflected signal. Errors in these measurements obviously affect the quality of the final DTM. The primary sources of positional error in the LiDAR collection process are associated with the GPS equipment onboard the aircraft, the inertial navigation unit for estimating positions between GPS fixes, and the inertial measurement unit (IMU) for monitoring the pointing direction of the laser (Hodgson and Bresnahan 2004). Another important aspect of DTM generation from ALS data is separation of ground points from non-ground points, known as filtering; see e.g. Sithole and Vosselman (2004). Data collection as such is however not emphasized in this thesis and therefore no detailed presentation on this topic is provided here. However, issues on quality and accuracy of DTMs are presented in some more detail in next subsection.

Quality and accuracy of digital terrain models

In the context of geo-spatial data, quality is often considered with respect to the “fitness for use” (Chrisman 1984, Martinoni and Bernhard 1998). Thus the quality of a DTM may not be an absolute measure, but depends on the application. A number of factors may influence the quality. Besides the positional (geometric) accuracy, the resolution, the attribute accuracy and the “currency” may also be important aspects of the DTM quality. The discussion here is however limited to the geometric accuracy of DTMs. Accuracy here refers to the geometric correctness of a DTM with respect to the corresponding physical terrain surface. While there are a remarkable amount of publications on quality and accuracy of DEM (i.e. regular grid based terrain models)

the number of publications explicitly addressing quality of TIN models is considerably less. However the discussion below applies, to some extent, to both DTMs and DEMs.

A terrain surface is reconstructed from a finite set of points, a sample. In order to reconstruct the initial continuous surface, intermediate values have to be estimated. A number of factors affect the accuracy of these intermediate points. MacEachren and Davidson (1987) point to five such factors; 1) data measurement accuracy, 2) data intensity, 3) location of data collection point, 4) intermediate value estimation procedure, and 5) spatial variability of the surface represented. In practice, the most widely used approach for quality assessment relies on comparisons with reference data (Kraus et al. 2004 and Höhle and Höhle 2009). Such reference data are typically separate datasets that are highly accurate (compared to the data or model being assessed) but may also be the initial data set from which the terrain model was created. Thus, the quality of a specific DTM is reflected by the discrepancies between the model and some reference data set.

However, other approaches for quality assessment not requiring reference data are also described. For example, Bjørke and Nilsen (2008) present a geostatistical approach that only requires a single dataset. This approach uses variogram calculations to obtain an estimate of the measurement error as the estimated nugget effect represents the measurement error. As shown by Carlisle (2005), DEM errors are related to terrain characteristics. He used regression analysis to model the relationship between the DEM error and terrain characteristics. This enables generation of accuracy surfaces representing the spatially varying DEM errors. The accuracy of surface derivatives such as slope, aspect, curvature and surface roughness also depends on the accuracy of the initial terrain model. Hunter and Goodchild (1997) showed that the accuracy of slope and aspect is dependent on the spatial autocorrelation. Oksanen and Sarjakoski (2005) found that increase in DEM vertical error will increase the error in surface derivatives. They also pointed out that the spatial autocorrelation of the errors affects the accuracy of the surface derivatives and that uncorrelated DEM errors may not lead to the worst case scenario with respect to the accuracy of surface derivatives.

A substantial amount of literature on quality aspects of digital terrain models exist. In addition to the above mentioned references, suggested references on this topic include Li et al. (2005) and the references therein.

Generalization and simplification of terrain models

There may be a number of reasons for simplifying and reducing the amount of data in a DTM. A fundamental limitation often encountered in practice is the available processing and memory capacity of the hardware and software being used for DTM construction, analysis and visualization. Thus, data reduction is particularly relevant

with data acquisition methods that generate extensive amounts of raw data (e.g. LiDAR and multibeam echo sounder) or if the resulting DTMs are intended for real time visualization or dissemination via internet. There is a substantial amount of scientific literature addressing simplification and generalization of DTMs. Depending on the discipline (e.g. computer graphics versus geomatics or geosciences) the focus and the terminology seem to be somewhat different. For example, the main focus a computer graphics perspective is on visual appearance (e.g. Cline and Egbert 2001), algorithmic complexity and compression (e.g. Balmelli et al. 2003) whereas the geoscience community is more focused on how the simplification affects the geometry of the DTM in terms of elevation values and other terrain parameters. Some studies also investigate how the results of DTM based calculations are affected by DTM generalizations (e.g. Franklin et al. 2008 and Stuetzle et al. 2009). However, the researches originating from the different disciplines show a high degree of relatedness and overlaps and thus the literature is considered complementary.

Ideally, a DTM generalization method should be time efficient as well as provide good quality geometric approximations. Which property being the most important depends on the application; whether the simplification method is used as part of a pre-processing step or for real time applications such as for generating continuous levels of details (LOD, see e.g. Danovaro et al. (2006) and Section 2.3.3 in this thesis). In order to measure the approximation performance of the simplification method used, error metrics are used. One such error metric is Root Mean Square (RMS), also referred to as the L^2 norm.

Although different definitions are found in the literature, here the terms *simplification*, *data reduction* and *generalization* are used interchangeably. Two main approaches for DTM simplification can be identified, that is, decimation and refinement. Decimation refers to the situation where less significant data points are successively removed, from an initial high resolution mesh, as long as the simplified model maintain an acceptable approximation to the initial model. Contrary, refinement refers to the situation where a coarse initial mesh is successively updated with data points until a certain level of approximation is reached (e.g. Paper I). An example of combining refinement and decimation is found in Pedrini (2001).

As DTM generalization has been an active field of research for decades the amount of scientific literature is substantial. Only some selected references are mentioned here. One recognized refinement method is *adaptive triangulation*, first described by Heller (1990). Further investigations into this method are reported in Bjørke and Nilsen (2002) and in Paper I of this thesis. Paper I provides an assessment of different strategies for point selection in combination with both a standard Delaunay triangulation and a modified (data dependent) Delaunay triangulation. Comparisons of the performance of different generalization methods based on wavelets, adaptive triangulation and universal kriging are found in Bjørke and Nilsen (2002). The performances of their methods were measured using the L^2 error between the

thinned models and the original models. They concluded that average interpolating wavelets show attractive properties, such as better numerical stability and time complexity than the other methods, which make them very well suited for compact representation of digital terrain models. Further studies on wavelet based methods are reported in Bjørke and Nilsen (2003) and in Pradhan et al. (2005). Hierarchical approaches and multi resolution methods for terrain simplification are also well documented in the literature (see e.g. De Floriani and Puppo 1995 and Yang et al. 2005).

2.3 Geovisualization

2.3.1 Introduction

The term geovisualization is a contraction of *geographic visualization* and have been commonly used for a decade or so. Geovisualization can be regarded as an approach for exploring and analysing geospatial data where the ultimate goals typically are knowledge construction and decision making. According to Dykes et al. (2005), geovisualization can be described as a loosely bounded domain that addresses the visual exploration, analysis, synthesis, and presentation of geospatial data by integrating approaches from cartography with those from other information representation and analysis disciplines, including scientific visualization, image analysis, information visualization, exploratory data analysis, and GIScience. This description underlines the cross disciplinary nature of geovisualization. However, the foundation for geovisualization is intimately connected to interactive 3D computer graphics. Therefore, a brief presentation of the basics of interactive 3D computer graphics is provided in Section 2.3.2.

Geovisualization approaches may be particularly useful in complex rockslide investigations. A 3D visualisation of “geometrical solutions” helps one to understand the extension at depth of geological objects and avoid unrealistic interpretations”, (Zanchi et al. 2009). Another benefit from 3D geovisualization is that it may enable evaluation across scales; “Being able to test ideas at the outcrop scale and then quickly zoom out to obtain a perspective on the likely impact at the regional scale is extremely powerful.” (Jones et al. 2009). One of the fundamental ideas in such a context is to integrate a multitude of data in a 3D model in order to form a basis for geoscientists to perform their interpretations, analyses and judgements. Data integration and model building are addressed in Wu et al. (2005), Kaufmann and Martin (2008), Caumon et al. (2009), Jones et al. (2009) and Zanchi et al. (2009). Although some tasks may be adequately performed using mainstream GIS software, the required data analysis methods tend to be highly specialized in geoscientific applications (Jones et al. 2009). This in turn causes need for data transfer between

different software or possibly integration of software packages. An example of combining GIS and specialized geoscientific software is found in Zanchi et al. (2009). They combined GIS and the gOcad software for reconstruction of complex geological bodies.

A geovisualization application may employ different user interface concepts. Jones et al. (2009) differentiate between the windows based Graphical User Interface (GUI) denoted as the “desktop metaphor” versus the 3D geospatial GUI referred to as the “virtual world metaphor”. The desktop metaphor is characterized by the use of windows, icons and menu bars etc. Moreover, the depiction of the file system as hierarchy of files and folders is central to the desktop metaphor. The virtual world metaphor on the other hand is more objects centric; here the model *is* the interface as opposed to desktop metaphor context where the model exists *within* the user interface (Jones et al. 2009). Software using a 3D geospatial GUI, based on a „virtual world” metaphor, provides best user interactivity for complex geological models (Jones et al. 2009). The geovisualization application presented in Paper II and Paper III include elements from both the above mentioned “GUI classes”. For example, information associated with the model itself, such as the drill core images or interactive editing of geometric objects fit in with the “virtual world” metaphor whereas the head up display, enabling switching on and off data layers, falls under the “desktop metaphor”.

2.3.2 Foundation for geovisualization - interactive 3D computer graphics

The following brief description of interactive computer graphics is mainly based on Hern and Baker (2004) and Angel (2006). Furthermore, this description also has some references to OpenSceneGraph (OSG, Martz 2007), the high level application programming interface (API) used for Paper II and Paper III in this thesis.

Computer graphics basically deals with representations, digital synthesis and manipulation of pictorial data in a computer environment. At present, almost all graphics systems are raster based (Angel 2006). A schematic view of a raster based computer graphics system is shown in Fig. 4.

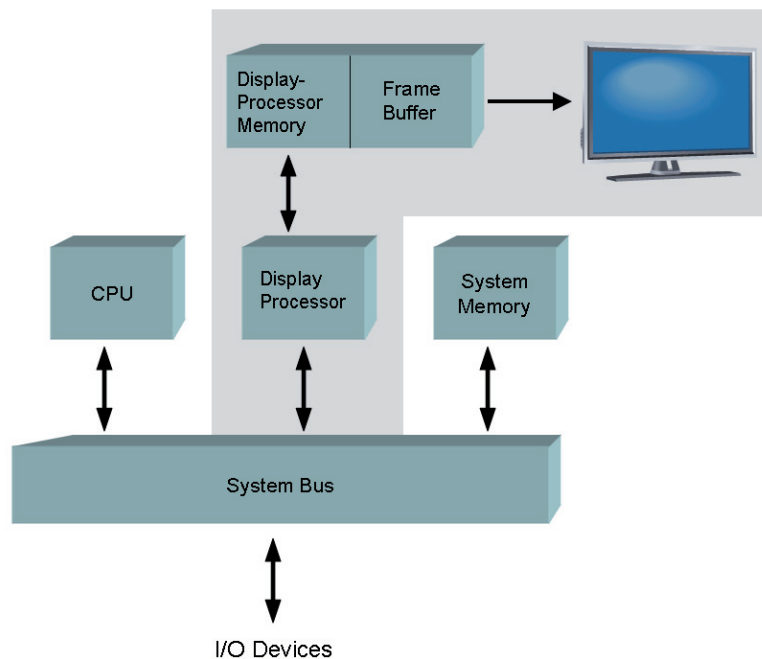


Figure 4. Architecture of a raster based graphics system (slightly modified from Hern and Baker 2004). The grey shaded area contains “graphics units” which come in addition to a general computer system. A display processor is optimised for graphics processing and has its own dedicated memory used for graphics processing including a frame buffer. The process of converting entities of a geometric model into pixel information for the frame buffer, which ultimately makes up the image definition, is known as rasterization or scan conversion

Viewing and projection

Although the digital models of real world spatial objects are three-dimensional, the corresponding images displayed on a computer screen are however two-dimensional. Converting from 3D model coordinates to 2D computer screen coordinates involves a number of steps including a projection transformation which actually transforms the 3D model coordinates into 2D image coordinates. *Perspective* projections are commonly used in geovisualization applications as they provide 3D effects such that far objects appear smaller than close objects. A *synthetic camera* metaphor is often used in computer graphics. That is; images of a scene are created dependent on the relative position and orientation of a synthetic camera as well as other settings associated with this synthetic camera such as projection parameters. Thus, the geometric 3D-model is rendered into a 2D image by simulating the view of the model through a synthetic camera and the relationship of the model and the light sources. Some basic principles of 3D computer graphics are illustrated in Fig.5.

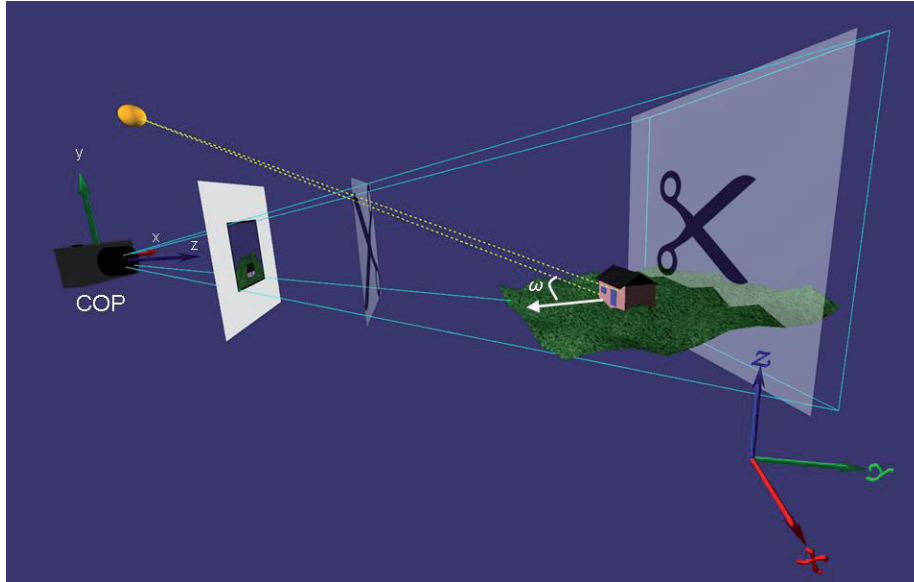


Figure 5. Principles of 3D computer graphics. The view frustum is the section of the view pyramid which lies between the near and the far clipping plane (indicated with scissors symbols). A synthetic camera is located at the apex of the view pyramid which corresponds to the centre of projection (COP). The projection plane or image plane is located in front of the camera which uses its own viewing coordinate system whereas the scene's geometric objects are (initially) specified in a modelling or world coordinate system. The viewing z-axis, corresponding to the camera's central axis, represents depth. Lighting or shading calculations are based on the angles between the surface normal vectors and the vectors pointing towards the light source(s). For example, the gable wall and the front wall of the building have the same colour specifications but the gable wall receive no direct incident light from the light source and therefore appears darker.

Clipping and back face culling

The clipping process determines which geometric objects are within the current view volume or view frustum (Fig. 5). Only those which are fully or partly inside the view volume need further processing. Moreover, to produce images that appear realistically only non-occluded objects should be displayed. This is also essential for the application's performance as the available resources should only be spent on the objects which actually contribute to the final images. Hidden surface removal algorithms aim to remove surfaces that are not visible to the viewer. Many algorithms for hidden surface removal work in the image-space, that is, after the geometric objects have been projected. The depth-buffer method is perhaps the most widely used image space algorithm. During scan conversion, this algorithm maintains a current depth value for each location in the frame buffer. After scan conversion is

completed, the object corresponding to the smallest depth value, at each frame buffer location, determines the final colour to be displayed. To improve the performance, images space algorithms are often combined with object space methods i.e. algorithms working on the 3D object coordinates. For example, back face culling can be applied prior to the depth-buffer method. As back face culling removes all polygons facing away from the viewer, roughly half of the polygons can be eliminated from further processing at an early stage of the rendering pipeline.

Level of details

However, real world spatial data sets are often large and therefore exceed the capabilities of the available graphics hardware. Various approaches for data reduction can be used to cope with this problem. For example, variable levels of details (LOD) can be implemented. Variable LOD can be implemented such that the software application switches to less detailed representations as the distance from the viewer to the object increases. Depending on the application, LOD can be accomplished by pre-processing a set of representations with variable levels of details, or by a continuous approach where generalizations of the full datasets are carried out in real time. The data reduction methods described in Paper I are highly suitable for generating pre-processed multiple “LOD versions” of surfaces.

Lighting and textures

The lighting of a scene is an important factor for providing 3D effects. As real time visualization is the major consideration for geovisualization, the applied lighting methods should not be too computing intensive. Thus, only local lighting models are usually used in real time visualization. The local lighting models generally provide satisfactory lighting effects although not photorealistic. For example, they do not account for reflections among the different objects in the geometric models. Only the direct incident light from the specified light sources is considered. However, usually general graphic programming packages such as OSG provide a large number of options both for light source properties and material properties which enables quite flexible lighting. Assuming a geometric model consisting of polygonal surfaces, a local lighting model uses the angles between the normal vector for each surface facet (triangle) and the vectors pointing towards the light sources as a basis for shading calculations (Fig. 5). Also texture mapping is often used to improve the visual appearance of geometric models. A common example within geovisualization is to drape aerial photos on terrain models. However, 3D texturing can also be useful for geovisualization purposes (Fig. 6).

Stereo viewing

In addition to the above mentioned techniques such as perspective projection, lighting and texture mapping, stereoscopic viewing can be used for further improvement of the viewer's 3D impression. Stereoscopic viewing mimics the real world human 3D perception of (close) objects. Although different techniques (anaglyph, shutter glasses etc.) can be used to obtain a stereo-view they all rely on the same principle. This is simply to display two different images of a 3D model, one for each eye, created from two slightly different camera locations, analogous to the slightly different view perceived by the left and right eye when looking at real world objects. These two images are subsequently synthesised into a 3D view by the human brain.

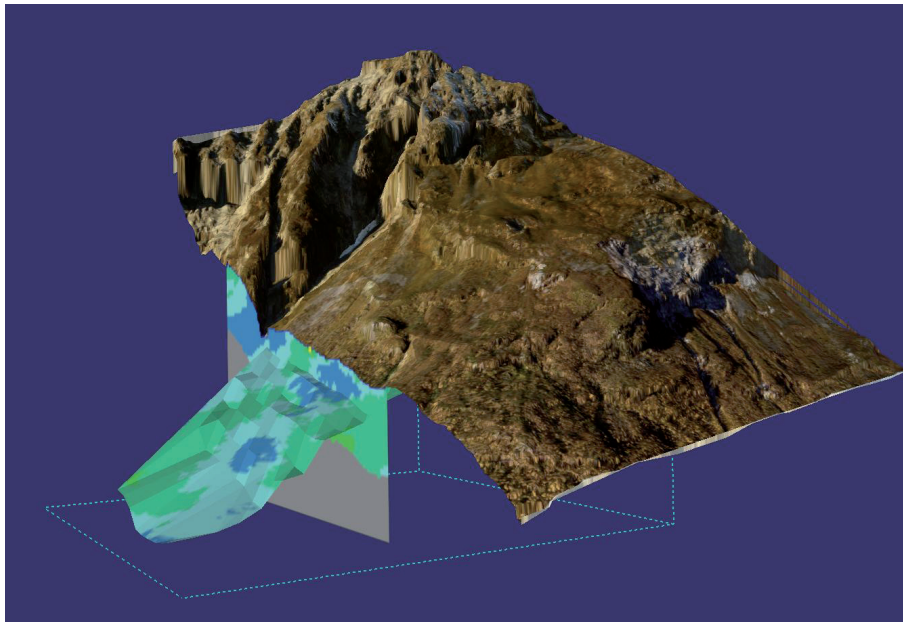


Figure 6. Example of 2D and 3D texturing (Åknes rockslide). 2D: An aerial photo is draped on a terrain model. 3D: A sliding surface and a vertical cross section painted with geo-electric resistivity values; when the location of the sliding surface or the cross section is changed, the colour values are automatically updated according to the resistivity values for the current location.

Scene graphs

Almost every graphics application employs a scene graph in some way (Staneker 2005). Scene graphs can help simplifying application development and making optimal use of the available graphics hardware (Reiners 2002). A scene graph is basically a hierarchical data structure which defines geometric objects, lights, cameras

and their properties as a 3D scene. An example of a scene graph is shown in Paper II, Fig. 3.

Interactivity

Interactivity is a key concept within geovisualization as it enables the direct exploration of spatial data. This requires some sort of interactive input device such as a mouse, a game controller or a haptic device. From the operation of these input devices, *events* are generated. For example, using a mouse as the input device, events are generated from mouse move, button press and button release. Each event is associated with certain information such as the position of the cursor, the button that generated the event and whether the button was depressed or released. This information is subsequently used by specific functions, denoted as callback functions, which govern how the application program responds to the events. Besides the common Graphical User Interface (GUI) operations, such as the selection of menu options, interaction with dialog boxes and window operations, navigation is the most notably form of interaction in 3D. Navigation involves rotation, pan and zoom.

Object selection or *picking* is another important function. Picking is used for identifying objects displayed on the screen by hitting a 3D object with a ray shot from the 2D mouse position on the user's screen. The selected objects may in turn be manipulated in different ways; both with respect to the geometry (rotation, translation, deformation) as well as to the object's visual appearance such as colour or transparency.

Picking involves mapping of 2D screen coordinates to the corresponding object(s) or node(s) in the scene graph. Various strategies are used for performing picking operations. For example, one strategy is based on intersection calculations. In principle, the intersections of interest are those between an imaginary ray into the model, originating from specific position on screen e.g. the current cursor position, and the geometric objects in the model. To efficiently perform the intersection calculations, often a hierarchy of bounding volumes are implemented as part of the scene graph. These bounding volumes are usually axis-aligned bounding boxes as this eases the computational load. The intersection calculations utilize this hierarchy of bounding volumes such that only those objects contained in bounding volumes intersected with the ray needs further processing. However, to avoid numerical problems related to intersection calculations with a ray and line primitives or point primitives as well as picking at large "distances", a volume object can be used instead of a ray. This strategy is implemented in OSG (Martz 2007). OpenSceneGraph uses a narrow pyramid in stead of a ray. The pyramid's apex corresponds to a specific screen location and the pyramid's central axis corresponds to an imaginary intersection ray. Generally, there will be multiple intersections between this pyramid and the objects in the model, resulting in a hit-list. Depending on the situation, usually the intersection

having the smallest depth value is the one of interest. This corresponds to the object closest to the viewer.

2.4 Statistical methods

Statistical methods are applicable to a wide range of problems arising from spatial data. Statistical methods comprise tools ranging from pure descriptive statistics and exploratory analysis to parameter estimation, hypothesis testing and prediction. The following sections provide a brief presentation of some core concepts within statistical analysis, including the methods used in this thesis (i.e. in Paper I, Paper IV and Paper V).

Measurement errors

All real world measurements are associated with errors. Errors are often classified either as random, systematic or gross. *Random errors* have expectation value zero and represent unpredictable fluctuations in all directions. *Systematic errors* typically represent constant offsets, in specific directions, or scale factors. *Gross errors* or *blunders* are generally associated with erroneous observations due to malfunctioning instruments or human mistakes. Ideally, all gross errors should be removed either in advance of the statistical analyses or possibly as part of the analyses. Systematic errors may be included in statistical models and estimated along with other relevant parameters. Random errors act as noise added to the true, but unobservable values, such that a single observation represents the true value plus a random error. Various parameter estimation techniques aim to provide (optimal) estimates of underlying parameters given the presence of errors. The method of Least Squares (LS) is widely used for parameter estimation.

Principal component analysis

Principal component analysis (PCA) is concerned with explaining the covariance structure of a set of variables through linear combinations of these variables (Johnson and Wichern 2002). Typical applications of PCA include data reduction, by replacing variables of a multivariate dataset with a subset of the most important principal components (PCs), or data interpretation.

If \mathbf{x} is a random vector with covariance matrix \mathbf{C} , then the 1st PC is the linear combination $\mathbf{a}_1^T \mathbf{x}$ that maximizes $\text{Var}(\mathbf{a}_1^T \mathbf{x})$ subject to the condition $\mathbf{a}_1^T \mathbf{a}_1 = 1$.

Generally, the i^{th} PC is the linear combination $\mathbf{a}_i^T \mathbf{x}$ that maximizes $\text{Var}(\mathbf{a}_i^T \mathbf{x})$ subject to the conditions; $\mathbf{a}_i^T \mathbf{a}_i = 1$ and $\text{Cov}(\mathbf{a}_i^T \mathbf{x}, \mathbf{a}_k^T \mathbf{x}) = 0$ for $k < i$. This means that the principal components correspond to the *eigenvectors* of a covariance matrix. Each eigenvector - or principal component - is associated with an *eigenvalue* representing the variance explained by this particular principal component. Thus PCA can be used to form an uncorrelated orthogonal basis from a set of correlated variables. Principal component analysis is a well established and widely used method and is treated in many textbooks regarding multivariate analysis. The reader is therefore referred to the literature for further details on PCA, see e.g. Johnson and Wichern (2002).

Linear regression

Linear regression is central to the analyses reported in Paper IV and Paper V. Here, linear regression was used for time series analysis of rock slope displacement measurements. A brief presentation of the foundation for linear regression is therefore presented in this section. Thorough descriptions of the theory for linear regression are found in e.g. Koch (1999) and Montgomery et al. (2001) which the below description is based on.

In a linear regression model the expectation values $E(\mathbf{y})$ of the observations \mathbf{y} are assumed to be linear combinations of unknown parameters;

$$E(\mathbf{y}) = \mathbf{X}\boldsymbol{\beta} = \mathbf{y} + \mathbf{e} \quad \text{with} \quad \text{Cov}(\mathbf{y}) = \text{Cov}(\mathbf{e}) = \mathbf{C}_{ee} = \sigma^2 \mathbf{Q}_{ee} \quad (1)$$

where \mathbf{X} is a known design matrix, $\boldsymbol{\beta}$ is a vector of unknown parameters and \mathbf{e} is a vector of errors. Eq. 1 shows that the error covariance matrix \mathbf{C}_{ee} can be expressed as the product of the variance σ^2 of unit weight and the cofactor matrix \mathbf{Q}_{ee} .

Estimates of the unknown parameters can be obtained using various methods. Here only the method of least squares (LS) is presented. The method of LS provides best linear unbiased estimates (BLUE) of the unknown parameters if the errors have zero expectation and are uncorrelated and have equal variances. This is known as the Gauss Markov theorem. An Ordinary Least Squares (OLS) solution is obtained from:

$$\hat{\boldsymbol{\beta}} = (\mathbf{X}^T \mathbf{X})^{-1} \mathbf{X}^T \mathbf{y} \quad \text{with} \quad \text{Cov}(\hat{\boldsymbol{\beta}}) = \hat{\sigma}^2 (\mathbf{X}^T \mathbf{X})^{-1} = \hat{\sigma}^2 \mathbf{Q}_{\hat{\boldsymbol{\beta}}} = \mathbf{C}_{\hat{\boldsymbol{\beta}}} \quad (2)$$

Here, \mathbf{X}^T denotes the transpose of \mathbf{X} and the hat symbol $\hat{}$ is used to denote estimates of the corresponding true (but unknown) values.

Positive autocorrelation is frequently encountered in real world spatial and temporal data. To account for the general case assuming correlated observations, a weight

matrix \mathbf{P} is introduced and the resulting estimate is known as a Weighted Least Squares (WLS) estimate. The solution for the method of WLS is given by Eq. (3):

$$\hat{\boldsymbol{\beta}} = (\mathbf{X}^T \mathbf{P} \mathbf{X})^{-1} \mathbf{X}^T \mathbf{P} \mathbf{y} \quad \text{with} \quad \text{Cov}(\hat{\boldsymbol{\beta}}) = \hat{\sigma}^2 (\mathbf{X}^T \mathbf{P} \mathbf{X})^{-1} = \hat{\sigma}^2 \mathbf{Q}_{\hat{\boldsymbol{\beta}}} = \mathbf{C}_{\hat{\boldsymbol{\beta}}} \quad (3)$$

where $\mathbf{P} = \mathbf{Q}_{ee}^{-1}$ is the weight matrix of the observations. An unbiased estimate of the variance σ^2 of unit weight is obtained from:

$$\hat{\sigma}^2 = \frac{\hat{\mathbf{e}}^T \mathbf{P} \hat{\mathbf{e}}}{n - u} \quad (4)$$

where n is the number of observations and u is the number of unknown parameters. Thus, $n - u$ denotes the degrees of freedom. An estimate $\hat{\mathbf{e}}$ of the error vector \mathbf{e} is obtained from:

$$\hat{\mathbf{e}} = \mathbf{X} \hat{\boldsymbol{\beta}} - \mathbf{y} \quad (5)$$

The error estimates $\hat{\mathbf{e}}$ are usually referred to as residuals. Although OLS also provides unbiased estimators for the regression parameters in the presence of autocorrelation, OLS does not provide optimal (minimum variance) estimators. But more important; using OLS in the presence of positive autocorrelation leads to underestimation of the variance (e.g. Montgomery et al. 2001). This in turn leads to unrealistically optimistic (narrow) confidence- and prediction intervals and may also lead to wrong conclusions with respect to hypothesis testing since the regression parameters may appear statistically significant even though they are truly non-significant. In Paper V the weight matrices (\mathbf{P} in Eq. 3) needed for WLS estimation were obtained from the estimated autocorrelation of the residuals from corresponding initial OLS estimates. Autocorrelation values were calculated for *lag 0*, *lag 1*, ..., *lag n - 1*, where n denotes the total number of time steps for the time series in question. These autocorrelation values were then used as elements in the weight matrix.

Generally speaking, a regression model should be as simple as possible while providing satisfactory fit to the data. With this respect trigonometric terms could be useful for modelling cyclic behaviour. This is demonstrated in Paper IV and Paper V. Here the trigonometric terms were obtained from spectral analysis (see next subsection) of the residuals obtained from an initial simple linear model only accounting for the linear trends. The reader is kindly referred to the literature for details on model building and parameter selection in linear regression models. Some useful references include Montgomery et al. (2001) and Miller (2002).

Spectral analysis

Spectral analysis or *frequency domain analysis* enables analysis in the frequency domain instead of in the ordinary time or space domain. Such analyses are applicable to various spatial data problems, among others in digital terrain modelling as mentioned in Section 2.2. In this thesis (Paper IV and Paper V) spectral analysis was utilized for analysis of time series of rock slope displacement. Since cyclic behaviour was expected in these time series, Fourier analysis was used as a mean to establish the most significant periodic components. The established sinusoidal components were subsequently used as regression parameters to obtain an adequate model which also includes the periodic variations.

Using the discrete Fourier transform, a time series $y(t)$ can be represented as (Wei 1990):

$$y(t) = \sum_{k=0}^{n/2} [a_k \cos(2\pi kt / n) + b_k \sin(2\pi kt / n)], \quad t = 1, 2, \dots, n \quad (6)$$

In case of non stationary data, the model should contain both trend and spectral parameters (Haakonsen 2005). Equation (6) can be set up as a Gauss Markov model (Eq. 1) and the LS method can be used for estimation of the Fourier coefficients a_k and b_k . The first Fourier frequency is obtained from $\omega_1 = 2\pi / T$, where T denotes the total time span of the time series. For a unit sampling frequency, T equals n . Consecutive Fourier frequencies are obtained by $\omega_k = k\omega_1$, where $k = 2, 3, \dots, n/2$, and their amplitudes are obtained from:

$$\hat{A}_k = \sqrt{\hat{a}_k^2 + \hat{b}_k^2} \quad (7)$$

The Fourier frequencies form an orthogonal basis. This independent set of frequencies can be used as a starting point for the formulation of an adequate (regression) model by selecting the most important frequencies. Some relevant references regarding time series analysis and spectral analysis include Wei (1990), Shumway and Stoffer (2000) and Haakonsen (2005).

Hypothesis testing

A statistical hypothesis can be defined as an “assertion or conjecture about the distribution of one or more random variables” (Miller and Miller 1999). Hypothesis testing constitutes the core of statistical inference and is often performed as an integral part of statistical analyses. Typical examples include testing the significance of estimated regression parameters or comparing sample means between populations.

Hypothesis testing usually involves the following steps (Miller and Miller 1999):

1. Based on the problem at hand, formulate the null hypothesis H_0 and the alternative hypothesis H_1 , and specify the significance level α .
2. Using the sampling distribution of an appropriate test statistic, determine a critical region of size α .
3. Determine the value of the test statistic from the sample data.
4. Check whether the value of the test statistic falls into the critical region, accordingly, reject the null hypothesis, or accept it, or reserve judgement.

As hypothesis testing involves random variables, one may never be a 100% sure that a hypothesis is correctly accepted or rejected. There are two possible types of errors;

Type I: Rejection of the null hypothesis when it is true.

Type II: Acceptance of the null hypothesis when it is false.

The probability of committing a type I error is referred to as the significance level of the test and denoted α . As type I errors are considered the most critical, this means that the “burden of proof” lies with the alternative hypothesis and usually a conservative value of α is chosen (typically 0.05 or less). If also the probability of committing type II errors are of major importance, the *power function* of the test should be calculated, see e.g. Miller and Miller (1999). In practice it is often convenient to use the *p-value* for decision regarding rejection. The p-value is the probability of obtaining a test statistic at least as extreme as the one that was actually observed, assuming that the null hypothesis is true (Wikipedia). Thus, if the calculated p-value is below the chosen level of significance this implies that the null hypothesis should be rejected.

Other relevant references

In addition to the references provided in the text above, some more text books should be mentioned. For example Cressie (1993) provides a comprehensive presentation of classical spatial statistics including geostatistics. A more recent presentation of spatial statistics is found in Banerjee et al. (2004). This monograph also addresses computing intensive methods and touches upon spatiotemporal methods. Spatiotemporal methods are also addressed Andrienko and Andrienko (2006).

3 Discussion and some suggestions for future work

3.1 Digital terrain modelling and data reduction

The use of Light Detection and Ranging (LiDAR) technology for data collection is increasing. Light Detection and Ranging generates substantial amounts of point data which often serve as input for terrain model construction algorithms. However, since the available computing resources imply restrictions with respect to the number of data points which can be efficiently handled, some kind of data reduction (decimation) is usually required. To the author's knowledge no comprehensive evaluations of point data reduction methods are available. A natural extension to the investigation reported here (Paper I) would be to include grid based models as well as a wider spectre of evaluation criteria. This can for example be slope or curvature but also outputs from various terrain surface analysis algorithms such as calculation of catchment areas, drainage networks, run out areas or the extraction of structural terrain features. A key problem will be to determine how the outputs from these surface analysis algorithms are affected by different data reduction methods. Moreover, an evaluation of more sophisticated data reduction methods, in terms of using multiple criteria for point selection, could also be a useful contribution.

3.2 Statistical analysis of rock slope deformation

Displacement data from rockslide areas typically pose challenges with respect to data analysis because of their varying quality. Errors are not only due to limitations in the measuring methods and the instruments themselves. As rockslide areas usually are located in inhospitable environments, this means for example that control points may disappear or power supply and instruments may get damaged from rock falls or minor avalanches. Immediate recovery of the instruments may not be practically possible due to the usually difficult access to rockslide areas. This in turn leads to missing or erroneous observations for shorter or longer periods of time. Moreover, the instruments' exposure to weather may be completely different from summer to winter as the instruments may be covered with snow during winter. Instruments may also be reset from time to time due to maintenance. All such factors complicate data analysis

and may cause violations of the assumptions associated with the statistical methods used for analysis. For example, the use of linear regression analysis implies several assumptions, such as independent errors and constant error variance. In time series analysis and spatial data analysis, the assumption regarding independency is often not fulfilled due to autocorrelation (e.g. O'Sullivan and Unwin 2003). In general, a positively auto-correlated sample provides less information than an independent sample of same size. Assuming independent errors when positive autocorrelation is present may seriously underestimate the variance and consequently confidence regions for the estimated parameters will be too narrow. Similarly, autocorrelation will also affect the validity of hypothesis testing conducted under the assumption of independency. It is therefore important to consider the influence from autocorrelation. Autocorrelation may be a result of un-modelled effects. Thus, including such effects in the statistical models may remove the autocorrelation problem. However, in practice, observations of such additional variables may not be available. Another approach is therefore to use methods which account for the autocorrelation structure, such as Weighted Least Squares (WLS, e.g. Paper V).

Despite, or rather *because of*, the aforementioned problems on data quality, the benefits from statistical analysis should not be ignored. If statistical methods appear useless for a particular application, the alternative, using a pure deterministic or discretionally approach may even be worse since estimates may be worthless without accompanying accuracy measures. Arguably, statistical methods provide an objective basis for data analysis. Thus, results obtained from proper statistical analysis may both strengthen conclusions as well as increase the awareness of the limitations of the data in question. For example, to evaluate deviations from the expected displacements for a rock slope, the statistical properties of the observations has to be considered. Thus, a proper statistical analysis of observations from the past provides a basis to determine whether the observed deviations reflect critical changes to the rock slope.

Statistical approaches may be useful in different stages of a rockslide investigation; from the initial design of control networks and specification regarding required accuracy of instruments, through analysis of monitoring data, including quantification of the impact on displacements from controlling factors, to definition of alert thresholds for early warning systems. However, it should be emphasised that the usefulness of statistical methods is dependent on careful geoscientific evaluations of the results. Even though the results may be statistically significant they may not be significant from a geoscientific point of view.

3.2.1 Change detection using temporal LiDAR based DTMs

A pertinent question in the context of this thesis is whether airborne LIDAR based terrain models could be used for monitoring of unstable rock slopes such as those

addressed in Paper IV and Paper V. More specifically, would it be feasible to combine the terrain modeling approach reported in Paper I (TIN based DTMs) to supplement the statistical displacement analyses in Paper IV and Paper V? This question is discussed in the following section. No new analyses have been carried out; the discussion is solely based on the existing body of literature as well as on knowledge and experience from the work of this thesis. The objective here is to point to some key factors for success as well as to highlight some limitations and practical challenges which need to be coped with in order to make this a useful method for rock slopes monitoring.

In order to make use of LiDAR for rock slope monitoring a number of issues should be addressed. Some central issues are;

Filtering. In the presence of vegetation or other above-ground-objects, filtering methods are essential to obtain bald earth measurements. Filtering is thus a prerequisite for further processing as obviously only bald earth measurements should be used for comparison. The performance of the filtering method may in turn affect the accuracy of the resulting terrain model as well as the surface matching process.

Matching. In order to detect deformation between two epochs, a matching procedure is required. Surface matching is a well known problem from photogrammetry. Similar approaches are also applicable to LiDAR data and are typically employed for adjustment of adjacent scan strips. As the exact same locations are not sampled at each epoch, this means that some kind of interpolation scheme is required. This could be achieved by creating a model based on the two acquired point sets. However other approaches are also described. The method suggested in Maas (2000) and Maas (2002) avoids the error propagation associated with gridding (re-sampling) of both datasets involved in the matching process. Instead he uses linear interpolation of only one of the data sets. This is achieved by using one of the datasets as is and a TIN for linear interpolation of the other dataset such that “..matching is performed between discrete points in one patch and points derived from the corresponding TIN mesh in the other patch.” (Maas 2000).

Accuracy. Accuracy of digital terrain models is addressed in Section 2.2. The accuracy of airborne LiDAR data is specifically addressed in Maas (2002) and Hodgson and Bresnahan (2004). In particular *filtering* and *data redundancy* are important aspects with regard to accuracy of terrain models generated from LiDAR data. Filtering, i.e. the removal non ground points, is a crucial step in order to provide the necessary basis for detection of change (deformation) between two or more epochs. Furthermore, the key to achieve better accuracy is the high data density associated with LiDAR. This redundancy could be used for noise reduction such that for terrain model generation purposes, individual point samples are replaced by average values of close-by data points. Thus, a considerably better accuracy is achieved compared to the individual sample points.

Data coverage. Light Detection and Ranging data are collected at discrete locations along scan lines generating semi-random samples. Since “blind zones” may occur, data coverage may be a practical issue. Obviously, this depends on the topography and position of the air craft relative to the terrain but may also be dependent on vegetation or snow cover etc. The usefulness of LiDAR for monitoring depends, among other, on sufficient data coverage. Therefore this issue should be taken into consideration.

Discussion

A number geo-scientific studies draw on comparisons of temporal DTMs for change detection such as the estimation of volume change or displacement rates, e.g. Etzelmüller (2000); White and Wang (2002), Dewitte and Demoulin (2005); Chen et al. (2006); Dewitte et al. (2008); Lan et al. (2009). Common to these studies are that they address assessment of rather large regions using relatively coarse data resolution. Thus, this implies less stringent accuracy requirements compared to detection of centimeter or millimeter displacements at a particular, potentially unstable, rock slope. However, Terrestrial Laser Scanning (TLS) are now becoming common place for rock slope monitoring (e.g. Prokop and Panholzer 2009; Abbelán et al. 2009). Abbelán et al. (2009) point to TLS as one of the most promising surveying techniques for rockslope characterization and monitoring. As both airborne and terrestrial LIDAR rely on the same basic principles, both methods are relevant to this discussion.

There are several potential advantages of using airborne LiDAR for rock slope monitoring. One of the most attractive properties of airborne LiDAR is that it provides 3D deformations, as opposed to Satellite Aperture Radar (SAR) for instance which only provides radial changes. Moreover, the LiDAR technology enables large areas to be covered without any need for ground access such as onsite installation of equipment and reflectors. The high LiDAR point density, compared to a network of GPS receivers for instance, allows for virtually continuous determination of deformation over the entire area in question. On the other hand there is a hand full of challenges associated with airborne LiDAR, cf. the five issues mentioned above. In addition, the time resolution may be a practical limitation with respect to the intended application. For example to monitor and analyze seasonal changes (e.g. Paper V) as well as establishing the impact of controlling factors, a high resolution in time is required.

Considering the Åknes rock slope as a specific example, there may be challenges with respect to occlusions due to the high relief terrain. Moreover, vegetation and snow cover during large parts of the year may also be problematical. Similarly, changes to the surface (e.g. subsidence of scree material or minor rock falls) not reflecting the

overall displacement of the larger body of detached bedrock suggest that other monitoring methods are more suitable. Depending on the above mentioned critical issues, the attainable accuracy would probably be sufficient to detect the major displacements at Åknes (annual displacement at the decimeter level and possibly also at the centimeter level). The attainable geometric accuracy will however be inadequate for analysing the finer seasonal variation with respect to potential controlling factor such as the deformation response to precipitation or snow melt.

In general, using airborne LiDAR based DTMs for rock slope monitoring is probably more relevant as a first step towards detection of unstable slopes and to obtain initial estimates of displacement rates. The usefulness of LiDAR in this context depends on the objectives and characteristics of the slope being monitored but in general this method is considered less suitable for detailed studies or for prediction. Methods for prediction of slope failures (e.g. Crosta and Agliardi 2002) rely on continuous supply of data which is not practical with airborne LiDAR data. In addition the attainable accuracy may also be a limiting factor in this respect. However, more research is needed to determine the potential as well as the limitations of airborne LiDAR with regard to rock slope monitoring.

3.3 Geovisualization in rockslide investigations

The Åknes rockslide in western Norway were considered highly suitable for case studies as this is one of the world's most investigated rockslides (Ganerød et al. 2008). Consequently, the volume and the diversity of spatial data are considerably, as are the need for appropriate methods to facilitate and improve the extraction of useful information from the available datasets. Analyzing these data pose challenges not only due to the diversity (heterogeneity) but also the due to the complex spatial (and temporal) relations among datasets. Therefore, it was essential to make all relevant data available in a comprehensible manner in an environment suitable for data interpretation and knowledge construction (Paper II and Paper III). A crucial intermediate task was to determine the shape and location of potential basal sliding surfaces. It was considered advantageous to be able to perform the geometrical modelling of these sliding surfaces within the same visual environment displaying all relevant data at their correct spatial location.

Except from the interactive modelling of these sliding surfaces, the geovisualization part of this thesis was confined to static geometric models. However, both within geovisualization in general and particularly in a rockslide investigation context, there is a wide range of problems with dynamic nature. Such problems include real time 3D visualization of the spatio-temporal varying groundwater level, deformation and movement of rockslides and possibly the propagation of resulting tsunamis. A possible approach for addressing these dynamic visualization problems could be to

take advantage of flexible and parallel nature of current graphics hardware and to perform calculations directly on the graphics processing unit (GPU) instead of the central processing unit (CPU), e.g. Owens et al. (2007). This allows for greater flexibility and efficiency when working with dynamic visualization and simulation algorithms. As even commodity gaming graphics cards support GPU programming, this could be a viable approach for applications running on ordinary PCs. Future research could therefore focus on the potential of using programmable rendering pipelines for dynamic geovisualization problems.

At present, geovisualization is a continuously evolving field and is likely to involve a wider spectre of applications in the future. However this implies certain requirements to GI Science community as stated by Gold (2006); "...the future clearly involves more integration at a discipline level, as well as at the system design level – which requires more system, graphics and programming knowledge within the GI Science community".

Further extension of the Åknes geovisualization application

A natural extension to the work reported in Paper II and Paper III is to include visual presentation of the results obtained from the time series analyses in Paper IV, or taking it one step further; to perform these analysis within an integrated geovisual analytics environment. *Geovisual analytics* can be defined as "the science of analytical reasoning and decision-making with geospatial information, facilitated by interactive visual interfaces, computational methods, and knowledge construction, representation, and management strategies", MacEachren (2008). An important issue here is the integration of geovisualization methods and analytical or statistical methods (Andrienko et al. 2007). Some examples of efforts in this direction are found in Demšar et al. (2008) and Steed et al. (2009). Steed et al. (2009) developed a prototype of an interactive geovisual analytic system to support in cyclone data analysis. Their system facilitates visual selection of most important variables in multivariate datasets using parallel coordinates and is thus an example of an interactive integration of visual and statistical methods. Demšar et al. (2008) report a "first attempt" showing how a geovisual exploratory approach can be used to study spatially varying model coefficients. The case study reported used Geographically Weighted Regression (GWR) on a multivariate spatial dataset regarding educational attainment. Although the two above mentioned studies are not directly comparable to the Åknes geovisualization approach (Paper II and Paper III), they represent an important initiative in combining visual and analytical methods. However, one of the major challenges with regard to integration analytics is that each specific application tends to require highly specialized functionality. Challenges also remain in producing models and visualizations that clearly incorporate and display uncertainties in data or interpretation (Turner 2006).

4 Summary and conclusions

Several important aspects of spatial data handling with respect to rockslide investigations have been addressed. As the paramount objective was to take advantage of methods from spatial data handling to support in rockslide investigations, the research reported in this thesis was carried out in a cross disciplinary and highly applied context.

The first sub-topic addressed was data reduction (decimation) of topographic Light Detection and Ranging (LiDAR) data (Paper I). Data reduction is regarded as a prerequisite for further analysis including terrain modelling and interactive 3D visualization. The objective of data reduction is to reduce the amount of data whilst preserving as much as possible of the useful terrain characteristics. A comparison of various data reduction methods, concerning construction of Triangulated Irregular Networks (TIN) from point data, was conducted. The criteria used for evaluation were deviation in volume and surface area as well as the Root Mean Square (RMS) of vertical errors and the maximum vertical error. The results showed that the method using a vertical point selection threshold combined with a data dependent triangulation had the overall best performance when tested on 30 different test datasets. Results from the experiment also indicated that there is a certain level for which the approximation errors start to grow rapidly. For the test datasets, this critical level was similar for all methods being tested; about 2.5% of full datasets. However, this critical level will be highly dependent on the initial datasets (sampling density, terrain characteristics) and the intended applications of the resulting terrain models.

The next sub-topic addressed was geovisualization including interactive geometrical modelling of sliding surfaces at the Åknes rockslide in western Norway (Paper II and Paper III). Åknes is among the world's most investigated rockslides and poses many challenges with respect to the volume and diversity of the datasets involved in the investigation. The aim was therefore to utilize geovisualization as an integral part of the rockslide investigation methodology. A prototype of a geovisualization application was developed to visualize combinations of various geoscientific datasets at their correct spatial location as well as to support interactive geometric modelling of sliding surfaces inferred from (subsurface) data. The geometries of the sliding surfaces are essential for stability analyses of the rock slope as well as for the volume estimation of the unstable rock mass. The geovisualization application was based on the open source graphics application programming interface (API) OpenSceneGraph (OSG). This geovisualization application enabled geoscientists to propose different potential sliding scenarios based on different interpretations of the available data. The outcome comprises volume and area estimates corresponding to the different

scenarios as well as the geometries for the all-important basal sliding surfaces. A scenario having a basal sliding surface located at a depth of 105m to 115m below the topographic surface, with a volume of unstable rock mass of 43 million m³, was considered as the most realistic.

The last sub-topic addressed was statistical analysis of surface displacement data. A proper statistical approach for analyzing different displacement data from the Åknes rockslide site was described in Paper IV. These analyses paid special attention to time series from GPS and extensometer measurements. The estimated annual displacement rates, obtained from linear regression analysis, ranged from a few millimetres to about 8 centimetres. Moreover, to establish and quantify periodic variations in displacement rates, spectral analysis (Fourier analysis) was used. The periodic variations typically showed maximum amplitudes of about 1 to 2 millimetres. Annual and semi-annual fluctuations were established for some of the control points, whereas the time series for other control points suggested long-length periodic variation which could not be reliably established from the currently available time series. The annual and semi-annual variations were most likely caused by increased precipitation in autumn and snow melt in spring as well as the resulting changes in groundwater level. High correlations between the groundwater level and displacements measured across the back scarp were established.

Analysis of laser and crackmeter measurements at the Nordnes rockslide (northern Norway) was reported in Paper V. The main objective of this analysis was to obtain accurate estimates for the displacement rates as well as to gain better insight into the sliding processes. All ten crackmeters showed statistically significant displacements whereas two out of the three lasers showed statistically significant displacements. The estimated displacement for the north-westernmost part of the unstable rock slope was more than 5 cm per year, which makes this part the most critical in terms of generation of a rapid rockslide. Results from the analysis of crackmeter measurements suggested that the opening of large fractures in the upper part of the slope is compensated by compression of cracks in lower parts of the slope. Although the temperature changes clearly affect the deformation of the slope, the seasonal fluctuations in displacement rates could not be fully explained by temperature terms in the regression models, suggesting that there are additional factors which contribute to the seasonal fluctuations. Based on the current time series, prediction intervals for future observations were derived. These prediction intervals are considered useful for the evaluation of future observations and may also be used as a basis for defining alert thresholds for a possible early warning system.

The approaches and methodology reported in this thesis have proven to be successful to investigations of large rockslides, and thus assumed to be useful for other rockslide investigations. This thesis is, therefore, regarded as a contribution to the general rockslide investigation methodology.

References

- Abellán A., Jaboyedoff M., Oppikofer T. and Vilaplana J. M. (2009). Detection of millimetric deformation using a terrestrial laser scanner: experiment and application to a rockfall event, *Natural Hazards and Earth System Sciences*, 9, 365-372.
- Andrienko G., Jern M., Dykes J., Fabrikant S. and Weaver C. (2007). Panel Session gIV07, Geovisualization and synergies from InfoVis and Visual Analytics, 11th International Conference Information Visualization (IV'07).
- Andrienko N. and Andrienko G. (2006). *Exploratory analysis of spatial and temporal data: a systematic approach*, Springer.
- Angel E. (2006). *Interactive Computer Graphics 4th ed.*, Pearson Education Inc., USA.
- Balmelli L., Liebling T. and Vetterli M. (2003). Computational analysis of mesh simplification using global error, *Computational Geometry*, 25, 171-196.
- Banerjee S., Carlin B.P. and Gelfand A.E. (2004). *Hierarchical modelling and analysis for spatial data*, Monographs on statistics and applied probability 101, Chapman & Hall.
- Bjørke J.T. and Nilsen S. (2002). Efficient representation of digital terrain models: compression and spatial decorrelation techniques, *Computers & Geosciences* 28, 433-445.
- Bjørke J.T. and Nilsen S. (2003). Wavelets applied to simplification of digital terrain models, *Int. J. Geographical Information Science*, 17 (7), 601-621.
- Bjørke J.T. and Nilsen S. (2008). Derivation of quality parameters for terrain models, *Visualization technical*, PositionIT July/August 2008, 58-59.
- Bóo M., Amor M. and Döllner J. (2007). Unified Hybrid Terrain Representation Based on Local Convexifications, *Geoinformatica*, 11, 331-357.
- Carlisle B.H. (2005). Modelling the Spatial Distribution of DEM Error, *Transactions in GIS*, 9 (4), 521-540.
- Caumon G. Collon-Drouaillet P., Le Carlier de Veslud C., Viseur S. and Sausse J. (2009). Surface-Based 3D Modeling of Geological Structures, *Mathematical Geosciences*, 41 (8), 927-945, DOI: 10.1007/s11004-009-9244-2.
- Chen R.-F., Chang K.-J., Angelier J., Chan Y.-C., Deffontaines B., Lee C.-T. and Lin M.-L. (2006). Topographical changes revealed by high-resolution airborne LiDAR data: The 1999 Tsaoiling landslide induced by the Chi-Chi earthquake, *Engineering Geology*, 88, 160-172.

- Chrisman, N. R. (1984). The role of quality information in the long-term functioning of a geographic information system, *Cartographica*, 21, 79-87.
- Cline D. and Egbert P.K. (2001). Terrain decimation through quadtree morphing, *IEEE Transactions on Visualization and Computer Graphics*, 7 (1), 62-69.
- Cressie N.A.C. (1993). *Statistics for Spatial Data*, John Wiley & Sons, USA.
- Crosta G.B. and Agliardi F. (2002). How to obtain alert thresholds for large rockslides, *Physics and Chemistry of the Earth*, 27, 1557-1565.
- Danovaro E., De Floriani L., Magillo P., Puppo E. and Sobrero D. (2006). Level-of-detail for data analysis and exploration: A historical overview and some new perspectives, *Computers & Graphics*, 30, 334-344.
- De Floriani L. and Puppo E. (1995). Hierarchical triangulation for multiresolution surface description, *ACM Transactions on Graphics*, 14 (4), 363-411.
- Delaunay B. (1934). Surla sphere vide, *Bull Acad Sci USSR*, 7, 793-800.
- Demšar U., Fotheringham A.S. and Charlton M. (2008). Combining Geovisual Analytics with Spatial Statistics: the Example of Geographically Weighted Regression, *Geovisualisation Special Issue*, August 2008, *The Cartographic Journal*, 45 (3), 182-192.
- Dewitte O. and Demoulin A. (2005). Morphometry and kinematics of landslides inferred from precise DTMs in West Belgium, *Natural Hazards and Earth System Sciences*, 5, 259-265.
- Dewitte O., Jasselette J.-C., Cornet Y., Van Den Eeckhaut M., Collignon A., Poesen J. and Demoulin A. (2008). Tracking landslide displacements by multi-temporal DTMs: A combined stereophotogrammetric and LIDAR approach in Western Belgium, *Engineering Geology*, 99, 11- 22.
- Dykes J., MacEachren A.M. and Kraak M.-J. (eds.) (2005). *Exploring Geovisualization*, Elsevier Amsterdam, The Netherlands.
- Etzelmüller B. (2000). On the Quantification of Surface Changes using Grid-based Digital Elevation Models (DEMs), *Transactions in GIS*, 4 (2), 129-143.
- Franklin W.R., Tracy D.M., Andrade M.A., Muckell J., Inanc M., Xie Z. and Cutle B.M. (2008). Slope Accuracy and Path Planning on Compressed Terrain, In: Ruas A. and Gold C. (eds.). *Headway in Spatial Data Handling*, Proceedings of the 13th International Symposium on Spatial Data Handling, Springer, 335-349.

Ganerød G.V., Grøneng G., Rønning J.S., Dalsegg E., Elvebakk H., Tønnesen J.F., Kveldsvik V., Eiken T., Blikra L.H. and Braathen A. (2008). Geological model of the Åknes rockslide, western Norway, *Engineering Geology*, 102 (1), 1-18.

Gold C.M. (2006). What is GIS and What is Not?, *Transactions in GIS*, 10 (4), 505–519.

Grøneng G. (2010). Stability Analyses of the Åknes Rock Slope, Western Norway, Doctoral thesis at Norwegian University of Science and Technology, ISBN 978-82-471-2014-9.

Haakonsen T.A. (2005). Temporal and Spatial Analyses of Continuous GPS Observations, Doctoral theses at NTNU, 2005:171, ISBN 82-471-7230-5 (electronic version).

Heller M. (1990). Triangulation algorithms for adaptive terrain modelling, *Proceedings of Fourth International Symposium on Spatial Data Handling*, International Geographical Union, Zurich, 163-174.

Henderson et al. (Manuscript in preparation for Landslides), Working title: Integrated study of the Nordnesfjellet potential rockslide, Troms County, north Norway.

Hern D. and Baker M. P. (2004). *Computer Graphics with OpenGL*, 3rd ed., Pearson Prentice Hall, USA.

Hodgson M.E. and Bresnahan P. (2004). Accuracy of Airborne LiDAR-Derived Elevation: Empirical Assessment and Error Budget, *Photogrammetric Engineering & Remote Sensing*, 70 (3), 331-339.

Höhle J. and Höhle M. (2009). Accuracy assessment of digital elevation models by means of robust statistical methods, *ISPRS Journal of Photogrammetry and Remote Sensing*, 64, 398-406.

Hunter G.J. and Goodchild M.F. (1997). Modeling the Uncertainty of Slope and Aspect Estimates derived from Spatial Databases, *Geographical Analysis*, 29 (1), 35-49.

Johnson R.A. and Wichern D.W. (2002). *Applied Multivariate Statistical Analysis*, 5th ed., Prentice Hall, USA.

Jones R.R., McCaffrey K.J.W., Clegg P., Wilson R.W., Holliman N.S., Holdsworth R.E., Imber J. and Waggott S. (2009). Integration of regional to outcrop digital data: 3D visualization of multi-scale geological models, *Computers & Geosciences*, 35, 4-18.

Kaufmann O. and Martin T. (2008). 3D geological modelling from boreholes, cross-sections and geological maps, application over former natural gas storages in coal mines, *Computers & Geosciences*, 34 (3), 278-290.

Koch K.-R. (1999). *Parameter Estimation and Hypothesis Testing in Linear Models*, 2nd ed., Springer-Verlag, Germany.

Kraus K., Briese C., Attwenger M. and Pfeifer N. (2004). Quality measures for digital terrain models, XXth ISPRS Congress Istanbul, Commission II, Vol. XXXV, part B2, p. 113 ff.

Kumler M.P. (1994). An intensive Comparison of Triangulated Irregular Networks and Digital Elevation Models, *Cartographica*, Monograph 45, 31 (2).

Kveldsvik V. (2008). Static and dynamic stability analyses of the 800m high Åknes rock slope, western Norway. Doctoral theses at NTNU, 2008:128, ISBN 978-82-471-8608-4.

Lan Q., Fei L. Liu Y. and Zhang K. (2009). Application of multi-temporal DEM data in calculating the earth's surface deformation, *Proceedings of SPIE - The International Society for Optical Engineering*, v 7492, International Symposium on Spatial Analysis, Spatial-Temporal Data Modeling, and Data Mining, DOI: 10.1117/12.837926.

Li Z., Zhu Q. and Gold C. (2005). *Digital Terrain Modelling – Principles and Methodology*, CRC Press, USA.

Maas H.G. (2000). Least-Squares Matching with Airborne Laserscanning Data in a TIN Structure, *International Archives of Photogrammetry and Remote Sensing*. Vol. XXXIII, Part B3. Amsterdam 2000.

Maas H.G. (2002). Methods for Measuring Height and Planimetry Discrepancies in Airborne Laserscanner Data, *Photogrammetric Engineering & Remote Sensing*, 68 (9), 933-940.

MacEachren A.M. and Davidson J.V. (1987). Sampling and Isometric Mapping of Continuous Geographic Surfaces, *The American Cartographer*, 14 (4), 299-320.

MacEachren A.M. (2008). (Invited paper on Geovisual Analytics, Information Visualization.)

Mark D. (1975). Geomorphic parameters: a review and evaluation. *Geografiska Annaler*, 57A, 165-177.

Mark D. (1997). The History of Geographic Information Systems: Invention and Re-invention of Triangulated Irregular Networks (TINs), *Proceedings, GIS/LIS'97*, Accessed from URL: <http://www.ncgia.buffalo.edu/gishist/GISLIS97.html> 14 August 2010.

Martinoni D. and Bernhard L. (1998). A conceptual framework for reliable digital terrain modeling, In: *Proceedings of the 8th Symposium on Spatial Data Handling*, Vancouver, 737-750.

- Martz P. (2007). OpenSceneGraph Quick Start Guide, Skew Matrix Software, USA.
- Midtbø T. (1993). Spatial Modelling by Delaunay Networks of Two and Three Dimensions, Doctoral thesis at Norwegian Institute of Technology.
- Miller A. (2002). Subset selection in regression, 2nd edition, Chapman & Hall/CRC.
- Miller C. and Laflamme R. (1958). The digital terrain model – theory and applications, *Photogrammetric Engineering*, 24, 433-442.
- Miller I. and Miller M. (1999). John E. Freud's Mathematical Statistics, 6th ed., Prentice Hall, USA.
- Montgomery D.C., Peck E.A. and Vining G.G. (2001). Introduction to Linear Regression Analysis, John Wiley & Sons, USA.
- Oksanen J. and Sarjakoski T. (2005). Error propagation of DEM-based surface derivatives, *Computers & Geosciences*, 31, 1015-1027.
- O'Sullivan D. and Unwin D.J. (2003). Geographic Information Analysis, John Wiley & Sons, USA.
- Owens J.D., Luebke D., Govindaraju N., Harris M., Lefohn A.E. and Purcell T.J. (2007). A Survey of General-Purpose Computations on Graphics Hardware, *Computer Graphics Forum*, 26, 80-113.
- Pedrini, H. (2001). An improved refinement and decimation method for adaptive terrain surface approximation, In: Conference proceedings of the 8th International Conference in Central Europe on Computer Graphics, Visualization and Computer Vision.
- Podobnikar T., Stancic Z. and Oštir K. (2000). Data integration for the DTM production, ISPRS WG VI/3 and IV/3 meeting, Ljubljana, Slovenia, 2-5 February 2000.
- Pradhan B., Mansor S., Ramli A.R., Sharif A.R.B.M. and Sandeep K. (2005). LIDAR data compression using wavelets, Remote Sensing for Environmental Monitoring, GIS Applications, and Geology V, In: Ehlers M. and Michel U. (eds.), *Proceedings of SPIE Vol. 5983*, 598305, DOI: 10.1117/12.626579.
- Prokop A. and Panholzer H. (2009). Assessing the capability of terrestrial laser scanning for monitoring slow moving landslides, *Natural Hazards and Earth System Sciences*, 9, 1921-1928.
- Reiners D. (2002). Scene Graph Rendering, OpenSG Forum, Accessed from URL: <http://oldsite.vrjuggler.org/pub/scenegraph-rendering.ieeevr2002.pdf> 6 May 2009.

Samet H. (1990). *The Design and Analysis of Spatial Data Structures*, Addison Wesley, USA.

Shumway R.H. and Stoffer D.S. (2000). *Time Series Analysis and Its Applications*, Springer, USA.

Sithole G. and Vosselman G. (2004). Experimental comparison of filter algorithms for bare-Earth extraction from airborne laser scanning point clouds, *ISPRS Journal of Photogrammetry and Remote Sensing*, 59, 85-101.

Skrednett (2009). (National web database for landslides in Norway, hosted by the Geological Survey of Norway), URL: www.skrednett.no, cited 19 April 2009.

Staneker D. (2005). *Hardware-assisted Occlusion Culling for Scene Graph Systems*, Doctoral dissertation at the Eberhard Karls Universität Tübingen, Germany.

Steed C.A., Fitzpatrick P.J., Swan II J.E. and Jankun-Kelly T.J. (2009). Tropical Cyclone Trend Analysis Using Enhanced Parallel Coordinates and Statistical Analytics, *Cartography and Geographic Information Science*, 36 (3), 251-265.

Stuetzle C., Franklin W.R. and Cutler B. (2009). Evaluating hydrology preservation of simplified terrain representations, *SIGSPATIAL Special*, 1 (1), 51-56.

Turner A.K. (2006). Challenges and trends for geologic modelling and visualization, *Bulletin of Engineering Geology and the Environment*, 65, 109–127, DOI: 10.1007/s10064-005-0015-0.

Wei W.W.S. (1990). *Time series analysis: univariate and multivariate methods*, Addison-Wesley.

White S.A. and Wang Y. (2003). Utilizing DEMs derived from LIDAR data to analyze morphologic change in the North Carolina coastline, *Remote Sensing of Environment*, 85, 39-47.

Wikipedia (2010), *Wikipedia – The Free Encyclopedia*, URL: <http://en.wikipedia.org/wiki/P-value>, cited 26 April 2010.

Wilson J.P. and Gallant J. (eds.) (2000). *Terrain Analysis: Principles and Applications*. John Wiley & Sons, USA.

Wu Q., Xu H. and Zou X. (2005). An effective method for 3D geological modeling with multi-source data integration, *Computers & Geosciences*, 31(1), 35-43.

Yang B., Shi W. and Li Q. (2005). A Dynamic Method for Generating Multi-Resolution TIN Models, *Photogrammetric Engineering & Remote Sensing*, 71 (8), 917-926.

Zanchi A., Francesca S., Stefano Z., Simone S. and Graziano G. (2009). 3D reconstruction of complex geological bodies: Examples from the Alps, *Computers & Geosciences*, 35 (1), 49-69.

Paper I

Nordvik T. and Midtbø T. (2007). Application of Data Reduction Methods in Dynamic TIN Models to Topographic LIDAR Data. In: Bjørke and Tveite (eds.): *Proceedings of the 11th Scandinavian Research Conference on Geographical Information Science*, Print: Rotator SiÅs, ISBN 978-82-7636-020-2, p. 111-128.

Paper II

Nordvik T. and Harding C. (2008). Interactive geovisualization and geometric modelling of 3D data – a case study from the Åknes rockslide site, Norway. In: Ruas and Gold (eds.), *Headway in Spatial Data Handling*, 13th International Symposium on Spatial Data Handling, Series: Lecture Notes in Geoinformation and Cartography, Springer, ISBN 978-3-540-68565-4, p. 367-384.

Paper III

Nordvik T., Grøneng G., Ganerød G.V., Nilsen B., Harding C. and Blikra L.H. (2009). Geovisualization, geometric modelling and volume estimation of the Åknes rockslide, Western Norway, *Bulletin of Engineering Geology and the Environment*, 68 (2), 245-256, DOI: 10.1007/s10064-009-0198-x.

Paper IV

Nordvik T. and Nyrnes E. (2009). Statistical analysis of surface displacements – an example from the Åknes rockslide, western Norway, *Natural Hazards and Earth System Sciences*, 9, 713-724, DOI: 10.5194/nhess-9-713-2009.

Paper V

Nordvik T., Blikra L.H., Nyrnes E. and Derron M.H. (2010). Statistical analysis of seasonal displacements at the Nordnes rockslide, northern Norway, *Engineering Geology*, 114, 228 -237, DOI: 10.1016/j.enggeo.2010.04.019.

Appendix: Papers

Paper I

Application of Data Reduction Methods in Dynamic TIN Models to Topographic LIDAR Data

Trond Nordvik¹ and Terje Midtbø²

Division of Geomatics, Department of Civil and Transport Engineering, Norwegian
University of Science and Technology,
Høgskoleringen 7A, N-7491 Trondheim, Norway

¹Trond.Nordvik@ntnu.no

²Terje.Midtbo@geomatikk.ntnu.no

Abstract. Comparisons of five data reduction methods associated with dynamic TIN models were conducted. All methods were applied to real world Light Detection and Ranging (LIDAR) topographic data. Data reduction is based on point selection by thresholding in dynamic Delaunay triangulation together with random point selection. The triangulation criteria used include Delaunay and hybrids of Delaunay and data dependent triangulation. The performance of the various reduction methods was evaluated by means of surface area, volume, RMS of vertical errors and maximum vertical errors. All methods were evaluated for five levels of reduction; 10%, 5%, 2.5%, 1% and 0.5% of full datasets.

1 Introduction

Although the processing capacity of desktop computers are continually increasing, the large data volumes generated by some data collection technologies such as Light Detection and Ranging (LIDAR), are posing a big challenge when it comes to processing, including spatial analyses and visualization. This makes a need for efficient data reduction methods. The objective of a data reduction method is to reduce the amount of data and at the same time preserve as much as possible of the useful information. A wide range of data reduction methods associated with polygon meshes are reported in the literature. However two main approaches for data reduction can be identified. The first main approach starts with a full model containing all data points and excludes the less significant points which are deemed redundant at the chosen level of decimation. The other main approach starts with a course mesh of some key points and successively adds data points which are deemed significant.

Examples of the first approach include the surface simplification method suggested by Schröder and Roßbach [1]. This method initially generates a high resolution TIN representing the given surface and then repeatedly reduces the number of points in this mesh. The criterion which is used to assess the significance of a point calculates a measure of the roughness of the terrain at that point. When the roughness value of a

point indicates that it can be removed from the mesh without affecting the overall representation significantly, the area around the removed point is retriangulated. The simplification algorithm proposed by Garland and Heckbert [2] is based on contraction of vertex pairs in a full model. Also Demaret et al [3] used an approach based on successive removal of points from a full model.

Examples of the second approach include adaptive triangular mesh (ATM) filtering proposed by Heller [4]. This approach can be considered as a conceptual equivalent to the Douglas-Peucker (DP) approach for lines. The triangulation starts with a few initial points. Depending on the vertical distance to the current triangular mesh, new points are added to the triangulation until no relevant points remain. Also Bottelier et al [5] use a combination of a “DP”-like algorithm and thresholding in a dynamic TIN model for near real time decimation of high density echo sounder data. This latter approach is by far more favourable from a processing demand point of view and the methods which are to be evaluated in this paper fall under this approach.

The performance of data reduction methods can be evaluated in terms of various criteria such approximation errors and processing time. Garland and Heckbert [2] used error quadratics for the triangle planes joined at each vertex as a measure of approximation error. Demaret et al [3] used CPU time and maximum approximation error as evaluation criteria. Anderson et al [6] compared deviation in mean and standard deviation from full datasets to reduced datasets. Choice of criteria is highly application dependent. In visualization applications for example, one of the most important properties to preserve is the surface normal vectors Diebel et al [7]. In this study the class of polygonal meshes dealt with is confined to the Triangular Irregular Networks (TINs). The TIN model represents a surface as a set of contiguous non-overlapping irregularly shaped triangular facets. A TIN model can be regarded both as a terrain model as well as a data structure. It is a model because the space-filling triangular planar facets determine a value for the surface everywhere, but it also has a specific structure in which the points, triangles and topologies are stored [8]. The most common types of TIN models are Delaunay triangulations but also data dependent triangulations are well established.

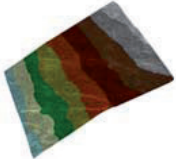


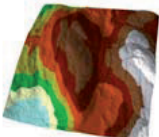
In order to discuss the advantages and disadvantages of TIN models it is natural to introduce grid models or digital elevation models (DEMs) as a reference. A DEM consists of a regular mesh of, usually square, cells. The TIN and DEM approaches are by far the most common types of terrain models. In general the TIN model is more complex with respect to algorithms and data structures and, dependent on implementation, may require more memory storage than a DEM. These are the main disadvantages of the TIN models. On the other hand the TIN model easily allow for variable resolution depending on topography. TIN can represent morphology directly and better than grid-based models, since they allow placing vertices at arbitrary positions, and embedding arbitrary poly-lines among their edges [9]. Also, using the sampled points directly and avoid the “gridding” process yield a more precise representation of a topographic surface as the introduction of errors associated with the “gridding” process are avoided. With this respect one can say that a TIN model is a model that fits the data and not vice versa. Moreover, many graphics systems are optimized for rendering triangles.

Comparison of data reduction methods in TIN models on real world topographic data has not gained too much attention in the literature. However, some research has been done e.g. Demaret et al [3]. The objective of the research reported in this paper is to quantify the performance of some data reduction methods on real world data. Five different data reduction methods; random subset, and two types of threshold in dynamic Delaunay triangulation, each combined with a final data dependent edge swap pass, have been applied to LIDAR topographic data. A common feature of all data reduction methods evaluated in this study is that they provide a subset of the full dataset by selection of points.

1.1 Description of Data

Analyses carried out in this study are based on data collected with airborne LIDAR. For a general description of the LIDAR technology, see for example Baltsavis [10] and the references therein. Technical specifications of the particular LIDAR system “Optech Airborne Laser Terrain Mapper (ALTM3100C)” used for data collection of this study can be obtained from [11]. The LIDAR data comprise point measurements; x-, y- and z-coordinates together with the intensity of the reflected signal. The background for this scan campaign is landslide hazard assessment. The area covered in this scan is along the fjord system of inner Storfjorden in Møre and Romsdal County, Norway. It covers nearly 600 square km, mostly steep hillsides from fjord to mountain. From this total area, 32 datasets each covering a square area of 1km by 1km, are selected as test datasets for this study. Data are pre-processed by the contractor and thus assumed to only contain bald earth measurement with no gross errors present. The point density of the test datasets ranges from 0.41 to 1.53 points per square meters with an average of 0.82 points per square metre. Some of the test areas have somewhat variable point density particularly where there is overlapping between two or more adjacent stripes. The difference of elevation from the highest to the lowest point within a single dataset varies from about 250 meters to about 1200 meters. In order to assess the performance of the data reduction methods on different topographies, the 32 test datasets were discretionary categorized into four categories. These categories are; “Hilly”, “Hillside”, “Ridge/Peak” and “Valley/Pit”. See Table 1 for a description of the categories and to see a sample of each category.

Table 1. Terrain categories. First row lists the category names, second row lists the category descriptions, third row provides an example of a representative dataset for the actual category.

"Hillside"	"Ridge/Peak"	"Valley/Pit"	"Hilly"
comprises planar slopes when the micro topography is disregarded	comprises concave terrain surfaces when the micro topography is disregarded	comprises convex terrain surfaces when the micro topography is disregarded	comprises broken and undulating terrain that does not fit into any of the other categories
			

2 Implementation and Calculations

2.1 Experiment

Five data reduction methods; RD, PD, PH, VD and VH (see Table 2 for details) were applied to 32 test datasets. Each dataset covers a square area of one by one kilometre with an average of 820.000 points per square kilometre. In order to evaluate the approximation errors of the various methods some criteria were chosen; surface area, volume, root mean square (RMS) of vertical residuals, mean of vertical residuals and maximum vertical residuals. Vertical residuals are calculated as the difference between the measured values of the control points and the corresponding interpolated values from the TIN surfaces. Since there was no accurate control measurements available the omitted points were used as control points. Surface area and volume calculations obtained from the reduced datasets are compared with those obtained from the corresponding full datasets. All methods were evaluated for five levels of reduction; 10%, 5%, 2.5%, 1% and 0.5% of full dataset.

Table 2. Specification of data reduction methods. A hybrid triangulation criterion means that the final Delaunay triangulation is modified by a data dependent edge swap pass. The embraced texts specify the data dependent swap criteria

Name	Point selection criterion	Triangulation criterion
RD	Random	Delaunay
PD	Perpendicular threshold	Delaunay
PH	Perpendicular threshold	Hybrid of Delaunay and data dep. (minimize vertical RMS)
VD	Vertical threshold	Delaunay
VH	Vertical threshold	Hybrid of Delaunay and data dep. (minimize max vertical error)

2.2 Description of TIN Data Structures and Algorithms

For the investigation reported in this paper a dynamic Delaunay triangulation algorithm was used as a basis. The dynamic algorithm starts with a course mesh of key points and allow for addition and removal of points during the triangulation process. See Midtbø [12] for a thorough description of data structures and algorithms for dynamic Delaunay triangulations. This basis algorithm was extended with functionality to accommodate the comparison study. Microsoft Visual Studio and C++ were used for the implementation. A twin edge data structure, proposed by Heller [4] makes up the backbone of the triangulation. All information about the triangles is implicitly stored in the edges and consequently no triangle table is required. However, to facilitate the triangle by triangle calculations needed for this study a triangle table was considered as a convenient extension. The topology of the network is maintained by pointers between edges (Figure 1).

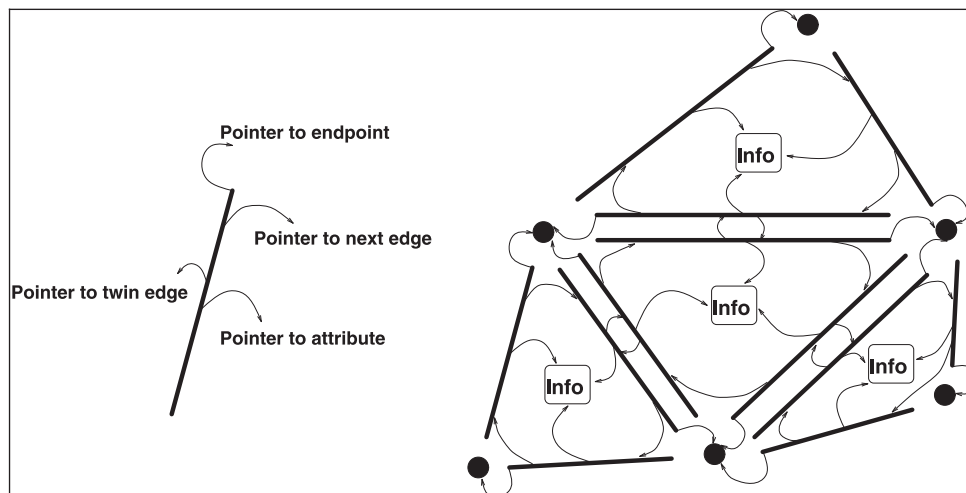


Figure 1. Twin-edge data structure (figure copied from [12])

Initially, a triangulation of the corner points of a circumscribing rectangle of the dataset is chosen as approximation mesh. The height of these initial auxiliary vertices is arbitrary set to -300 meters, which results in selecting the points with largest elevation as the first inserted point in each of the two initial triangles. When a new point is inserted into the network the enclosing triangle of the current point is split into three new triangles and the data structure is updated accordingly, see Figure 2.

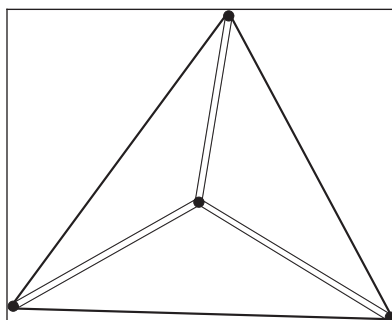


Figure 2. Insertion of a new point. The centre point is inserted and 6 new edges are added to the network (figure copied from [12])

In order to maintain the Delaunay criterion when a new point is inserted, a recursive edge swap procedure is applied if the criterion is not met. Extension to data dependent edge swap is a minor adaptation of the existing Delaunay triangulation framework. The following pseudo code outlines the idea:

Pseudocode for data dependent edge swap

```

for each edge[i] element of Delaunay triangulation
    if( isSwapable(edge[i]))
        if( getCostCur(edge[i]) > getCostAlt(edge[i]))
            swapEdge(edge[i])
  
```

The `isSwapable` function is needed since not all quadrangles are convex and will therefore not generate consistent triangles when the diagonal is interchanged, match Figure 3.

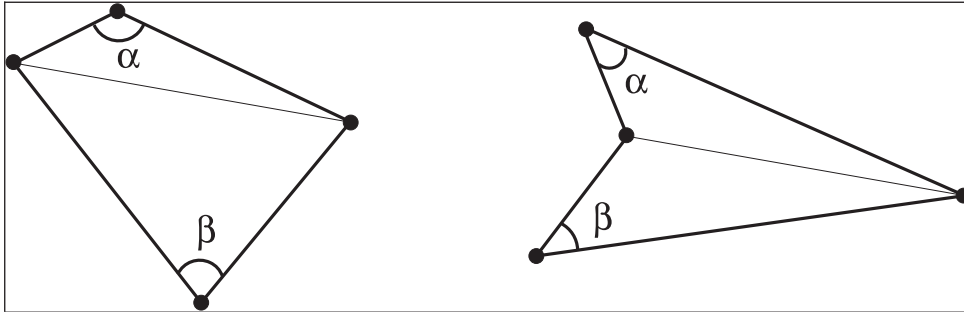


Figure 3. Quadrangles. The left quadrangle is convex and the diagonal is swappable. The right quadrangle is concave and the diagonal is not swappable (figure copied from [12])

The two functions `getCostCur` and `getCostAlt` calculate the costs associated with the two alternative configurations of the diagonal. The cost functions in case of method VH is maximum vertical residual. This will preserve the most useful property of the vertical distance method; that is to control the maximum vertical residual. The cost function in case of method PH is RMS. The `swapEdge` function performs the interchange of diagonal and updates the data structures.

2.3 Selection of Data Point

For the random selection criteria each data point is included in the TIN model with a probability p . For the vertical distance criterion, the point with maximum vertical distance from existing TIN surface is inserted into the triangulation, given that the distance is larger than some specified threshold (Figure 4). The procedure for the perpendicular criterion is identical to the vertical distance criterion, except that the vertical distance from the existing triangle plane is replaced by the perpendicular distance. Selecting the point with the largest perpendicular distance to the existing triangle plane corresponds to selecting the point having the most influence on volume for the splitting of this triangle. The point with the largest perpendicular distance forms the apex of an imaginary tetrahedron with the existing triangle plane as the base. Thus, this point is the one with the largest impact on volume. Both the vertical and the perpendicular distance criteria are combined with a final edge swap pass.

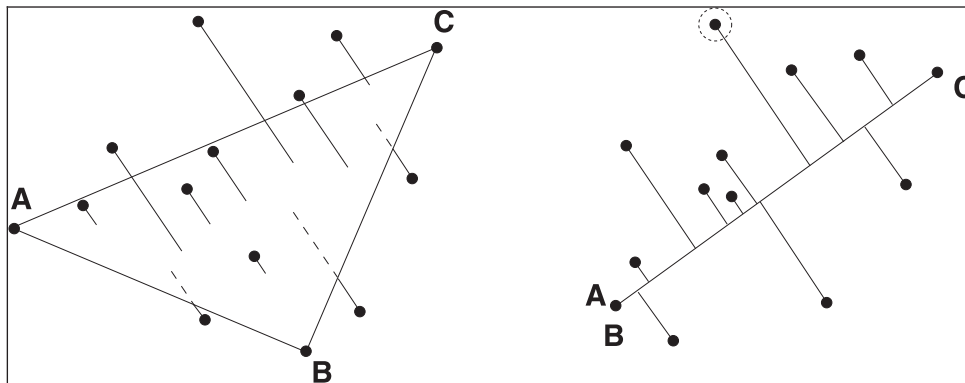


Figure 4. Point selection. The most distant point from the triangle plane will be inserted into the triangulation given that this distance is above some specified threshold (figure copied from [12])

2.4 Evaluation Criteria

In order to evaluate the approximation errors of the various methods some criteria were chosen; surface area, volume, root mean square (RMS) of vertical residuals¹, mean of vertical residuals and maximum vertical residuals. Surface area calculations and volume calculations obtained from the reduced datasets are compared with those obtained from the corresponding full datasets. Vertical residuals are calculated as the difference between the measured values of the control points and the corresponding interpolated values from the TIN surfaces (3). The omitted data points are used as control points. To avoid boundary effects, such as removing points which belong to the convex hull of the point set, a considerable larger area than the “clipping window” (i.e. the square area of 1 by 1km) is subject to data reduction. This buffer zone is 200 metres. The effect of data reduction on the selected criteria is then evaluated only for the area inside the clipping window. The vast majority of all triangles are either completely outside or completely inside the square clipping window. These two groups are pointed out by integer tests concerning coordinate extent since the clipping windows are axis aligned. The remaining triangles can possibly intersect with the clipping window and if they do intersect, the output can in principle range from triangles to heptagons (seven-sided polygons) depending on the actual configuration of the input triangle and the clipping window. The clipping of this group of triangles are handled by a “Sutherland-Hodgman” polygon clipping algorithm (see for example [13]). Nevertheless all triangles clipped by the square window will become convex polygons. The convex property makes it straight forward to split polygons into triangles and the same framework for calculations of evaluation parameters can be applied to all triangles. The TIN model is used for calculation of all evaluation criteria. Surface area of each individual triangle is calculated by (1) and then summarized for

¹ In this paper both *residual* and *error* refer to the same i.e. deviation from full model.

all triangles to get the total surface area within the clipping window. The volume of a single tri-prism is calculated by (2) and the total volume is obtained by summarizing the volume of each individual tri-prism.

$$SA(\Delta) = \frac{1}{2} |\bar{a} \times \bar{b}|, \text{ where } \bar{a} \text{ and } \bar{b} \text{ are vectors that span the triangle facet.} \quad (1)$$

$$V(\Delta) = A(\Delta) \frac{(z_1 + z_2 + z_3)}{3}, \text{ where } A(\Delta) \text{ denotes the horizontal triangle area.} \quad (2)$$

$$z(x, y) = \frac{-ax - by - d}{c}, \text{ where } a, b, c \text{ and } d \text{ are calculated from the enclosing triangle.} \quad (3)$$

3 Results and Discussion

A large number of circumstances will affect the construction of a TIN model and consequently the derived parameters. Examples of factors influencing the results include; selection of initial points for triangulation, handling of degenerated cases, order of point insertion etc. Limited testing shows that some of these factors are inferior to others. However this problem will not be addressed in this study. In this study all factors not related to the test datasets it selves are hold constant. Selection of evaluation criteria is highly application dependent. This study has assessment of slide hazard in mind; volume calculations are of course essential to slide assessment and the ratio of surface area to projection area can serve as a simple measure of terrain roughness. The vertical residuals provide a more general measure of approximation quality. A more advanced interpolation technique such as Kriging would probably lead to better results with respect to interpolated height values but the intention is to give an idea of how well the TIN surface itself approximates the topographic surface.

Figure 5 shows the average difference in surface area together with the associated standard deviations. The hypotheses of interest in connection with surface area can be stated as follows:

H_0 : All methods have the same means within each level of reduction

H_1 : At least one of the methods has, for at least one level of reduction, a different mean than the other methods

In order to test these hypotheses, they are split into hypotheses regarding pair of methods. Thus the testing can be carried out by means of a number of paired Student's t-tests (t-tests). Two conditions are required for a paired t-test; 1) Each pair of observations is statistically independent from the other pair of observations 2) The differences between each pair of observations are approximately normally distributed. The first condition is assumed to be fulfilled since there is no overlap between the 32

test datasets. According to histogram plots of the pair differences there are no indications of severe violations of the latter condition. These paired t-tests will involve all possible pair combinations of the five methods, i.e. first RD is tested against PD (for each level of reduction) than RD is tested against PH and so forth. The sub hypotheses are as follows:

$H_0: \mu_i = \mu_j$ (method i has the same mean as method j for reduction level k)

$H_1: \mu_i > \mu_j$ or $\mu_i < \mu_j$ (method i has a larger/smaller mean than method j for reduction level k)

where $i \in \{1..5\}, j \in \{1..5\}, k \in \{1..5\}, i \neq j$

The calculated difference value of the actual pair determines whether it should be a “less than” or a “greater than” test, thus the H_1 hypotheses are one sided. Testing of the two latter hypotheses is separately conducted for each level of reduction, i.e. for 10%, 5%, 2.5%, 1% and 0.5% of full dataset. The testing is carried out with a significance level of 5% and 31 degrees of freedom. All five methods have significantly different mean values for every level of reduction. The mutual order of mean values are $PH > VH > PD > VD > RD$ as suggested by Figure 5. Moreover, there is also an evident trend common to all methods; less data gives lower surface area. This is expected since a decrease in number of surface points will cause some smoothing of the finer topography, as well as a reduction in the random noise which also makes a significant contribution to surface area.

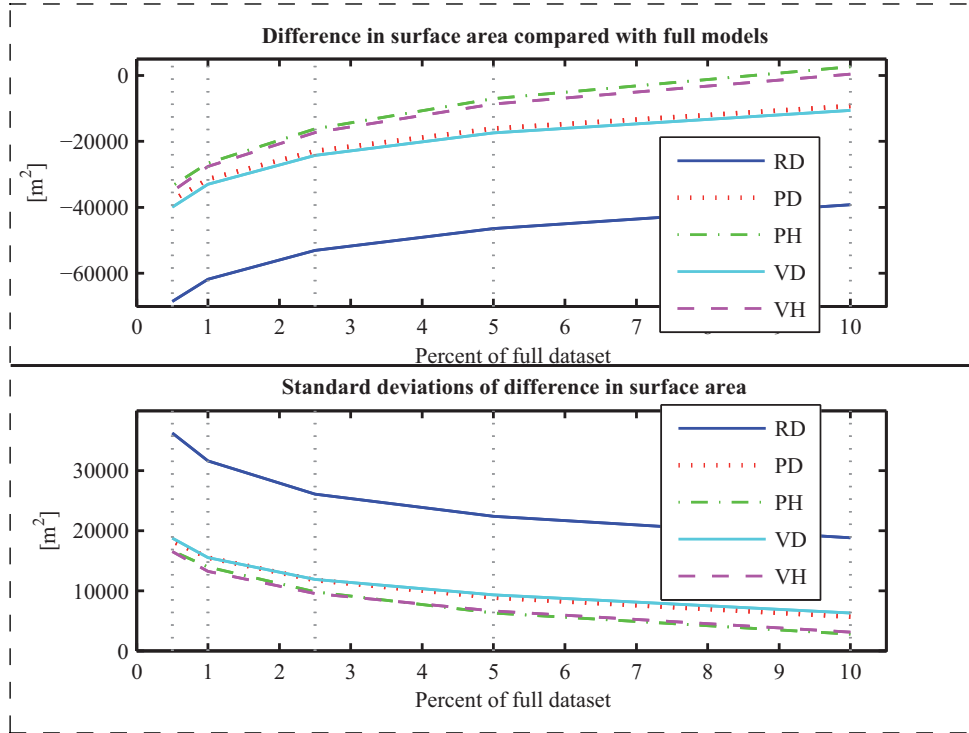


Figure 5. Surface area. Upper plot: average difference in surface area for the 32 test datasets. Lower plot: standard deviation of difference in surface area for the 32 test datasets. Vertical dotted lines indicate reduction levels applied for comparisons

Figure 6 shows the average difference in volume together with the associated standard deviations. Residual plots for the volume residuals indicate that they are closely normally distributed which makes the t-test applicable. The hypotheses to be tested are as follows:

- $H_0: \mu_i = 0$ (volume calculations associated with method i give unbiased estimates)
- $H_1: \mu_i \neq 0$ (volume calculations associated with method i give biased estimates)

Student’s t-tests with significance level of 5% and 31 degrees of freedom are used for testing. Each level of reduction is tested separately. None of the H_0 hypotheses could be rejected at any level of reduction, which means that the volume calculations associated with all five data reduction methods are unbiased for all levels of reduction.

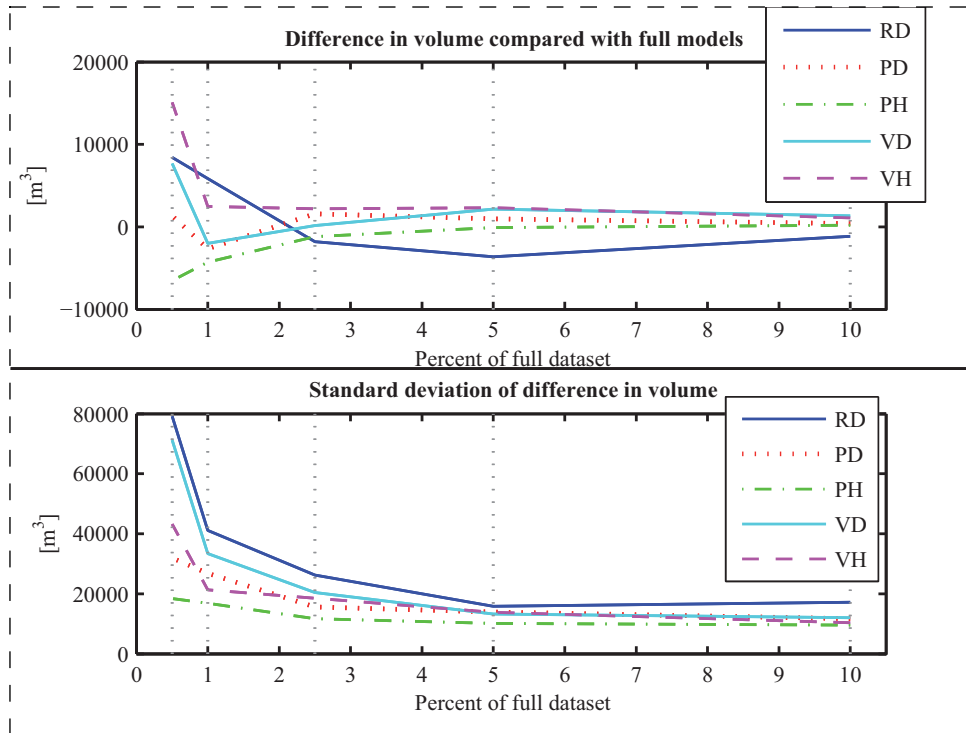


Figure 6. Volume. Upper plot: average volume difference compared with full models for the 32 test datasets. Lower plot: standard deviation of volume difference. Vertical dotted lines indicate reduction levels applied for comparisons

Figure 7 shows the vertical RMS values associated with the five methods. The RMS is tested pair by pair (as for the surface area) by means of a number of Fisher-tests (F-tests). In order to apply the F-tests, the RMS values are squared and thus assumed to be Chi-square distributed as implied by the F-test. The hypotheses are as follows:

$H_0: \sigma_i = \sigma_j$ (method i has the same RMS as method j for reduction level k)

$H_1: \sigma_i > \sigma_j$ or $\sigma_i < \sigma_j$ (method i has a larger/smaller RMS than method j for reduction level k)

where $i \in \{1..5\}, j \in \{1..5\}, k \in \{1..5\}, i \neq j$

The number of degrees of freedom is virtually unlimited if one consider all 32 datasets as a single area. The total number of data point processed is about $2.6 \cdot 10^7$ where 0.5% to 10% are used for construction of the TIN models. The remaining 90% to 99.5% are used as control points and thus corresponds to degrees of freedom. This is a somewhat pragmatic adaptation since the different datasets do not contain the same number of points. Due to the large number of degrees of freedom all RMS values are significantly different at any reasonable significance level. For the reduction levels 0.5%, 1% and 2.5% the mutual order of the RMS values are $RD > VD > VH > PD > PH$ where " $>$ " means significantly greater. However, for reduction

levels 5% and 10% this order is not valid. Still, RD has the highest RMS and PH has the lowest RMS but the order of the other methods is changed. Table 3 and Table 4 give comparisons of RMS for PD versus PH and for VD versus VH respectively.

Table 2. Vertical root mean square error of the control points for method PD and PH

Percent of full dataset	10%	5%	2.5%	1%	0.5%
PD RMS [m]	0.222	0.303	0.411	0.621	0.864
PH RMS [m]	0.189	0.262	0.357	0.540	0.752
Percent reduction of RMS	15.0	13.6	12.9	12.9	12.9

Table 3. Vertical root mean square error of the control points for method VD and VH

Percent of full dataset	10%	5%	2.5%	1%	0.5%
VD RMS [m]	0.216	0.314	0.463	0.789	1.158
VH RMS [m]	0.194	0.284	0.419	0.710	1.047
Percent reduction of RMS	10.1	9.5	9.7	10.0	9.6

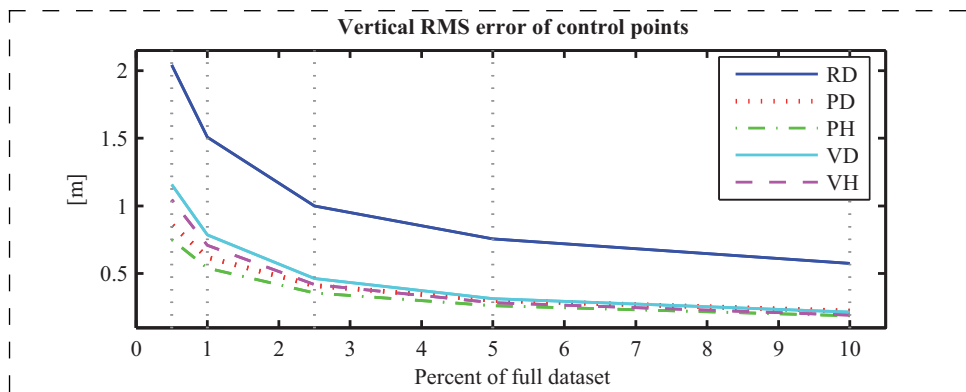


Figure 7. Vertical root mean square residuals of the control points. Residual values are calculated as interpolated value from the TIN surface minus measured elevation. Vertical dotted lines indicate reduction levels applied for comparisons

Similar hypotheses and testing procedures as for volume were also applied to the mean of the vertical residuals. Residuals in this context refer to the deviation of elevation values of control points from those interpolated from the TIN surface. Hypotheses testing indicate that the mean of residuals are unbiased for all methods except for method PH. It was not expected that PH should be biased since the volume estimates based on PH are unbiased. This situation might be related to the variable

TIN resolution. Figure 8 shows mean values of the vertical residuals together with the associated standard deviations.

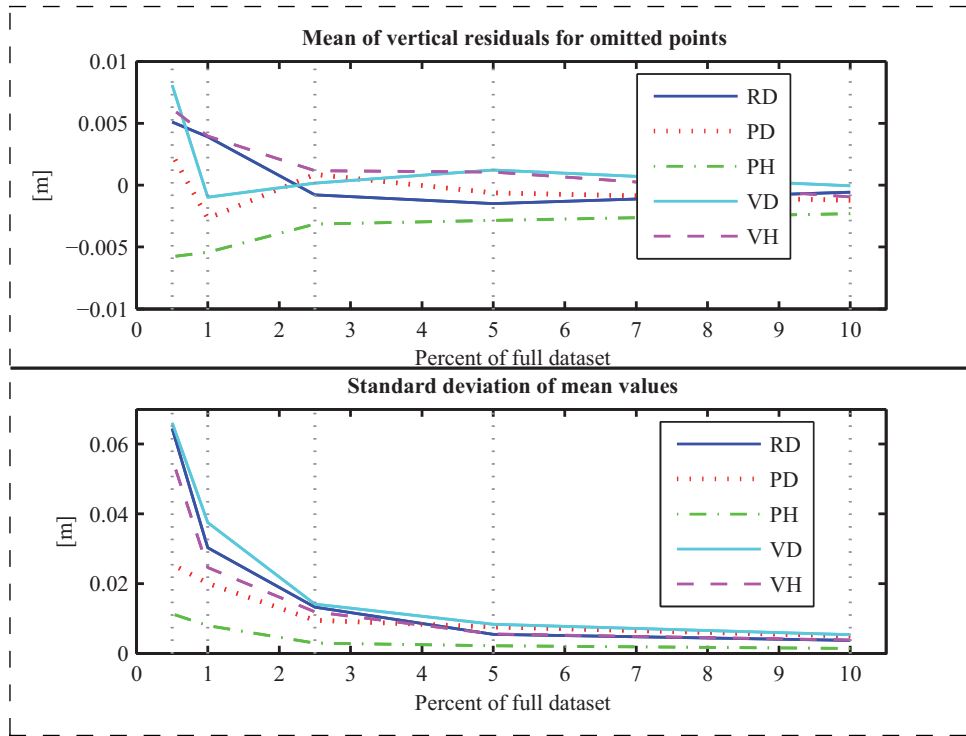


Figure 8. Mean of vertical residuals. Upper plot: mean values for the vertical residuals of control points. Lower plot: standard deviations of the mean values for the 32 test datasets. Vertical dotted lines indicate reduction levels applied for comparisons.

Figure 9 shows the average maximum vertical residuals together with the associated standard deviations. As for RMS, the max vertical residuals are squared in order to apply F-testing. Furthermore, the same pair wise testing scheme as for surface area is used. The hypotheses of interests are as follows:

$H_0: \sigma_{\max_i} = \sigma_{\max_j}$ (method i has the same mean of max residuals as method j for reduction level k)

$H_1: \sigma_{\max_i} > \sigma_{\max_j}$ or $\sigma_{\max_i} < \sigma_{\max_j}$ (method i has a larger or smaller mean of max residuals than method j for reduction level k)

where $i \in \{1..5\}, j \in \{1..5\}, k \in \{1..5\}, i \neq j$

Again, the calculated mean of maximum residuals of the actual pair determines whether it should be a "less than" or a "greater than" test, thus the H_1 hypotheses are one sided. A significance level of 5% and 31 degrees of freedom are used for testing.

Testing shows that RD has a significant larger mean of maximum residuals than the other methods. Moreover, PD and PH show no significant difference in mean of max values. The same applies to VD and VH. Method PD and PH have a significant larger mean of maximum residuals than VD and VH. The results from hypotheses testing regarding mean of maximum residuals can be summarized as follows; $RD > (PD \text{ and } PH) > (VD \text{ and } VH)$, where “>” means significantly greater.

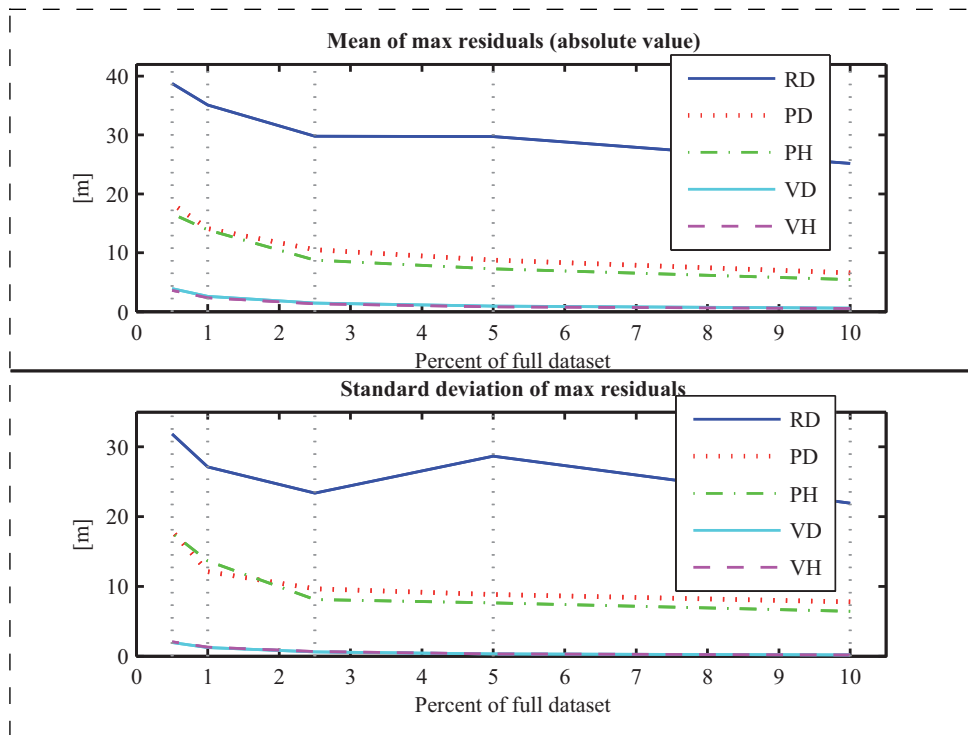


Figure 9. Max vertical residuals. Upper plot: means of the absolute value of the maximum vertical residual for the 32 test datasets. Lower plot: standard deviations of the maximum residuals. Vertical dotted lines indicate reduction levels applied for comparisons

The calculated evaluation parameters are dependent on the type of terrain and the properties of the actual datasets. However, no indications of significant change in *relative* performance (i.e. ranking of methods) of the five data reduction methods were found when applied to different types of terrain. However, this might be due to a poor categorization of terrain together with a small number of test datasets.

Although the Delaunay criterion produces a “good quality” triangulation in terms of its triangles' aspect ratios, it does not necessarily produce the triangulation which is the best approximation to a given height field for two reasons; 1) sliver triangles are necessary to give a good approximation to some surfaces and 2) the swapping of edges which the Delaunay criterion invokes can cause artificial break lines where

none exist in the original terrain [14]. A data dependent edge swap pass was performed for each of the two adaptive Delaunay triangulations. The processing cost associated with these edge swap passes is about 25% extra compared to the pure Delaunay triangulation. The gain of these data dependent edge swap passes is about 10-15 percent reduction of RMS error as well as better approximation of surface area. In accordance with the results in this paper, both Garland and Heckbert [15] and Rippa [16] report best results with a hybrid Delaunay – data dependent triangulation.

An ideal data reduction method should lead to unbiased results with low approximation errors as well as being cheap in terms of processing. Although the random subset method has some desirable properties, such as being unbiased for the parameters evaluated (except for surface area), the overall performance of this method is not adequate due to large variations in parameter estimates. This was expected, and the random method was introduced only to serve as a reference for the naive approach. The PH method has lower RMS than the PD method; this applies to all 32 test datasets as well as all 5 reduction levels. Similarly, the VH method has lower RMS than the VD method for all test datasets and for all levels of reduction. Statistical testing of PD RMS versus PH RMS is somewhat unnecessary since the data dependent edge swap is mostly a deterministic operation which solely aims to reduce the RMS. However there is a stochastic element involved since this is a greedy approach; during the edge swap process the same triangles can theoretically be subject to swapping several times and there is no guarantee that the optimal solution is found. The situation of VD and VH is slightly different; although there is a deterministic operation to swap diagonals to minimize the largest residuals; this is not directly related to the RMS which is to be evaluated.

Method PH has the smallest RMS and it also produces the largest surface area and lead to an unbiased volume estimate with the lowest standard deviation. Nevertheless, this method, as well as PD and RD, has a major drawback; it provides no control of the upper vertical approximation error. If this is considered as an important property only method VD and VH remain, where method VH provides the best overall approximation quality. However, it might be advantages to combine the vertical and perpendicular point selection criteria to get the best from both methods; slightly lower RMS and better approximation of surface area together with the ability to restrict the maximum vertical approximation errors. Some limitations of the applied methods should be mentioned; many conventional Geographical Information Systems (GIS) do not allow for dynamic triangulation and consequently these methods are not applicable for data reduction. Moreover the methods described in this paper is vulnerable to gross errors as they tend to give preference to gross errors if such are present in the data. Also, using a wider range of evaluation parameters including slope and curvature would have been beneficial.

4 Summary and Conclusions

Comparisons of five data reduction methods associated with dynamic TIN models were conducted. All methods were applied to the same test datasets of LIDAR topographic data. The performance of the various reduction methods were evaluated by means of surface area, volume, RMS of vertical errors and maximum vertical errors. Although the test datasets have somewhat variable properties with respect topography and point density one can point out some general guidelines. Most of the graphs for the test parameters seem to have an evident deflection at 2.5% of full dataset. This gives an indication of a suitable upper level of reduction. No indications of significant change in *relative* performance of the five data reduction methods were found when applied to different types of terrain. However this might be due to a poor categorization of terrain together with a small number of test datasets. Depending on importance of evaluation criteria, method VH is considered as the most favourable. Method VH employs point selection by vertical threshold in dynamic Delaunay triangulation combined with a final data dependent edge swap pass to reduce the maximum vertical approximation errors. The final data dependent edge swap pass requires about 25% extra processing time with the reduction levels and implementation used for this study. The gain is a reduction of about 10-15% in RMS together with better approximation of surface area.

Acknowledgement

Thanks to our colleagues at International Centre for Geohazards and at Division of Geomatics at Norwegian University of Science and Technology for suggestions and discussions. Special thanks to Dr. Marc-Henri Derron at the Geological Survey of Norway and Mr. Ivar Oveland at Blom Geomatics for support with data. We would also like to thank Dr. Erik Nyrnes at Statoil Research Centre for valuable comments regarding statistical testing. Moreover, thanks to the anonymous reviewers for their constructive comments.

References

1. Schröder, F., Roßbach, P., *Managing the complexity of digital Terrain Models*, Comput. & Graphics. Vol 18. No. 6, pp. 775-783, 1994.
2. Garland, M., Heckbert, P.S., *Surface Simplification Using Quadric Error Metrics*, Proceedings of SIGGRAPH, pp. 209-216, August 1997.
3. Demaret, L., Dyn, N., Floater, M.S., Iske, A., *Adaptive Thinning for Modelling and Image Compression*, Advances in Multiresolution for Geometric Modelling, Springer Verlag pp. 321-340, 2004.
4. Heller, M., *Triangulation algorithms for adaptive terrain modelling*, Proceedings of Fourth International Symposium on Spatial Data Handling. International Geographical Union, Zurich, pp. 163-174, 1990.
5. Bottelier, P., Haagmans, R., Kinneging, N., *Fast Reduction of High Density Multibeam Echosounder Data for Near Real-Time Applications*, The Hydrographic Journal, No. 98, October 2000.
6. Anderson, E.S., Thompson, J.A., Crouse, D.A., Austin, R.E., *Horizontal resolution and data density effects on remotely sensed LIDAR-based DEM*, Geoderma, No. 132, pp. 406-415, 2006.
7. Diebel, J.R., Thrun, S., *A Bayesian method for Probable Surface Reconstruction and Decimation*, ACM Transactions on Graphics, Vol. 25, No. 1, January 2006.
8. Kumlér, M.P., *An Intensive Comparison of Triangulated Irregular Networks and Digital Elevation Models*, Cartographica, Monograph 45, Vol. 31, No. 2, Summer 1994.
9. Danovaro, E., De Floriani, L., Magillo, P., Mesmoudi, M.M., Puppo, E., *Morphology-Driven Simplification and Multiresolution Modelling of Terrains*. GIS'03, New Orleans, Louisiana, USA, November 7-8, 2003.
10. Baltsavias, E.P., *Airborne laser scanning: existing systems and firms and other resources*, ISPRS Journal of Photogrammetry & Remotes Sensing, 54, pp. 164-198, 1999.
11. Optech, Webpage, Specifications for ALTM at URL: <http://www.optech.ca/prodaltm.htm>
12. Midtbø, T., *Spatial Modelling by Delaunay Networks of Two and Three Dimensions*, Norwegian Institute of Technology, Doctoral theses No. 23 1993.
13. Hern, D., Baker M.P., *Computer Graphics with OpenGL*, Third Edition, Pearson Prentice Hall, 331-335, 2004.
14. Brown, P.J. Cameron, *Selective Mesh Refinement for Rendering*, Emmanuel College, University of Cambridge, Doctoral theses 1998.
URL: <http://www.cl.cam.ac.uk/research/rainbow/publications/pjcb/thesis/>
15. Garland, M., Heckbert, P.S., *Fast Triangular Approximation of Terrains and Height Fields*, CS Department Carnegie Mellon University, Technical Report, May 1997.
16. Rippa, S., *Adaptive Approximation by Piecewise Linear Polynomial on Triangulations of Subsets of Scattered Data*, SIAM's Journal of Scientific and statistical Computing, Vol. 13, No. 5, pp. 1123-1141, September 1992.

Paper II

Interactive Geovisualization and Geometric Modelling of 3D Data - A Case Study from the Åknes Rockslide Site, Norway

Trond Nordvik¹, Chris Harding²

¹Division of Geomatics, Norwegian University of Science and Technology, N-7491 Trondheim, Norway

²Department of Geological and Atmospheric Sciences, Iowa State University of Science and Technology, Ames, Iowa 50011-2274, USA

Abstract

This paper reports on the 3D visualization and modelling of multiple 3D data sets from the Åknes rockslide site, one of the world's largest and most complex rock slide assessments. Using the open-source architecture OpenSceneGraph (OSG), we created an interactive 3D application which enables the project's geoscientists to visualize combinations of several different 3D data sets from the site. The application also allows them to model the subsurface geometry of suspected sliding surfaces which play a key role in the assessment of the rockslide and its prediction. This interactive modelling uses a constrained Delaunay triangulation method. This cross-platform application is designed to run on a typical desktop PC and does not contain any operating system specific components. While there are some caveats, OSG has provided us with a flexible and cost-effective high-level platform for the development of our geovisualization application.

Key words: 3D geovisualization, geometric modelling, rockslide, OpenSceneGraph

Introduction

Åknes is a headland (promontory) situated above the entrance of the Geiranger fjord (Fig. 1). This fjord is part of the world heritage list and attracts several hundred of thousands visitors per year (many of them onboard cruise ships). As the Åknes slope exhibits continuous creep of the rock mass which could lead to a massive rock slide, a comprehensive mapping program was initiated in 2004 (Derron et al. 2005, Kveldsvik et al. 2006) making Åknes one of the most investigated and instrumented slopes in the world (Ganerød et al. 2008). A large-volume rock slide from the slope into the nearby fjord could lead to a massive tsunami that would strike several inhabited villages (Blikra et al. 2005) and could endanger nearby cruise ships. A warning system has been established to allow the evacuation of the surrounding areas. The Åknes rock slide forms part of a steep mountain slope on the west side of the fjord. The slope rises from the fjord to about 1500 meters above sea level and is 30-40 degrees steep. Current investigations define the unstable parts of the slope as starting at a 800 m long back scarp zone (across slope) at roughly 800-900 m above sea level and extending for roughly 1000 m down the slope (Ganerød et al. 2008). Preliminary estimates put the overall volume of the potential rock slide at up to 80 million m³ (Rønning et al. 2006), 30 times the volume of the Great Pyramid of Giza (2.6 million m³, Edwards 2003).

Our work is part of a larger effort to analyse the many data sets obtained from the Åknes site and to determine the rock slide's 3D geometry and its material. This effort will help to estimate the potential volume of the unstable rocks and to predict the consequences of a potentially massive slide event. Surface data sets include; high resolution elevation data from Light Detection and Ranging (LIDAR), real-time Global Positioning System (GPS) data of critical locations along the slope and bathymetry data for the fjord's seabed, sub-surface data sets include geophysical surveys (geoelectrical resistivity, ground penetrating radar, seismic) and borehole measurements. Data from GPS, extensometers and interferometric Synthetic-Aperture Radar (inSAR) measurements are updated over time and thus add a temporal dimension to the research. Visualising these different types of surface and subsurface data sets as 3D ensembles helps geoscientists to validate incoming field measurements, to formulate and answer spatial questions, and to develop an idea of the "big picture". The accurate determination of Åknes' sliding surface(s) is of paramount importance. The extent and nature of these sliding surfaces, such as their slope and aspect and the volume of the rock units they delineate, are vital inputs for the numerical modelling of the slide dynamics and for the tsunami modelling,

which, in turn are used to predict the consequences of different sliding scenarios.

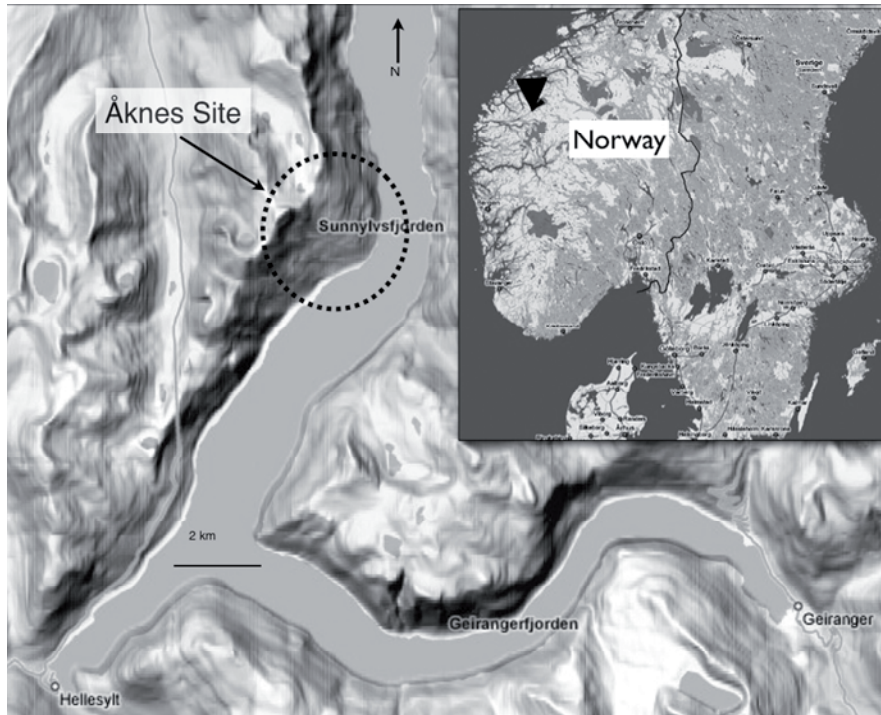


Fig. 1. Location of the Åknes site

While “off the shelf” software has been used for parts of the project, it has been difficult to find existing software that supports the requirements of the Åknes project. Instead, this custom software application has been created together with the project's geoscientist, to adapt to the project's needs and to its evolving data. Our application uses a high-level 3D graphics scene-graph architecture (OpenSceneGraph) and leverages many well known principles and techniques of 3D geovisualization, to address the specific visualization and modelling needs of the Åknes project. The application presents the currently available 3D data to the geoscientist in an easy-to-understand form and thus provides an intuitive overview of the spatial situation at the Åknes site. Because of the vital role of the sliding surfaces, the system also allows the geoscientists to interactively model (sculpt) the geometry of the main sliding surface within the spatial context

of the other 3D data sets. This interactive visualization and modelling application can be run on common personal computer hardware. The rest of this paper describes the use of OpenSceneGraph in this application, the Åknes site's 3D model and its visualization, the interactive modelling of the sliding surface's geometry and closes with a discussion and summary.

OpenSceneGraph

OpenSceneGraph (OSG) was chosen as a basis for this 3D application (OSG, 2007). OpenSceneGraph is a freely available, open source application programming interface (API) used to develop 3D graphics applications including applications for geovisualization, e.g. (Kada et al. 2003), (ossimPlanet 2007) and (Sherman et al. 2007). OpenSceneGraph uses a high level scene graph structure and Open Graphics Library (OpenGL) rendering to provide a full visualization framework. The scene graph architecture, a collection of nodes organised as a hierarchical tree data structure, is used to efficiently manage and render 3D data. The OSG project started almost a decade ago and it is currently used by more than 1600 developers to develop 3D applications (Martz 2007). OpenSceneGraph is written in C++ and uses OpenGL, the de facto standard rendering API for cross-platform computer graphics. OpenSceneGraph supports the standard template library (STL) and combines high performance graphics with object oriented (OO) programming. Besides providing high level access to computer graphics (Fig. 2), OSG supports smart pointers and other modern programming functionality.

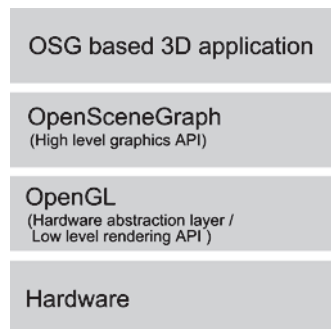


Fig. 2. A cross-platform 3D application uses the high level OSG scene graph API, which uses OpenGL as the rendering engine

The nodes of a scene graph (Fig.3) represent a tree structure that connects the scene's physical and abstract objects. In general, rendering this scene means traversing this tree from the root and perform a function at each node encountered that possibly carries over to the nodes "beneath", effectively compositing an image (frame) from the current state of the tree's nodes. When navigating, the scene graph is traversed roughly 30 times per second and creates the impression of a fluid response to the user's interactions. Types of nodes used in this project include: geometry nodes (to define a 3D geometric model as a collection of triangles), transformation-nodes (to move/rotate/scale the model in 3D space), lighting nodes (representing light sources that illuminate the model) and camera nodes (to "record" the view of the model seen on the monitor), group-nodes (to affect multiple nodes as a group) and switch nodes (selectively affect only a subset of the nodes).

Compared to using OpenGL alone for application development, OSG offers a number of convenient high level features and performs several levels of optimization automatically - for example, OSG automatically discards parts of the scene that are currently not visible (co-called culling). OpenSceneGraph's architecture allows the programmer to work with a wide range of 3D data types; its object oriented nature encourages the reuse of already tried and true methods. Other OSG functionality useful for visualization includes interactive object selection (picking via mouse or a 3D ray) and stereo viewing. OpenSceneGraph supports the import/export of 3D models in many 3D file formats, for example VRML (.wrl), ESRI Shape (.shp), 3D Studio Max (.3ds) and Alias Wavefront (.obj) for data interchange with other 3D applications. Although, OSG is a general purpose graphics API there are some features especially designed for geospatial data such as the osgTerrain module for generating paged (tiled) terrain databases. However, using OSG for our project made us also aware of its limitations and shortcomings, some of which will be addressed in the discussion section.

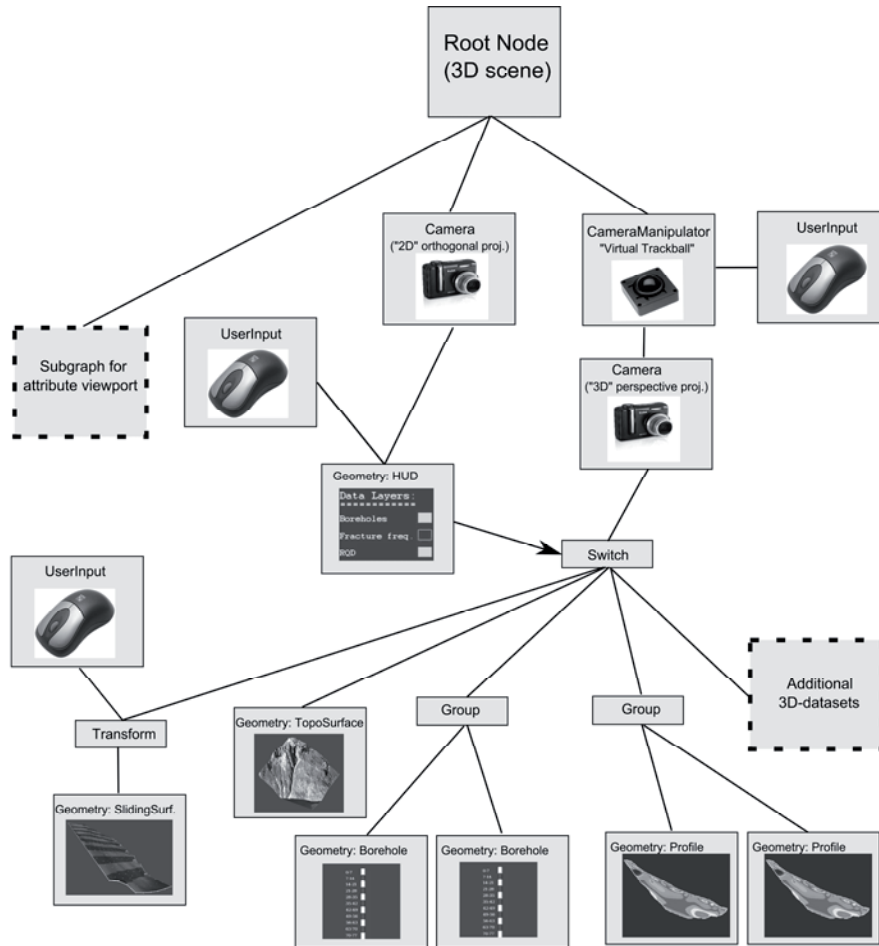


Fig. 3. Simplified subset of our application’s scene graph. The scene graph provides a traversal (rendering) tree for nodes with specific functions to create a user-driven view of the 3D data sets. The switch node, selecting the currently visible data sets, is controlled by interaction with the head-up display (HUD)

Design and implementation of the 3D Åknes model.

Our application was developed using OpenSceneGraph (version 2.0) and Microsoft Visual Studio (version 8.0) running on the Windows XP operating system. The visualization application supports several forms of stereo

viewing, such as active stereo (shutter glasses) and passive stereo (polarized projectors/glasses). Based on input and requirements from a group of geoscientists (geologists, geophysicists and geotechnical engineers) affiliated with the Åknes project, this geovisualization application was designed as a stand alone application to view and interact with the 3D model of the site on a common Windows PC. The 3D model of the site is organized as a hierarchical scene graph using a number of OSG node classes. Fig. 3 shows a simplified subset of the models scene graph. The main window displays one or more of the available 3D data sets in a perspective projection whilst an auxiliary 2D window displays additional 2D information such as drill core images (Fig. 4). The 3D data sets can be selected (switched on and off) by clicking on a set of check boxes with the mouse, currently around 30 different data sets. Because OSG itself does not integrate standard interface components such as menus and buttons etc., check boxes were implemented as a head-up display (HUD), which draws text and symbols in front of the 3D scene as "overlay graphics" (Fig. 4).

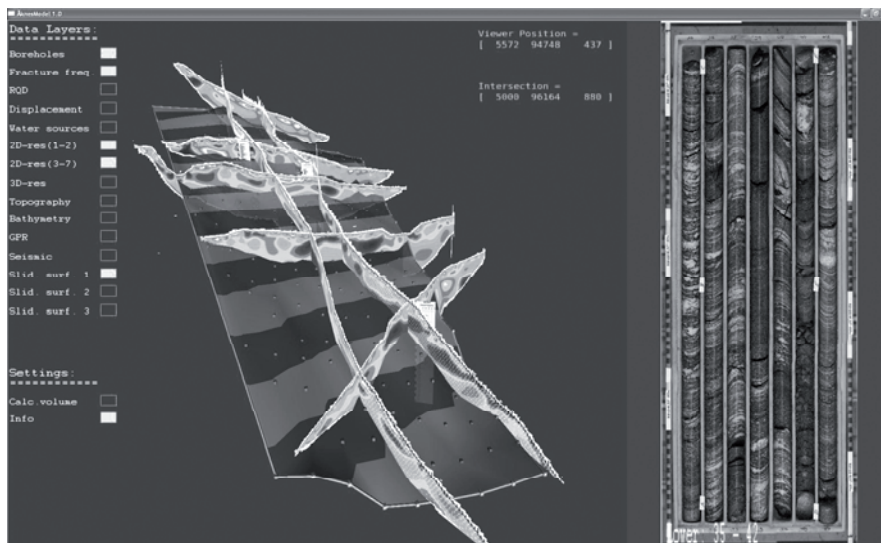


Fig. 4. Graphical User Interface. Left viewport, displaying the 3D model, has perspective viewing projection whilst the right viewport, displaying additional attribute information, has orthogonal viewing projection

A predefined OSG trackball camera manipulator class is used for navigation in the 3D scene (main viewport). This provides basic navigation functions, such as panning, rotation and zoom, by mimicking a virtual trackball via the mouse. For example; left mouse button dragging will ro-

tate the 3D model around its origin, while middle mouse button dragging pans (moves) around and right mouse button dragging will induce zooming (exo-centric navigation). To help the viewers to recover their bearings, we implemented an improved option for resetting the camera's position and attitude. In this improved reset, the position and the horizontal components of the viewing direction are maintained but the vertical view component is set to zero, that is the pitch and the roll are set to zero whilst the heading and the position are kept. This option is useful when moving vertically along objects in the model to examine geological structures and inspect data values. The navigation functions can also be used to create a fly-through, an animation that provides a continuous bird's eye view to the model and is well suited to communicate an overview of the site. Fig. 5 shows the topography and bathymetry of the Åknes area (the chessboard pattern was added to illustrate the rough extent of the Åknes site and can be switched off).

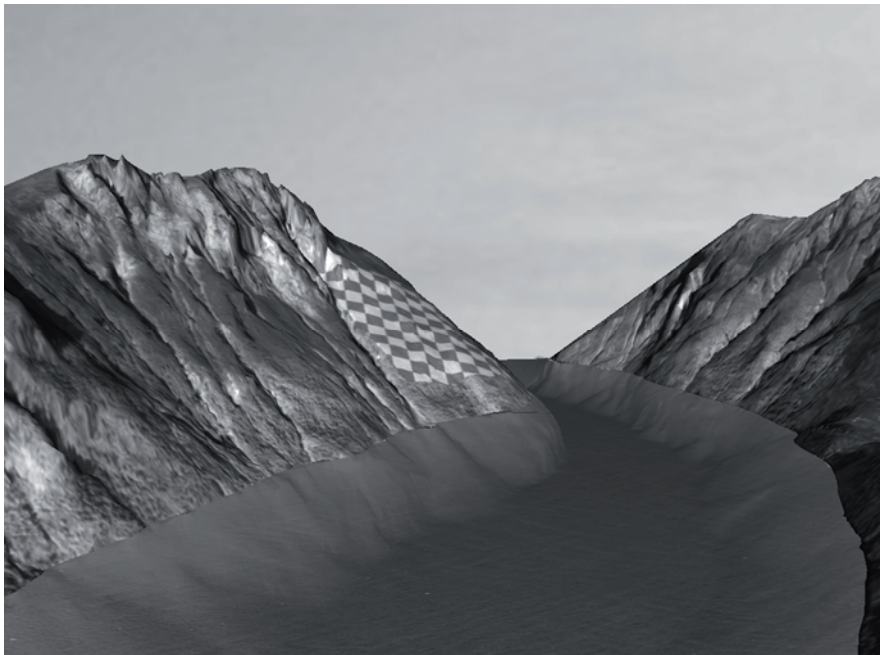


Fig. 5. Overview of the Åknes site. (The slide area is indicated with a chessboard pattern)

Methods used in the preparation and visualization of the 3D model

Since 2004, an extensive survey campaign of characterizing the geoscientific (surface and subsurface) conditions has been conducted at the Åknes site. This includes maps from field observations (geological, hydrological and geomorphological maps) and data from aerial photography, airborne and terrestrial LIDAR, geo-electrical resistivity, refraction seismic, ground-penetrating radar, various types of borehole measurements and bathymetric measurements. Several different types of permanent field stations were established to monitor rock changes throughout the Åknes site, these include GPS, inclinometers, extensometers, permanent radar reflectors (inSAR scatters), reflectors for total stations, climate sensors (precipitation, temperature) as well as permanent seismic installations. We integrated many of these different 3D data sets into the OSG 3D model of the Åknes site.

We used OSG Delaunay triangulations to represent 2.5D surface (elevation) data of the site's topography and bathymetry (Fig. 5), and its subsurface sliding surfaces (Fig. 4, 7, 8, 10 and 11). A triangulated irregular network (TIN) model represents both a contiguous mesh of non-overlapping triangular facets and a data structure: "A TIN model can be regarded both as a terrain model as well as a data structure. It is a model because the space-filling triangular planar facets determine a value for the surface everywhere, but it also has a specific structure in which the points, triangles and topologies are stored." (Kumler 1994). A Delaunay triangulation is one common way to create a TIN model, such a Delaunay type TIN is made from "*triangles where no points in the network are enclosed by the circumscribing circles of any triangle*" (Midtbø 1993). The Delaunay triangulation's solely mathematical criterion forces the creation of "well-shaped" triangles with edges that are not radically different in length (i.e. are not "skinny"); this has proven to be beneficial in many real world and theoretical applications. To further improve the shape of a triangulated surface, additional constraints can be imposed during its creation. For example, so-called break lines can be added which require the TIN to honour the geometry of these lines (i.e. none of its triangles can cut across a break line), however, such triangles will not necessarily fulfil the Delaunay criterion. Break lines are useful to model abrupt changes in the topography or to embed man-made objects, such as roads, into the terrain.

The site's raw topography and bathymetry data (measured by LIDAR and multi beam echo sounder, respectively) were given as geo-referenced points (x, y, z locations on the Earth's surface). The OSG surface model is

based on these points. The x and y coordinates are given in UTM coordinates, the z coordinate (elevation) is given with respect to the geoid. Both raw data sets are very detailed and contain a large number of data points, roughly 50 million points for the area shown in Fig. 5 at typically 1 to 2 points per square meter. To achieve a real time visualization of the 3D model (i.e. more than 30 frames per second) on modest hardware, we had to reduce the 3D model's number of points and the size and total amount of texture ("images") draped over the TIN. OpenSceneGraph provides a "DelaunayTriangulator" node which can be customized using its "DelaunayConstraints". When creating the OSG surface models from this original data, we used an adaptive triangulation approach (Heller 1990, Nordvik and Midtbø 2007) which intelligently lowers the number of vertices and triangles while keeping the mesh's quality adequate. Adaptive triangulation changes the "resolution" of the triangle mesh depending on the raw data's elevation. In areas with little change of slope, a relatively coarse mesh sufficiently represents the topography, in more complex areas; a larger number of triangles are used to archive an acceptable level of approximation error. This method could also be used to create multiple surfaces of different quality for the same spatial extent, which represent different levels of details (LOD) of this area.

To create a photo-realistic appearance, a high resolution ortho-photo was draped over the geometric model of the site's topographic surface. In the original ortho-photo 1 pixel corresponds to 12.5cm on the ground, roughly 15,000 x 15,000 pixels to cover the site. Although even commodity graphics adapters can now store many 100s of megabytes of total texture images, single texture images are typically limited to sizes from 2048 x 2048 pixels to 8192 x 8192 pixels. Larger texture images have to be either rescaled or split into smaller images (tiles) before they can be used. However, a reduction in resolution is undesirable; draping the split texture images on rectangular tiles requires calculating and inserting new "helper vertices" and would create artificial break lines along the straight borders. Using OSG's multi-texture facilities allowed us to split the large texture image into several smaller textures "tiles" and to blend these tiles together without breaking up the TIN internally. Although each texture tile is mapped to the entire mesh, valid texture coordinates ($s \in [0,1]$, $t \in [0,1]$) are only assigned to vertices within the area corresponding to that specific tile. Vertices outside the tile's area are given texture coordinates outside the valid 0.0-1.0 range resulting in a RGB colour value of (0,0,0) (i.e. the colour is clamped to black). After this procedure is completed for all tiles, the final colour values for the TIN are calculated by summarising all separate texture tiles. Although this method requires additional work in terms of texture coordinates, the final result is a mosaic corresponding to

the initial oversized texture (Fig. 6) where only pixels within each tile will contribute to the overall texture colour while the black pixels add nothing (0,0,0).

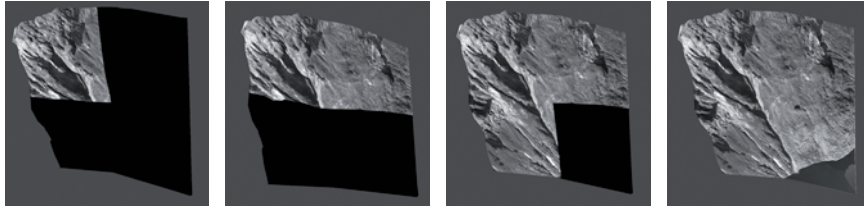


Fig. 6. Assembling a high resolution texture by adding four textures together using OSG's multi-texturing capability. From left to right, each images shows the addition of a new texture (quarter)

We visualized data from various geophysical surveys, including 2D and 3D inversions of geo-electric resistivity measurements and ground-penetrating radar. We show the 2D resistivity inversions as series of 2D textured, vertical slices at the correct spatial location within the 3D model, so-called fence diagrams. The 3D resistivity inversion was transformed into a 3D texture (a 3D texture array); this automatically “paints” any arbitrary geometry placed inside this volume with the resistivity values. Besides allowing the user to move vertical and horizontal sections through the volume, we also paint the 3D resistivity volume on the geometry (TIN) of the sliding surface (see next section). As the TIN of the topography may obscure the subsurface data beneath it, we use an OpenGL clip plane to temporarily cut away parts of the TIN. Fig. 7 shows the 3D textured sliding surface (TIN) and a horizontal section (profile) moved to two different positions.

Core samples of seven boreholes in three different locations of the slide area provide accurate information about the subsurface along these holes. After the drilling, the cores themselves were photographed and a large number of parameters were measured either in the drill holes or from the drill core samples (see Rønning et al. 2006 and Ganerød et al. 2007 for a complete list of measured parameters). In the 3D OSG model, the boreholes themselves are represented as sets of black-and-white segments (cylinders); each segment represents a 7 m stretch of core. Plots of the measured parameters are presented as textured “billboards” (panels) next to the boreholes in the 3D model. Billboards are “smart” rectangles which automatically rotate towards the viewer along the vertical axis and thus avoid situations where the viewer cannot see the front of the panel. Clicking on a

borehole's cylinders with the mouse shows high-resolution images of the rocks found along each segment of the borehole (core images) in a separate part of the application (right in Fig 8).

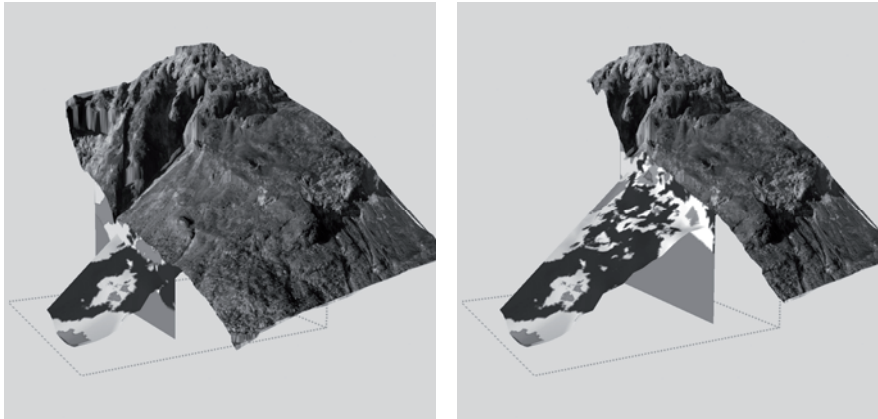


Fig. 7. Using 3D texture to visualize the 3D resistivity beneath the topography. Left and right figure show two different cross sections set by the user, the topography is clipped along the cross section

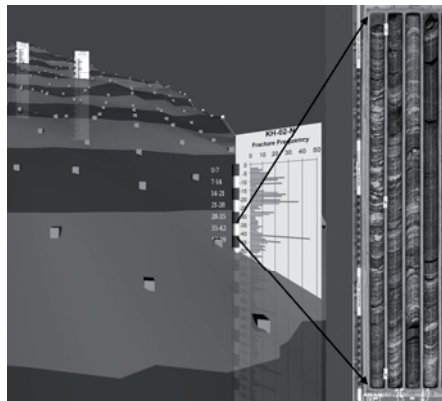


Fig. 8. A semi transparent sliding surface and boreholes with billboards containing fracture frequency plots displayed together with a core image

During field work campaigns the locations of water sources within the slide area were noted and their properties were established. These water sources are represented as animated OSG particle generators in the 3D

model. The properties of the particle generators are set to mimic the properties of these actual water sources; the size and frequency of the particles reflect the amount of water, the height of the fountain reflects the pressure. While certainly not realistic, these fountains serve as symbolic, yet quantitative visualizations of the location of these water sources and their properties (Fig. 9, left). The parts of the Åknes site that are suspected to form the sliding rock units are monitored for creep by extensometers, inSAR, GPS and total stations. The right section of Fig. 9 shows a set of displacement vectors derived from GPS measurements.

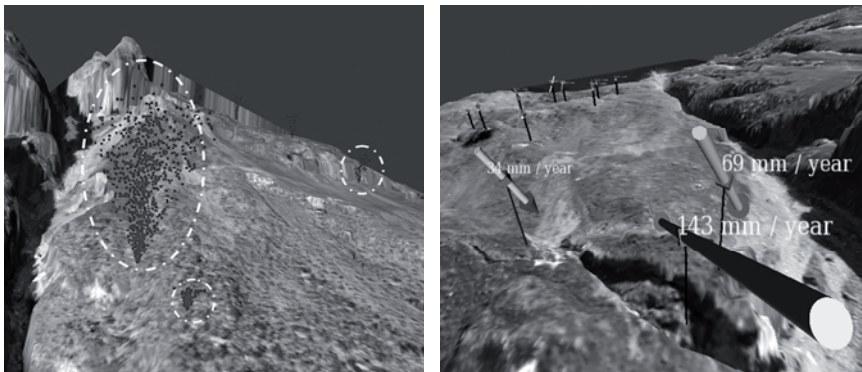


Fig. 9. Left figure: Water sources are represented as particle generators. Right figure: Vectors of the displacement at certain points of the slope over time (measured via GPS) are represented as 3D arrows in the model

Interactive modelling of the sliding surfaces

Besides offering a 3D visualization of the site's data sets, our application uses a constrained Delaunay triangulation to implement the interactive modelling of the sliding surfaces i.e., surfaces that, in 3D, delineate the unstable rock units from the solid bedrock below. To start this modelling process, an initial sliding surface is created at a constant depth beneath the site's topographic surface. Each TIN node is used as an editable "control point" (shown as small cubes in Fig. 8 and 10), that can be manually adjusted in x, y and z directions via the keyboard. Similarly, groups of control points can be selected by the mouse and shifted along the three coordinate axes, as can the entire surface mesh. Other 3D data sets (e.g. drill-hole data or resistivity data) can be displayed to provide the needed 3D spatial

context for defining the shape of the sliding surface. A horizontal mesh resolution of 50 m was considered sufficiently detailed to capture the initial shape of the surface, however the user can interactively add more control when and where more subsurface information becomes available, e.g., along the profiles and in the vicinity of boreholes. After the user has moved, added or deleted vertices, the surface is re-triangulated in real time to show the new shape and how it fits into the surrounding data (Fig. 10). This lets the user explore what-if scenarios and to compare different solutions. In general, a “good” surface needs to fit not only into the surrounding information but also into a mental model of the overall geological and geophysical "situation" of the site. It should be noted that this geometric modelling is not as simple as forcing the shape of the surface to follow the shape of the surface to follow the displayed data sets (boreholes, fence diagrams, etc.). As the scale and uncertainty of the displayed data sets differ considerably, it is quite possible that data sets seem to contradict each other at certain locations. While it is still up to the skill and knowledge of the geoscientists to create a geometric model as a personal interpretation of the available data, interactive 3D visualization and modelling tools automatically provide the users with visual context and thus allow them to better concentrate on the essential tasks.

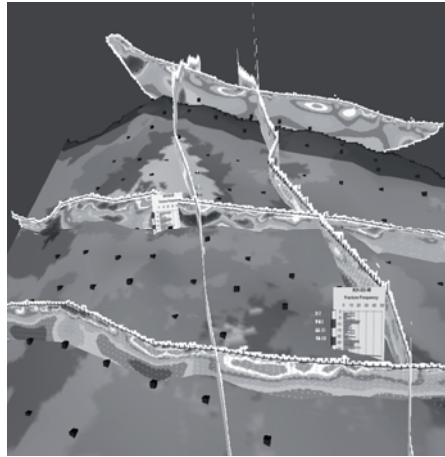


Fig. 10. Geometric modelling of a sliding surface (TIN) by moving control points, it is coloured by a 3D inverted resistivity data (3D texture); also shown: 2D inversion (fence diagrams) and borehole data

The boundary of the sliding surface is represented as a constrained poly-line which enables it to form a non-convex hull (unlike the unconstrained Delaunay triangulation's boundary, which will always form a convex hull).

The sliding surface and parts of the topographic surface are connected together by embedding a "projection" of the boundary polygon into the topography TIN above (fat poly-line in Fig. 11). Note that the vertices of this upper boundary can also be moved laterally and are not simply vertical extrusions of the lower boundary polygon. This vertex-to-vertex connection defines a 3D body between the sliding surface and the corresponding part of the topography above it. The body's volume is calculated as the difference of the volume between the upper surface (topography) and a horizontal reference plane; and the volume between the lower surface (sliding surface) and the same reference plane.

As inserting more than one new *boundary* control points at once could lead to unintended switch backs (i.e. the boundary line crossing itself), we re-triangulate both surfaces after a boundary control point is inserted or deleted. When the modelling process of a sliding surface is completed, it can be exported to a file for further processing with external software.

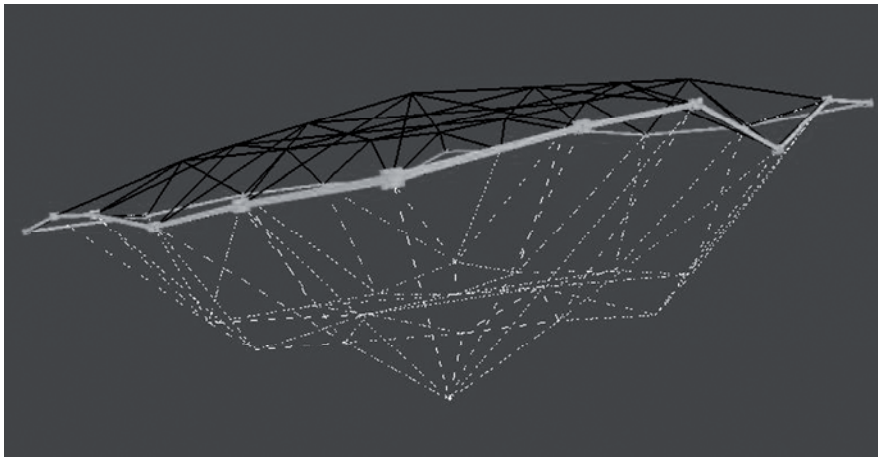


Fig. 11. Construction a 3D body from two TIN surfaces (bottom: sliding surface, top: topography), the surfaces' constraint boundary (poly-line) are connected vertically

Discussion and summary

We have created a visualization and modelling application that solves the specific needs of the geoscientists working on the Åknes site, including the creation of a geometric model of the sliding surfaces underlying the

site. Challenges included the complexity, volume, heterogeneity of the site's data sets, the fact that the data collection is ongoing and the number and diversity of groups involved in the Åknes project. While each group may use other software packages, such as ER Mapper, ArcGIS, QT Modeller and Plaxis, to fulfil a specific functionality, our application aims to provide a "communal" visualization solution that is easy to learn and can be used by all geoscientists involved.

Unlike regular grids, TIN models are capable to adapt to the underlying scattered data set (e.g. LIDAR data) and can efficiently capture both smooth and abrupt changes in height. As TIN models are based on the same underlying primitives (triangles) as OpenGL, their display can be optimized by the renderer. For the application to work at interactive rates on an ordinary PC, we used a *constrained 2.5D TIN* surface approach as a flexible way of reducing the size of the original surface data sets by intelligently adapting the TIN's resolution. This constrained TIN approach is also used in the interactive geometric modelling of the all-important sliding surfaces and allows geoscientists to shape a surface within the context of surrounding 3D data sets. While the use of Delaunay constraints enables us to integrate break lines, holes and vertical sections in the surfaces, there are fundamental limitations to such a 2.5D approach, most notably its fundamental inability to capture more complexly shaped (folded) surfaces with multiple z values, i.e. overhangs.

OpenSceneGraph provided us with the flexibility to combine different types of data sets, such as elevation data, 3D grid data, 2D vertical sections and 1D borehole data, into high-level 3D objects that the user can interact with. OpenSceneGraph also provided a flexible way for 3D navigation. While the open source nature provides everybody with OSG's source code, its documentation is still of variable quality and occasionally absent; this may provide a hurdle to newcomers who are not used to learning from code examples. The OSG version used for this project (version 2.0) does not provide direct support for parametric surfaces (2D/3D splines), 3D triangulations (tetrahedral meshes) or 2D/3D iso-surfaces (contours). Despite these caveats, our experience points to OSG as a flexible and cost-effective high-level platform for the development of cross-platform geovisualization applications. Because OSG is an open-source (non-commercial) system, our application can be freely distributed to all scientists involved in the project and can be further extended as the need for additional functionality arises. For example, while our application can already work in stereo and make use of a large single projection screen, it can be further extended via virtual reality (VR) toolkits (such as VR Juggler) to work on multiple stereo screens (e.g. a CAVE system) and to support 3D tracking and 3D input devices. While our application is developed on a Windows desktop com-

puter, it uses only OSG and OpenGL libraries and can be adapted to multi-node (cluster) systems and other operating systems. We have experimented with such a VR-version of our application, using a four-sided CAVE and a wireless gamepad, and envision its use for collaborative visualization and modelling.

Acknowledgements

The authors would like to acknowledge a number of scientists affiliated with the International Centre for Geohazards, the Geological Survey of Norway and the Norwegian University of Science and Technology for their contribution to this project either by exchange of ideas or by providing data. The first author wishes to thank the faculty and the staff at the Virtual Reality Applications Center at Iowa State University of Science and Technology, USA, for having him as a visiting scholar during the initial stage of this project.

References

- Blikra LH, Braathen A, Derron MH, Kveldsvik V, Grøneng G, Dalsegg E, Elvebakk H (2005) Rockslope failure at Åknesremna, Stranda, western Norway. Report by the Geological Survey of Norway
- Derron MH, Blikra LH, Jaboyedoff M (2005) High resolution digital elevation model analysis for landslide hazard assessment (Åkneset, Norway). In: Seneset k, Flaate K, Larsen JO (eds) Proceedings of the 11th International Conference and Field Trip on Landslides (ICFL). 1st-10th September 2005, Norway. Taylor & Francis Group, London
- Edwards JF (2003) Building the Great Pyramid - Probable Construction Methods Employed at Giza. *Technology and Culture*. The Johns Hopkins University Press, Vol.44, No. 2, pp 340-354
- Ganerød GV, Grøneng G, Rønning JS, Dalsegg E, Elvebakk , Tønnesen JF, Kveldsvik V, Eiken T, Blikra LH, Braathen A (2008, in press) Geological Model of the Åknes Rockslide, western Norway. *Engineering Geology*
- Ganerød GV, Grøneng G, Aardal IB, Kveldsvik V (2007) Logging of drill cores from seven boreholes at Åknes, Stranda municipality, Møre and Romsdal County. Report 2007.020 by the Geological Survey of Norway

- Heller M (1990) Triangulation algorithms for adaptive terrain modeling. In: Brasel K, Kishimoto H (eds) Proceedings of the 4th International Symposium on Spatial Data Handling, International Geographical Union, Zurich, Vol. 1, pp 163–174
- Kada M, Roettger S, Weiss K, Ertl T, Fritsch D (2003) Real-time visualization of urban landscapes using open-source software. In: Proceedings of the 24th Asian Conference on Remote Sensing & Internatioanl Symposium on Remote Sensing, 3rd-7th November, 2003, Busan, Korea.
- Kumler MP (1994) An Intensive Comparison of Triangulated Irregular Networks and Digital Elevation Models. *Cartographica*, Monograph 45, Vol. 31, No. 2, pp 1-49
- Kveldsvik V, Eiken T, Ganerød GV, Grøneng G, Ragvin N (2006) Evaluation of movement data and ground conditions for the Åknes rock slide. The International Symposium on Stability of Rock Slopes. The African Institute of Mining and Metallurgy. April 2006, pp 279-299
- Martz P (2007) OpenSceneGraph Quick Start Guide. Skew Matrix Software LLC
- Midtbø T (1993). Spatial Modelling by Delaunay Networks of Two and Three Dimensions, Doctoral thesis No. 23, 1993, Norwegian Institute of Technology
- Nordvik T, Midtbø T (2007) Application of Data Reduction Methods in Dynamic TIN Models to Topographic LIDAR Data. In: Bjørke JT, Tveite H (eds) Proceedings of the 11th Scandinavian Research Conference on Geographical Information Science, 5th - 7th September, 2007, Ås, Norway, pp 111-128
- OSG (2007) OpenSceneGraph website (Cited 26 November 2007) URL: <http://www.openscenegraph.org/projects/osg>
- ossimPlanet (2007) ossimPlanet website (Cited 27 November 2007). URL: <http://www.ossim.org/OSSIM/ossimPlanet.html>
- Rønning JS, Dalsegg E, Elvebakk H, Ganrød G, Tønnesen JF (2006) Geofysiske målinger Åknes og Tafjord. Report 2006.002 by the Geological Survey of Norway, (Norwegian text)
- Sherman WR, Penick MA, Su S, Brown TJ, Harris Jr FC (2007) VR Fire: an Immersive Visualization Experience for Wildfire Spread Analysis. IEEE Virtual Reality Conference, 10th – 14th March, 2007, Charlotte, North Carolina, USA, pp 243-246

Paper III

Is not included due to copyright

Paper IV

Statistical analysis of surface displacements – an example from the Åknes rockslide, western Norway

T. Nordvik¹ and E. Nyrnes²

¹Norwegian University of Science and Technology, Trondheim, Norway

²StatoilHydro Research Centre, Trondheim, Norway

Received: 3 December 2008 – Revised: 29 April 2009 – Accepted: 7 May 2009 – Published: 14 May 2009

Abstract. Analyses of displacement measurements may provide valuable insight into the characteristics and behaviours of landslides. This paper demonstrates the application of statistical analysis to displacement data collected with Global Positioning System (GPS), total stations and extensometers at the Åknes rockslide site, western Norway. The Åknes rockslide has particular interest due to the potential for catastrophic consequences if the rockslide accelerates into a rock avalanche and hits the fjord below. This would generate a tsunami in the adjacent fjord system and pose a threat to local settlements and infrastructure as well as to the many tourists visiting nearby areas. The analyses reported in this paper pay special attention to the newly available time series obtained from seven permanent GPS stations. The results from these continuously monitored GPS stations are believed to be an important contribution to the understanding of the complex displacement pattern evident from previous investigations. Results from the statistical analyses show that the displacement rates can be modelled as linear trends superimposed with periodic (sinusoidal) components. This indicates constant *average* displacement rates with no persistent accelerations. The annual displacement rates estimated from GPS and extensometer measurements range from a few millimetres to about 8 cm, whereas the periodical fluctuations typically have maximum amplitudes of 1–2 mm. Some interpretations of the periodical fluctuations are presented. High correlations between displacements and the groundwater level, measured in a borehole at the upper part of the slope, are evident for extensometers located across the back scarp. For the GPS control points located further down the slope, this correlation is, however, not so clear.

1 Introduction

This paper focuses on statistical analysis of displacement data and demonstrates the application of statistical methods to rock slope displacement data collected at the Åknes rockslide site, western Norway. The Åknes rockslide is among the world's most investigated rockslides (Ganerød et al., 2008). This rockslide has particular interest due to the potential for catastrophic consequences if the rockslide accelerates into a rock avalanche and hits the fjord below. This would generate a tsunami in the adjacent fjord system and pose a threat to local settlements and infrastructure as well as to tourists onboard the many cruise ships visiting the fjord located below the unstable rock slope. The objective of this paper is not to give a comprehensive evaluation of all available displacement data at Åknes, but rather to emphasize on the gain from using statistical methods as part of the overall landslide assessment methodology. Displacement measurements are often evaluated without paying much attention to their statistical properties. For example, this is the case when only visual examinations of raw-data plots are used. As statistical methods explicitly account for the statistical properties of the data, they may provide a more objective basis for data analysis.

The following list contains some key problems which will be addressed by the statistical analyses;

- Identify moving and stable control points by detection of statistically significant displacements.
- Estimate the displacement rate with corresponding confidence interval (CI) for each control point.
- Establish and quantify periodic variations in displacement rates.
- Estimate correlations between displacement rates and the groundwater level.



Correspondence to: T. Nordvik
(trond.nordvik@ntnu.no)



Fig. 1. Top: Location of the Åknes site. Bottom: A perspective view of the site. The boundary of the assumed unstable part of the slope is indicated with a green polygon.

- Identify control points showing similar displacement pattern.
- How to cope with imperfections in real world data, such as noise, offsets and missing observations as well as separating artefacts from actual displacements.

This paper starts with a brief description of displacement analysis in general. Then short introductions of the Åknes rockslide and the relevant displacement datasets are given. The core of this paper is the description of the methods used for analyzing displacement data from the Åknes rockslide along with the results obtained. Finally, some conclusions are drawn from the results.

1.1 Displacement analysis

Displacement or deformation analysis is an important tool for landslide assessment. The desired type of output from these analyses depends on a number of factors such as the objective of the analysis, the type of slide, the material in-

volved (clay, rock etc.) as well as the spatiotemporal resolution and accuracy of the available measurements. Caspary et al. (1990) describe a general approach for deformation analysis which may also serve as basis for landslide analyses. Most approaches for deformation analysis are closely related to Least Square (LS) estimation using the Gauss-Markov (GM) model which will be addressed in Sect. 2.2. In some applications the outcome from a deformation analysis is simply the identification of points showing significant displacement, in absolute position, between two or more epochs (e.g. Savšek-Safi et al., 2006), whilst in other applications the final outcome may be the identification blocks within a sliding area (e.g. Haberler-Weber, 2005) or the estimation of model parameters concerning translation, shear, rotation and scale, also known as strain estimation (e.g. Tzenkov and Gospodinov, 2003; Teza et al., 2008). The estimated model parameters are subsequently used for interpretations (e.g. Tzenkov and Gospodinov, 2003) and predictions of a slide's progress (e.g. Petly et al., 2002). As one of the major issues in displacement analyses is to detect *significant* displacement of individual control points or significant network deformations, statistical analyses and particularly hypothesis testing are essential tools. For example, the *global congruency test* (e.g. Cooper, 1987; Kennie and Petrie, 1990; Denli and Deniz, 2003) may be a useful first step towards the examination of the total deformation of a network between two epochs. If the observed deformation is small compared to the accuracy of the measurements, the network is regarded as congruent at those two epochs, otherwise the observed deformation is deemed significant, which usually requires further analyses. This may be the estimation of kinematics parameters such as velocity and acceleration (e.g. Sitros et al., 2004; Brückl et al., 2006; Pytharouli et al., 2007).

If time series data are available, spectral analysis may be a useful technique to establish periodical variations such as seasonal variations (e.g. Pytharouli et al., 2007). The most widely used spectral analysis is the Fourier analysis of which the basics are outlined in Sect. 2.3.

1.2 The Åknes rockslide

Åknes is located in western Norway (Fig. 1). In 2004, an extensive mapping and monitoring program was initiated for the unstable rock slope at Åknes. This program is still ongoing and includes, amongst others, various types of surface displacement measurements which form the basis for the statistical analyses reported in this paper. Kveldsvik et al. (2006) give a geological evaluation of the early displacement measurements collected at Åknes. They concluded that the Åknes rockslide currently was in a steady creep phase and that an accelerating phase is expected prior to a possible catastrophic failure.

The upper boundary of the unstable area is clearly defined by an 800 m long scarp located about 800–900 m above sea level. However, the extent and volume of the unstable

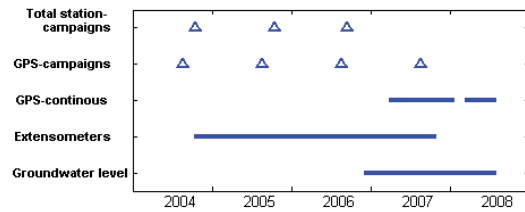


Fig. 2. Chronological overview of the datasets used in this paper.

rock mass, as well as the number and extents of the individual rock blocks involved, are not fully known. Nordvik et al. (2009) point out three different scenarios having volume estimates ranging from 20 to 85 million cubic metres. For a detailed description of the geological conditions at Åknes see Ganerød et al. (2008).

1.3 Description of data

Seven permanent GPS control points, three extensometer control points as well as the groundwater level were repeatedly measured for periods of time providing time series data. A number of total station control points and some additional GPS control points were only measured for a few epochs, denoted as survey campaigns in this paper, Fig. 2.

During a period of nearly 500 days, seven permanent GPS receivers have been operating at the Åknes rockslide site. Measurements were carried out as relative measurements using a GPS base station located at a fixed point close to the unstable rock slope. The locations of the control points and the base station together with the assumed boundaries of the unstable part of the rock slope are shown in Fig. 3.

The GPS antennas were mounted on top of about 3 meter tall aluminium pillars with cone-shaped caps to prevent snow and ice from interfering with the GPS signals. Six of the control points were located inside the suspected unstable part of the slope. The remaining control point (GPS 2) was located above the back scarp and thus assumed stable. During operation this control point was moved to a new location, a few metres away from the initial position, causing a shift in its time series.

The x-, y- and z-coordinates of the seven control points were recorded with a nominal sampling interval of 12 h. However, due to various circumstances this constant sampling interval was not maintained for the entire time series. For example; during a period of nearly 40 days, the power supply was down due to damages caused by lightning. Consequently no measurements were recorded during this period, leaving major gaps in the time series. Moreover, some settings related to the atmospheric correction model used for processing were also altered during operation. This is evident as shifts in the time series as well as changes in the noise levels (Fig. 4).

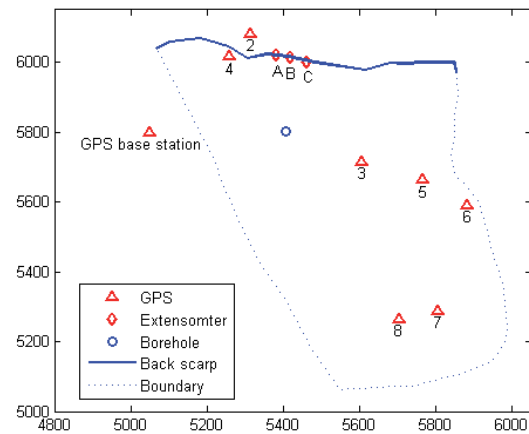


Fig. 3. Locations of permanent GPS and extensometer control points together with the assumed boundaries for the unstable part of the slope. (Coordinates are given in a local system; the transformation to UTM Zone 32 N is simply + 390 000 and + 6 890 000 for the x- and y-coordinate, respectively).

Data from three extensometers measuring the extension across the back scarp (Fig. 3) were included in this investigation. Even though the extensometer measurements were recorded with a nominal sampling interval of five minutes, only a single observation per day was considered for the analyses in this paper. An approximate orientation was measured for each extensometer. Assuming constant orientations of the extensometers, this allows for an approximate decomposition of the extensometer readings into changes in the x-, y- and z-direction. This is convenient for comparing results from extensometer with those obtained from GPS and total stations. However, the extensometers in question are oriented in the North-South direction along the slope; therefore changes in the x-components are not detectable.

As the groundwater level is assumed to have major influence on the displacement rates, daily groundwater records from a borehole located at the upper part of the slope (Fig. 3) were also considered for this investigation.

2 Methods

2.1 Principal component analysis

The Principal Components (PCs) are simply the eigenvectors of a (covariance) matrix. The eigenvector corresponding to the largest eigenvalue is denoted as the first principal component (PC1), the eigenvector corresponding to the second largest eigenvalue is denoted as the second principal component (PC2) and so on. Principal components depend solely on the covariance matrix of the data, and thus, their

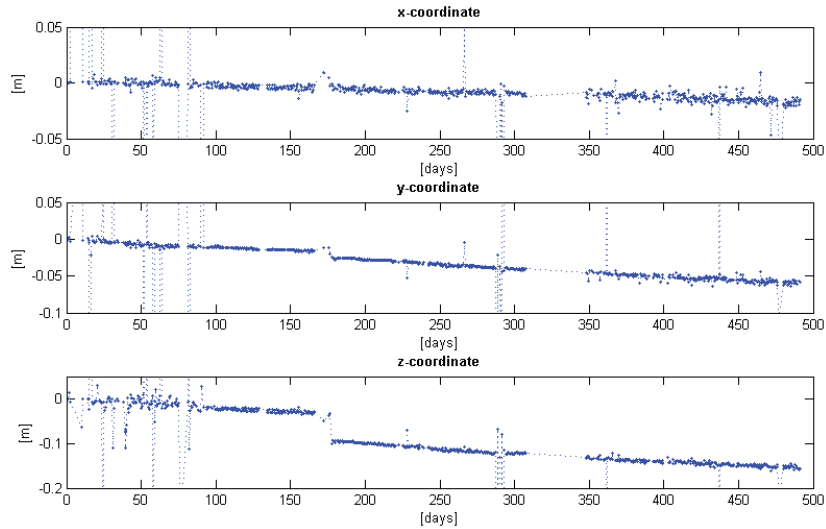


Fig. 4. Plots of raw GPS time series for point 4. (Day 0 corresponds to 26 March 2007).

development does not require a multivariate normal assumption (Johnson and Wichern, 2002). In this investigation Principal Component Analysis (PCA) is solely used for interpretation but PCA is also commonly used for data reduction purposes. The reader is referred to Johnson and Wichern (2002) and Davis (2002) for a more detailed description of PCA.

2.2 Trend estimation from time series

As a first step towards extracting the useful information from the available time series, trend models were fitted to each individual time series. This subsection outlines the chosen procedures and principles used for the trend modelling.

Each GPS control point has three corresponding time series; one for each of the x-, y- and z-coordinates. The recorded coordinates are given with respect to the UTM system. In order to get a more appropriate scale for the observations, the first observation from each series was simply subtracted from the subsequent observations to obtain Δx , Δy and Δz . Using delta values, as opposed to UTM coordinates, this eases human readability and is also preferable with respect to numerical stability.

Plots of the time series suggest linear trends (Fig. 4). However, there are a number of shifts which have to be considered as well as a number of gross errors, particularly at the first parts of the time series (Fig. 4). In order to calculate the magnitudes of the potential offsets, along with their significance levels, the models were extended with offset parameters which were estimated simultaneously with the other regression parameters. The estimated offsets for each of the

x, y, z time series were corrected before the corresponding absolute displacement (distance) time series were calculated.

To eliminate the major portion of gross errors, all delta values exceeding a discretionally chosen threshold were removed before the actual trend estimation.

In this paper, the parameter estimation is based on the GM model (e.g. Koch, 1999), where the expectation of the observations is described as linear combinations of unknown parameters. The GM model is defined by Eq. (1):

$$E(y) = X\beta = y + e \text{ with } \text{Cov}(y) = \text{Cov}(e) = \sigma^2 Q_{ee} = C_{ee} \quad (1)$$

where y is a vector of observations, β is a vector of unknown parameters, X is a known design matrix, Q_{ee} is the co-factor matrix of the errors e and σ^2 is the variance of unit weight, usually unknown. In this paper the errors e are assumed to be normally distributed; $e \sim N(0, \sigma^2 Q_{ee})$. The product of σ^2 and Q_{ee} is the error covariance matrix C_{ee} , and the inverse of Q_{ee} is the weight matrix; $P = Q_{ee}^{-1}$.

Assuming a GM model containing different regression parameters such as constant term, linear trend and offsets, the structure of the design matrix X is:

$$X = \begin{bmatrix} 1 & t_1 & 0 & \dots & 0 \\ 1 & t_2 & 0 & \dots & 0 \\ \vdots & \vdots & \vdots & \vdots & \vdots \\ 1 & t_k & 1 & \dots & 0 \\ 1 & t_{k+1} & 1 & \dots & 0 \\ \vdots & \vdots & \vdots & \vdots & \vdots \\ 1 & t_{n-1} & 1 & \dots & 1 \\ 1 & t_n & 1 & \dots & 1 \end{bmatrix} \text{ and } \beta = \begin{bmatrix} \beta_1 \\ \beta_2 \\ \vdots \\ \beta_u \end{bmatrix}, y = \begin{bmatrix} y_1 \\ y_2 \\ \vdots \\ y_n \end{bmatrix} \quad (2)$$

where the first and the second column of \mathbf{X} represent the constant term and linear trend respectively. Offset terms were introduced to model sudden unexpected shifts in the time series, and are represented by the digit one in the consecutive columns of \mathbf{X} . If no covariance information exists on the observations \mathbf{y} , the weight matrix \mathbf{P} is diagonal. Further, if the variances are equal, the weight matrix \mathbf{P} equals the identity matrix. The least squares estimates $\hat{\boldsymbol{\beta}}$ of the unknown parameters $\boldsymbol{\beta}$ are given by:

$$\hat{\boldsymbol{\beta}} = (\mathbf{X}^T \mathbf{P} \mathbf{X})^{-1} \mathbf{X}^T \mathbf{P} \mathbf{y} \text{ with } \text{Cov}(\hat{\boldsymbol{\beta}}) = \hat{\sigma}^2 (\mathbf{X}^T \mathbf{P} \mathbf{X})^{-1} = \hat{\sigma}^2 \mathbf{Q}_{\hat{\boldsymbol{\beta}}\hat{\boldsymbol{\beta}}} = \mathbf{C}_{\hat{\boldsymbol{\beta}}\hat{\boldsymbol{\beta}}} \quad (3)$$

where $\hat{\sigma}^2$ is the unbiased estimator of the variance σ^2 of unit weight obtained from:

$$\hat{\sigma}^2 = \frac{\hat{\mathbf{e}}^T \mathbf{P} \hat{\mathbf{e}}}{n - u} \quad (4)$$

where the quadratic form $\hat{\mathbf{e}}^T \mathbf{P} \hat{\mathbf{e}}$ is the residual sum of squares and $n - u$ is the degrees of freedom, i.e. the difference between the number of observations in \mathbf{y} and the number of unknowns in $\boldsymbol{\beta}$. The least squares estimates $\hat{\mathbf{e}}$ of the errors \mathbf{e} are the residuals, and can be obtained from Eq. (5):

$$\hat{\mathbf{e}} = \mathbf{X} \hat{\boldsymbol{\beta}} - \mathbf{y} \text{ with } \text{Cov}(\hat{\mathbf{e}}) = \hat{\sigma}^2 [\mathbf{Q}_{ee} - \mathbf{X}(\mathbf{X}^T \mathbf{P} \mathbf{X})^{-1} \mathbf{X}^T] = \hat{\sigma}^2 \mathbf{Q}_{\hat{\mathbf{e}}\hat{\mathbf{e}}} \quad (5)$$

After the first coarse approach for removal of obvious blunders, a certain amount of potential gross errors remained. The process of removing the remaining gross errors was carried out by analysing the standardized residuals. A standardized residual \hat{d}_i is defined by:

$$\hat{d}_i = \frac{\hat{e}_i}{\hat{\sigma}} \quad (6)$$

that is, each residual \hat{e}_i is divided by the estimated standard deviation of unit weight. The standardized residuals have zero mean and approximately unit variance (Montgomery et al., 2001). All observations corresponding to a standardized residual greater than 3.0 were considered as gross errors and removed from the dataset.

The hypotheses for testing the significance of the j th parameter β_j can be expressed as:

$$H_0 : \beta_j = 0 \text{ versus } H_1 : \beta_j \neq 0, j \in \{0, 1, \dots, u - 1\} \quad (7)$$

The test statistic for testing the above hypotheses is given by:

$$t_0 = \frac{\hat{\beta}_j}{\sqrt{\mathbf{C}_{jj}}} \quad (8)$$

where \mathbf{C}_{jj} is the variance of $\hat{\beta}_j$, i.e. the j th diagonal element in the covariance matrix $\mathbf{C}_{\hat{\boldsymbol{\beta}}\hat{\boldsymbol{\beta}}}$. The null hypothesis H_0 is rejected if:

$$|t_0| > t_{\alpha/2, n-u-1} \quad (9)$$

where α is the significance level of the test and $t_{\alpha/2, n-u-1}$ is the upper $\alpha/2$ quantile of a Student's t -distribution with $n-u-1$ degrees of freedom. A rejection of H_0 implies that the actual parameter β_j is significantly different from zero, and should therefore be included in the model. A significance level α of 5% is used for all hypotheses testing in this paper.

Processing one time series at a time, a complete model containing all possible regression parameters was first fitted to the time series. Then the parameter yielding the smallest absolute value of test statistic in Eq. (8) was chosen for deletion and a new least squares estimation was performed. The same procedure was repeated until only significant parameters remained. This parameter selection approach is known as Backward Elimination (e.g. Miller, 2002).

2.3 Spectral analysis

The residuals obtained from the final trend models were further investigated by spectral analysis to detect possible periodic components in the time series. The most common spectral decomposition technique is the Fourier transform which enables the decomposition of any periodic function into a set of cosine and sine components that represent the frequency spectre. In order to apply Fourier analysis, the data should be equidistant. This implies that there should be no gaps within the time series. For the time series in question, this requirement was not met as there were subintervals with missing observations. Moreover, removal of gross errors also caused additional gaps in the time series which had to be corrected. The initial residuals were therefore interpolated to obtain equidistant data. However, no interpolations were carried out for the "missing residuals" within the longer gaps (>10 days); these were simply set to zero.

Using the discrete Fourier transform, a time series $y(t)$ can be represented as in Eq. (10) (Wei, 1990).

$$y(t) = \sum_{k=0}^{n/2} [a_k \cos(2\pi kt/n) + b_k \sin(2\pi kt/n)], \quad t = 1, 2, \dots, n \quad (10)$$

Equation (10) can be set up as a GM model (Sect. 2.2) and the LS method can be used for estimation of the Fourier coefficients a_k and b_k . A model containing only a single wave component with frequency ω_1 has the following structure:

$$\mathbf{X} = \begin{bmatrix} \cos(\omega_1 t_1) & \sin(\omega_1 t_1) \\ \cos(\omega_1 t_2) & \sin(\omega_1 t_2) \\ \vdots & \vdots \\ \cos(\omega_1 t_n) & \sin(\omega_1 t_n) \end{bmatrix}, \quad \boldsymbol{\beta} = \begin{bmatrix} a_1 \\ b_1 \end{bmatrix}, \quad \mathbf{y} = \begin{bmatrix} y_1 \\ y_2 \\ \vdots \\ y_n \end{bmatrix} \quad (11)$$

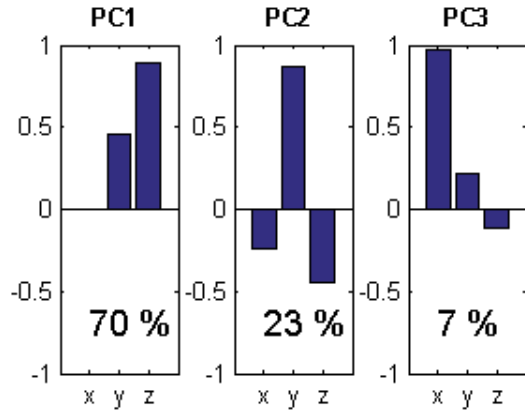


Fig. 5. Coefficients of the Principal Components (PCs) calculated from displacement vectors derived from GPS and total station surveys (cf. Figs. 6 and 7). The x-coefficient of PC1 is zero; this means that PC1 lies in the yz-plane. The percentage associated with each PC is the portion of the total variability explained by this PC.

Each new Fourier frequency introduced adds two new columns to the design matrix \mathbf{X} ; one cosine term and one sine term as well as the two corresponding Fourier coefficients to the parameter vector β . The \mathbf{y} vector contains residuals from a trend model. If only the Fourier frequencies are used, the estimated coefficients \hat{a}_k and \hat{b}_k will be uncorrelated as the Fourier frequencies form an orthogonal basis. The first Fourier frequency is obtained from $\omega_1=2\pi/T$, where T denotes the total time span of the time series. For a unit sampling frequency, T equals n . Consecutive Fourier frequencies are obtained by $\omega_k=k\omega_1$, where $k=2, 3, \dots, n/2$, and their amplitudes are obtained from:

$$\hat{A}_k = \sqrt{\hat{a}_k^2 + \hat{b}_k^2} \tag{12}$$

The significance of a single wave component k is evaluated by means of its contribution to the weighted sum of squares. Relevant hypotheses become:

$$H_0 : a_k = b_k = 0 \text{ versus } H_1 : a_k \neq 0 \vee b_k \neq 0 \tag{13}$$

The null hypothesis H_0 is rejected if:

$$F = \frac{(\mathbf{y}^T \mathbf{P} \mathbf{y} - \hat{\mathbf{e}}^T \mathbf{P} \hat{\mathbf{e}})/2}{(\hat{\mathbf{e}}^T \mathbf{P} \hat{\mathbf{e}})/(n-2)} > F_{(2, n-2, \alpha)}, \tag{14}$$

that is, if the test statistic F exceeds the upper α -percentage point of a Fisher distribution with 2 and $n-2$ degrees of freedom. In case of equal variance and uncorrelated observations, the weight matrix \mathbf{P} becomes the identity matrix which can be omitted from Eq. (14). The same test statistics (Eq. 14) can also be used for testing the simultaneous significance of a set of wave components, providing that the

degrees of freedom are updated accordingly. However, in this paper only one wave component was reported for each time series; the one that gave the largest value of the test statistic in Eq. (14).

2.4 Testing for equality of displacement vectors

A relevant question with respect to displacement analyses is whether two or more vectors are equal, i.e. whether the estimates $\hat{\mathbf{x}}_i$ and $\hat{\mathbf{x}}_j$ of two different displacement vectors have the same expectation value:

$$H_0 : E(\hat{\mathbf{x}}_i) = E(\hat{\mathbf{x}}_j) \text{ versus } H_1 : E(\hat{\mathbf{x}}_i) \neq E(\hat{\mathbf{x}}_j) \tag{15}$$

Under the assumption of normally distributed and uncorrelated displacement vectors;

$$\hat{\mathbf{x}}_i \sim N(\boldsymbol{\mu}_i, \mathbf{C}_i) \text{ and } \hat{\mathbf{x}}_j \sim N(\boldsymbol{\mu}_j, \mathbf{C}_j) \text{ with } \text{Cov}(\hat{\mathbf{x}}_i, \hat{\mathbf{x}}_j) = \mathbf{0}, \tag{16}$$

the null hypothesis H_0 can be evaluated by means of a chi-squared distributed random variable. The null hypothesis is rejected if:

$$T^2 = (\hat{\mathbf{x}}_i - \hat{\mathbf{x}}_j)^T (\mathbf{C}_i + \mathbf{C}_j)^{-1} (\hat{\mathbf{x}}_i - \hat{\mathbf{x}}_j) > \chi_{k, \alpha}^2 \tag{17}$$

where $\chi_{k, \alpha}^2$ is the upper α quantile of the chi-squared distribution with k degrees of freedom. In this case k equals 3, i.e. the dimension of the displacement vectors.

2.5 Cross-correlation

The cross-covariance between two jointly stationary stochastic processes x_t and y_t with lag parameter k is defined by (Wei, 1990):

$$\gamma_{xy}(k) = E[(x_t - \mu_x)(y_{t+k} - \mu_y)], \tag{18}$$

$$k \in \{0, \pm 1, \pm 2, \dots\},$$

where the index t refers to an observation made at time t . For large de-trended samples of size n with constant variance, the estimated cross-covariance is obtained from:

$$\hat{\gamma}_{xy}(k) = \frac{1}{n} \sum_{t=0}^{n-k-1} x_t y_{t+k} \tag{19}$$

The conversion from cross-covariance to cross-correlation involves the normalization;

$$\hat{\rho}_{xy}(k) = \frac{\hat{\gamma}_{xy}(k)}{\hat{\sigma}_x \hat{\sigma}_y}, \tag{20}$$

where $\hat{\sigma}_x$ and $\hat{\sigma}_y$ are the estimated standard deviations of x_t and y_t .

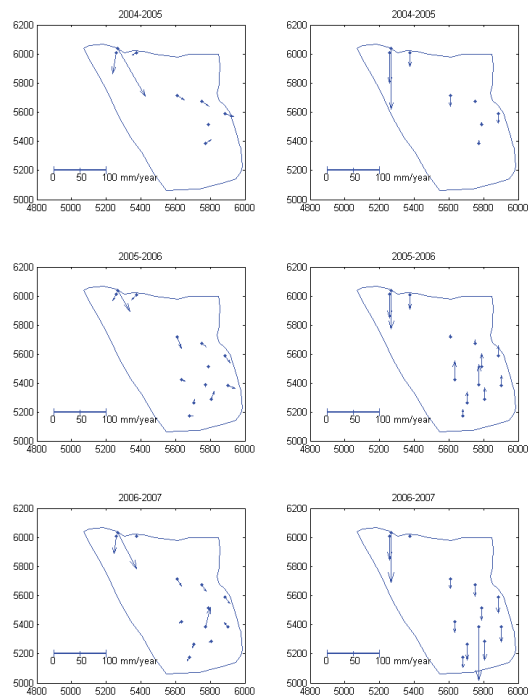


Fig. 6. Displacement vectors derived from GPS survey campaigns. Left column: horizontal displacements. Right column: vertical displacements.

3 Results

A principal component analysis was carried out for displacement vectors derived from GPS and total station survey campaigns (Fig. 5). The principal components are simply a rotation (orthogonal transformation) of the three initial coordinate axes such that the first principal component (PC1) represents the direction of most variability in the displacements. PC1 roughly corresponds to the down slope direction which is sensible since the largest displacement vectors go in this direction together with the fact that some of the control points show displacements close to zero. PC2 indicates the direction orthogonal to PC1 showing the second largest displacement variability. The direction of PC2 roughly corresponds to the slope's normal vector. The direction of PC3, orthogonal both to PC1 and PC2, roughly corresponds to the across slope direction. That is, there is the least variability in displacement across the slope.

Figures 6 and 7 show displacement vectors derived from GPS and total station survey campaigns carried out in 2004, 2005, 2006 and 2007. These vectors were obtained by taking the differences between LS adjusted coordinates at two consecutive epochs.

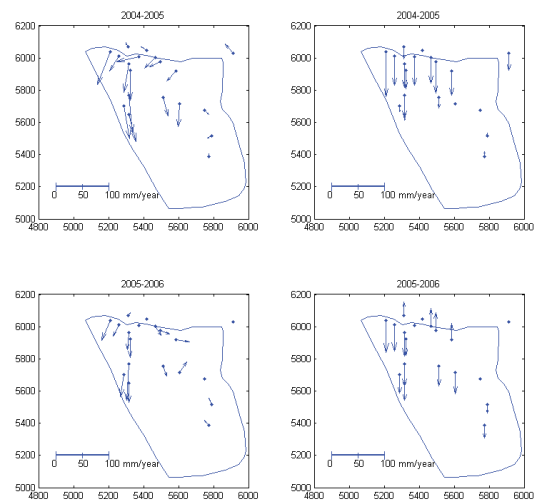


Fig. 7. Displacement vectors derived from total station survey campaigns. Left column: horizontal displacements. Right column: vertical displacements.

An example of fitted trend models is shown in Fig. 8. Figure 9 shows displacement-vectors derived from time series (comparable to those shown in Figs. 6 and 7). The estimated annual displacements and the most significant periodic components are listed in Tables 1 and 2. The periodic components corresponding to the middle time series in Fig. 8, i.e. for the y-coordinate, are shown in Figs. 10 and 11.

Spectral analysis of the time series for the groundwater level shows that the most significant period is 378 days with corresponding amplitude of 1.62 m.

From Fig. 9 the question arises whether the displacements vectors for point 3, 5 and 6 are equal, meaning that the observed deviations in directions and magnitude are only caused by random errors. This question can be summarised by the following hypotheses;

$$H_0 : E(\hat{x}_3) = E(\hat{x}_5) = E(\hat{x}_6) \text{ versus } H_1 : E(\hat{x}_3) \neq E(\hat{x}_5) \vee E(\hat{x}_3) \neq E(\hat{x}_6) \vee E(\hat{x}_5) \neq E(\hat{x}_6) \quad (21)$$

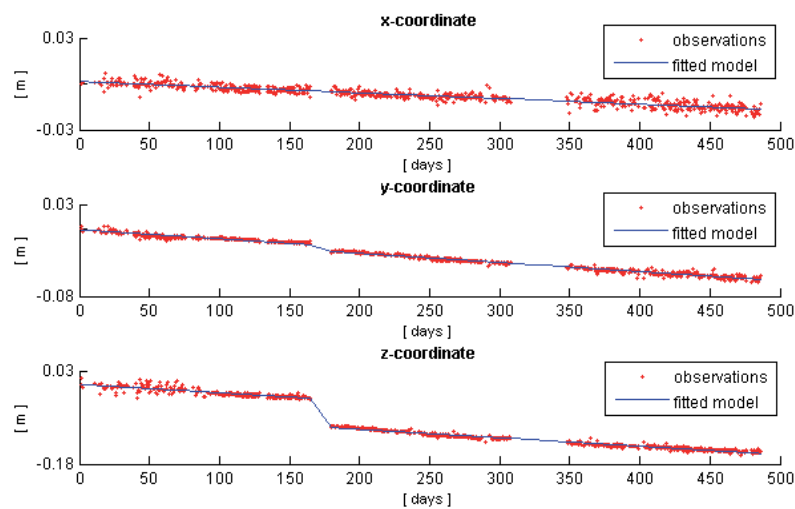
These hypotheses can be tested by splitting into vector pairs. Test statistics from Eq. (17), for each feasible vector pair, are shown in Table 3. The null hypothesis H_0 is rejected if at least one individual test statistics exceeds the critical value. Table 3 shows that all individual test statistics far exceed the critical value. Consequently, H_0 was rejected.

A cross correlation analysis of displacements and the groundwater level in a borehole located in the upper part of the unstable slope was carried out. All datasets were detrended before the cross correlations were calculated. The results indicate strong correlations ($|\rho_{xy}| > 0.7$) between the

Table 1. Absolute displacements (distance). Linear trends and most significant periodic components from GPS and extensometer time series.

Point	Trend [mm/year]	95% CI for trend [mm/year]	Period [days]	Amplitude [mm]
GPS 2	2.8	[2.3, 3.2]	162	0.8
GPS 3	30.6	[29.6, 31.5]	66	0.8
GPS 4	81.4	[80.5, 82.4]	134	1.6
GPS 5	17.6	[17.0, 18.2]	6	0.6
GPS 6	25.8	[25.2, 26.5]	22	0.8
GPS 7	14.7	[13.3, 16.2]	333	1.6
GPS 8	4.9	[3.8, 6.0]	46	1.3
Ext A	13.3	[13.2, 13.4]	>	>
Ext B	23.0	[22.9, 23.1]	>	>
Ext C	15.3	[15.3, 15.4]	355	0.7

> indicates long periods which can not be reliably established from the current time series.

**Fig. 8.** Example of trend models. Linear trend models containing offset terms fitted to the time series of GPS control point 4 (correspond to the raw observations in Fig. 4).

groundwater level and the displacements measured by the extensometers at the back scarp (Table 4, Fig. 12). Increase in displacements for extensometer A and B tends to occur about three weeks after increase in groundwater level. For extensometer C the situation is, however, different as the maximum absolute correlation appears at lag zero. The correlation for extensometer C is negative which indicates that the displacement rate tends to slow down as the groundwater level increases. There are no strong correlations between groundwater level and displacements for the GPS control points (Table 4).

4 Discussion

The PCA carried out here is regarded as part of the exploratory analysis to gain overview of the situation. Not surprisingly, most of the variability is related to the down slope movement and subsidence of the slide (PC1 and PC2). The portion explained by PC3 is probably mostly due to observational noise.

As the GPS data were sampled with at least 12 h time spacing, the autocorrelation was neglected for these observations. The offsets detected from the GPS time series might correspond to minor failures in the slope but this is considered as highly unlikely as the same offset features are present for most of the GPS control points, but are not detectable from the extensometer time series.

Table 2. Linear trends and most significant periodic components in x-, y- and z-direction from GPS time series.

Point	Coordinate	Trend [mm/year]	95% CI for trend [mm/year]	Period [days]	Amplitude [mm]
GPS 2	x	–	–	>	>
	y	–2.8	[–4.0, –1.8]	158	0.8
	z	–	–	118	2.5
GPS 3	x	12.8	[12.3, 13.3]	118	0.7
	y	–23.5	[–24.2, –23.0]	172	0.4
	z	–14.2	[–15.9, –12.5]	62	1.1
GPS 4	x	–13.5	[–13.9, –13.1]	29	0.5
	y	–39.9	[–40.5, –39.2]	339	0.8
	z	–69.3	[–70.7, –67.8]	134	1.7
GPS 5	x	11.2	[10.4, 12.1]	127	0.8
	y	–9.4	[–10.0, –8.7]	55	0.4
	z	–9.8	[–11.3, –8.3]	23	1.1
GPS 6	x	16.2	[14.0, 18.5]	120	0.7
	y	–17.9	[–19.6, –16.3]	176	0.8
	z	–7.7	[–9.7, –5.7]	23	1.8
GPS 7	x	–10.9	[–13.8, –8.1]	282	1.2
	y	–	–	159	0.6
	z	8.9	[2.9, 14.9]	16	1.8
GPS 8	x	4.6	[3.0, 6.2]	62	1.2
	y	1.7	[0.9, 2.6]	203	0.6
	z	–	–	147	2.1

– indicates non-significant values.

> indicates long periods which can not be reliably established from the current time series.

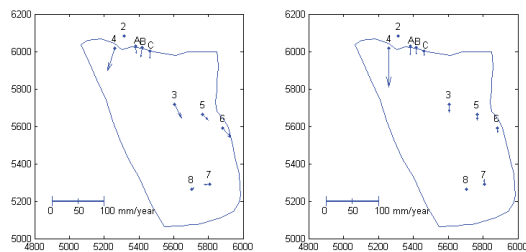


Fig. 9. Displacement vectors derived from GPS and extensometer time series. Left: horizontal displacements. Right: vertical displacements.

From the GPS time series, trends were estimated both for the absolute displacements (i.e. when only distances were considered) and for the individual coordinates x, y and z. All continuously monitored control points show significant displacements for at least one of their coordinates. This applies even to control point 2 which was assumed stable. Even though the estimated annual displacement for control point 2 is less than 3 mm, this calls for further monitoring.

The estimated periodic components for the y-coordinate of GPS 4 (339 days, Table 2) as well as for Ext C (355 days, Table 1) are likely caused by changes in the groundwater level

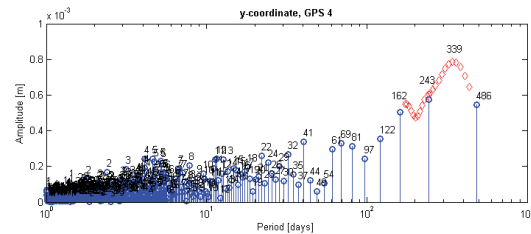


Fig. 10. Periodogram for the y-coordinate of GPS 4. Each vertical line represents a Fourier frequency with the corresponding wavelength indicated above. To obtain the most significant frequency for this time series, the Fourier frequency having the largest amplitude (wavelength 243) was used as a starting point. Repeated calculations, using only one periodic component, were then carried out until an approximate optimum frequency was reached (wavelength 339, cf. Fig. 11).

as the most significant periodic component for the groundwater level is also close to one year. Some of the time series show periodic components close to six months e.g. the y-coordinates of GPS 3 and GPS 6 (172 and 176 days respectively, Table 2) which indicate bi-annual variations. This may be related to snowmelt in the spring and increased precipitation in the autumn. Moreover, the time series for the y-coordinates of GPS 2, GPS 7 and GPS 8 (158, 159 and

Table 3. Test statistics regarding equality of displacement vectors.

Vector combination i, j	Test statistic ($T_{i,j}^2$)	$T_{i,j}^2 > \chi_{3,0.05}^2 = 7.81$
3, 5	1026	Yes
3, 6	72	Yes
5, 6	109	Yes

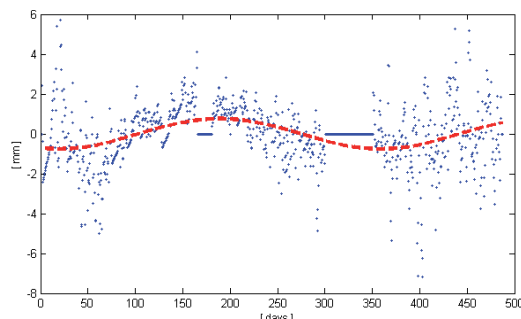
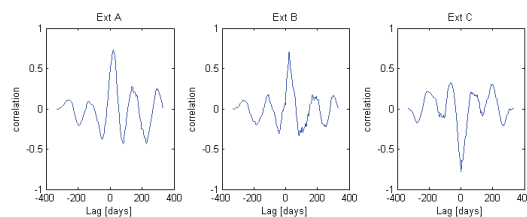
Table 4. Cross-correlations between groundwater level and absolute displacements.

Control point	ρ_{xy} [-1, 1]	Lag [days]
GPS 2	0.32	-54
GPS 3	0.20	-45
GPS 4	-0.22	9
GPS 5	0.18	-42
GPS 6	0.20	-51
GPS 7	0.29	-16
GPS 8	-0.27	48
Ext A	0.73	21
Ext B	0.71	22
Ext C	-0.78	0

203 days respectively, Table 2) may also be related to this bi-annual variation but their estimated periods may be affected both by noise in the observations as well as the physical conditions of the rocks lope.

A well known problem when dealing with real world time series is that the total time span is too short to prove the existence of the longer periods. This applies to some of the time series analyzed here (e.g. Ext A and Ext B, Table 1). For example, Pytharouli et al. (2007) established the existence of periods between 4 and 7.5 years for two landslides in Greece. Moreover, it can be considered as a trade off whether to use the “fixed set” of Fourier frequencies which are uncorrelated but indirectly determined by the total length of the time series, or to use an arbitrary (probing) frequency being the optimal. If any arbitrary frequency is used, this implies some limitations with respect to interpretation of consecutive frequency estimates as these will no longer be uncorrelated. If the frequencies in question correspond to long wavelengths, with respect to the total time span, the approximation errors introduced by using Fourier frequencies are generally more notable. Therefore, in this paper only the single optimal frequencies, in terms of highest test statistic in Eq. (14), were listed. However, this implies that remaining periodical components are omitted even though they may be statistically significant. All periodical components reported in this paper were statistically significant which gives good indications that these periods are realistic, even though some of them are long compare to the total time span of the time series.

An important issue associated with the spectral analysis is

**Fig. 11.** Periodic fluctuations. The most significant wave component is fitted to the y-coordinate of GPS 4. The period is 339 days and the amplitude is approximately 0.8 mm. The peak appears in early autumn as day 0 corresponds to 26 March 2007. (Apparent artefacts stem from interpolation and insertion of “zero-residuals” to get equidistant data).**Fig. 12.** Cross-correlations between groundwater level in borehole and displacements for extensometer A, B and C.

to separate the periodical components related to un-modelled effects from those related to the actual displacement of the rock slope. As the GPS measurements were calculated as relative measurements i.e. as vectors from a fixed base station, one should not expect to find the typical periodical components as for absolute GPS measurements such as ocean loading, Earth tide and the Chandler wobble. However, there may be other periodical components that can affect the time series but still not related to the physical motion of the rock slope. For example, the heat expansion of the aluminium pillars, used as base for the GPS antennas, will be in the order of magnitude 2 mm from one extreme to the other assuming a variation in temperature of 30 degrees Celsius (thermal expansion coefficient for Aluminium is $2.3 \cdot 10^{-5}$ m/m K). It is assumed that the heat expansion effect will even out with respect to the trend estimates but will contribute to the observed noise as well as to the periodical components, though mainly on the z-coordinate. The contribution to the periodical components may be both to the seasonal variations as well as to the diurnal variations. The latter will appear as noise in the measurements due to the short wavelengths with respect to the sampling interval. As the amplitudes for the

periodic components detected for the z-coordinates for some of the control points are in the order of magnitude 2 mm, they are likely influenced by the heat expansion of the pillars.

The time series used in this investigation were not fully ideal for spectral analysis, as there were some violations of the conditions of the Fourier analysis such as offsets, blunders and variable noise levels as well as missing observations which had to be corrected. Among others, this required interpolation to get equidistant data. This interpolation may indeed influence the results from the spectral analysis. In order to get an idea of how the results were affected, various interpolations methods such as linear, nearest neighbour and cubic splines were tested. However, the choice of interpolation method seemed to only have minor influences on the resulting periods. Also, imperfections in the trend model may affect the outcome from spectral analysis. Parameter estimates will generally be affected depending on whether all parameters are estimated simultaneously or the trend part is estimated separately i.e. before the periodical components are estimated. Some limited testing indicated, however, that this effect is relatively small. Therefore the estimation was carried out in a two step manner by first removing the linear trends before the periodical components were estimated from the resulting residuals. Moreover, inserting zero-residuals within the gaps probably caused some reduction of the estimated amplitudes of the periodic components.

All extensometers show high correlation with the groundwater level (Table 4, Fig. 12). However, the behaviour of Ext A and Ext B are probably affected by some fractures in the vicinity of these extensometers. Therefore, Ext C is regarded as the most representative for the upper part of the slope. Correlations for the other GPS control points were low (Table 4) and therefore considered as neglectable from a practical point of view.

It is already established that there are certain periodic variations in displacement rates at the Åknes rockslide due to seasonal variations in precipitation and temperature. During spring and autumn the displacement rates are larger due to snowmelt and increased precipitation, respectively (Grøneng et al., 2009). However, statistical evaluations carried out in this analysis provide a formalized means for quantifying these relations which may be useful both for interpretation and prediction of future displacements.

Even though some of the time series, particularly those from extensometers, can be well described by higher order polynomials, it is advantageous to use a model based on linear trends combined with periodical components. With respect to prediction of future displacements, the performance of a model based on higher order polynomials may be completely unsatisfactory outside the observation interval. Moreover, interpreting estimated model parameters from linear trend models with periodic components are more straightforward than for higher order polynomial models.

On the basis of the analysis reported in this paper some recommendations regarding design of future displacement

measurements can be given; the continuous measurements are preferably to the yearly survey campaigns. This is evident from the currently available GPS time series. If the displacement vectors were derived from the difference in coordinate values, from the mean of the initial part of the time series to the mean of the end of the same time series, this would lead to erroneous results compare to the displacement rates derived from trend estimates. This is a result of the offsets within the time series (Fig. 8). Similarly, the contradictions between *vertical* displacements, in the south-eastern part of the slope, for the period 2005–2006 (Figs. 6, 7) were most likely caused by a systematic error (vertical shift) related to the GPS measurements carried out in 2006.

Moreover, a larger number of control points and better spatial coverage of the unstable area is preferable with respect to future analyses. More control points located at the assumed stable parts of the slope may also be beneficial. As there may be un-modelled effects related to the GPS measurements, more control points located at the stable parts of the slope would help identifying such un-modelled effects as well as being a validation of the estimated accuracy. However, in most cases there will be practical limitations regarding the number and locations of the control points. For the Åknes case, some parts of the slope are exposed to frequent snow avalanches whereas others have limited GPS satellite coverage which makes those areas less suitable.

5 Summary and conclusions

A statistical approach for analyzing various types of surface displacement data is presented. Different displacement datasets, including data from survey campaigns, carried out with GPS and total stations, as well as time series from continuously monitored GPS and extensometers control points, were analysed. These datasets were collected at the Åknes site in western Norway, one of the world's most investigated rockslides.

The main focus for this investigation was time series analysis. Results from time series analyses show that displacements at Åknes can be modelled as linear trends superimposed with periodic components. This means that there are periodical fluctuations but no *persistent* acceleration.

The annual displacement rates, estimated from GPS and extensometer time series, range from a few millimetres to about 8 cm, whereas the periodical fluctuations typically have maximum amplitudes of 1–2 mm. Some of the estimated periodic components show annual or biannual variations which are most likely caused by changes in groundwater level, precipitation and snowmelt.

High correlations between displacements and the groundwater level, measured in a borehole at the upper part of the slope, were evident for extensometers located across the back scarp. However, for the GPS control points located further

down the slope, the correlations were low and therefore considered as neglectable from a practical point of view.

The three most similar displacement vectors, derived from GPS time series, were formally tested for equality by means of hypothesis testing. The hypothesis regarding equality was rejected. This supports the complex displacement pattern evident from previous GPS and total station survey campaigns as well as the assumption of a number of individual moving blocks.

Some data sets, particularly the GPS time series, were not fully ideal in terms of missing observations, offsets and gross errors. These problems were resolved by various techniques such as gross error removal, interpolation and offset estimation. However, such flaws in data make additional contributions to the uncertainties associated with the estimated displacements.

We believe that the statistical approach reported in this paper can be useful to other landslide assessments as well as for future analyses of the Åknes rockslide.

Acknowledgement. Thanks to T. Eiken, University of Oslo, for providing results from LS adjustment of GPS and total station survey campaigns. We also thank H. Nahavandchi, Norwegian University of Science and Technology and T. A. Haakonsen, Trondheim municipality, for valuable comments and suggestions regarding spectral analysis. L. H. Blikra and G. Grøneng, Norwegian University of Science and Technology, are acknowledged for their useful comments regarding geological aspects.

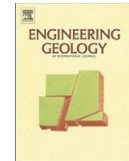
Edited by: T. Glade

Reviewed by: J. Dehls and another anonymous Referee

References

- Caspary, W. F., Haen, W., and Borutta, H.: Deformation analysis by statistical methods, *Technometrics*, 32, 49–57, 1990.
- Brückl, E., Brunner, F. K., and Kraus, K.: Kinematics of a deep seated landslide derived from photogrammetric, GPS and geophysical data, *Eng. Geol.*, 88, 149–159, 2006.
- Cooper, M. A. R.: Control surveys in civil engineering, Collins Publisher, London, UK, 1987.
- Davis, J. C.: *Statistics and Data Analysis in Geology*, 3rd ed., John Wiley & Sons, USA, 2002.
- Denli, H. H. and Deniz, R.: Global Congruency Test Methods for GPS Networks, *J. Surv. Eng.*, 129, 95–98, 2003.
- Ganerød, G. V., Grøneng, G., Rønning, J. S., Dalsegg, E., Elvebakk, H., Tønnesen, J. F., Kvelde, V., Eiken, T., Blikra, L. H., and Braathen, A.: Geological Model of the Åknes Rockslide, western Norway, *Eng. Geol.*, 102, 1–18, 2008.
- Grøneng, G., Christiansen, H. H., and Blikra, L. H.: Meteorological Control on Seasonal Rock Deformation in the Åknes Sliding Area, Western Norway, in preparation, 2009.
- Haberler-Weber, M.: Analysis and interpretation of geodetic landslide monitoring data based on fuzzy systems, *Nat. Hazard. Earth Sys.*, 5, 755–760, 2005.
- Johnson, R. A. and Wichern, D. W.: *Applied Multivariate Statistical Analysis*, 5th ed., Prentice Hall, New Jersey, USA, 2002.
- Kennie, T. J. M. and Petrie, G.: *Engineering surveying technology*, Thomson Litho Ltd, Scotland, 1990.
- Koch, K. R.: *Parameter estimation and hypothesis testing in linear models*, 2nd ed., Springer-Verlag, Germany, 1999.
- Kvelde, V., Eiken, T., Ganerød, G. V., Grøneng, G., and Ragvin, N.: Evaluation of movement data and ground conditions for the Åknes rock slide, *The International Symposium on Stability of Rock Slopes*, The African Institute of Mining and Metallurgy, 279–299, 2006.
- Miller, A. J.: *Subset selection in regression*, 2nd ed., Chapman & Hall/CRC, 2002.
- Montgomery, D. C., Peck, E. A., and Vining, G. G.: *Introduction to linear regression analysis*, 3rd ed. John Wiley & Sons, USA, 2001.
- Nordvik, T., Grøneng, G., Ganerød, G. V., Nilsen, B., Harding, C., and Blikra, L. H.: Geovisualization, geometric modelling and volume estimation of the Åknes rockslide, western Norway, *B. Eng. Geol. Environ.*, 68(2), 245–256, doi:10.1007/s10064-009-0198-x, 2009.
- Petly, D. N., Bulmer, M. H., and Murphy, W.: Patterns of movement in rotational and translational landslides, *Geology*, 30, 719–722, 2002.
- Pytharouli, S. I., Kontogianni, V. A., and Stiros, S. C.: Kinematics of two deep-seated landslides in Greece, *Geotechnical Engineering*, 160, 179–183, 2007.
- Savšek-Safie, S., Ambrožič, T., Stopar, B., and Turk, G.: Determination of Point Displacements in the Geodetic Network, *J. Surv. Eng.-ASCE*, 132, 58–63, 2006.
- Sitros, S. C., Vichas, C., and Skourtis, C.: Landslide Monitoring based on geodetically derived distance changes, *J. Surv. Eng.-ASCE*, 130, 156–162, 2004.
- Teza, G., Pesci, A., Genevois, R., and Galgaro, A.: Characterization of landslide ground surface kinematics from terrestrial laser scanning and strain field computation, *Geomorphology*, 97, 424–437, 2008.
- Tzenkov, T. and Gospodinov, S.: Geometric Analysis of Geodetic Data for Investigation of 3D Landslide Deformations, *Natural Hazard Review*, 4, 78–81, 2003.
- Wei, W. W. S.: *Time Series Analysis*, Addison-Wesley Publishing Company, USA, 1990.

Paper V



Statistical analysis of seasonal displacements at the Nordnes rockslide, northern Norway

Trond Nordvik^{a,b,*}, Lars Harald Blikra^{a,c}, Erik Nyrnes^d, Marc-Henri Derron^a

^a Geological Survey of Norway, Trondheim, Norway

^b Division of Geomatics, Norwegian University of Science and Technology, N-7491 Trondheim, Norway

^c Åknes/Tafjord Early Warning Centre, Stranda, Norway

^d Statoil Research Centre, Trondheim, Norway

ARTICLE INFO

Article history:

Received 5 May 2009

Received in revised form 21 April 2010

Accepted 24 April 2010

Available online 4 May 2010

Keywords:

Rockslide

Displacements

Seasonal displacements

Permafrost

Statistical analysis

Lasers

Crackmeters

ABSTRACT

The Nordnes rockslide in northern Norway poses a threat to local settlements along the nearby fjord due to its potential of generating tsunamis. Therefore, a monitoring program was initiated in 2007. Evaluation of the resulting monitoring data is expected to provide important contributions to the understanding of the sliding mechanisms.

This paper focuses on statistical analyses of continuous laser and crackmeter measurements at the Nordnes rockslide during a period of 16 months. Annual linear displacements and seasonal fluctuations were estimated from time series of 3 lasers and 10 crackmeters.

Results from the analyses show that the north-westernmost part of the area has the largest movement of more than 5 cm per year, which makes this part the most critical in terms of generation of a rapid rockslide. The amplitudes of the seasonal fluctuations estimated from crackmeter time series were approximately 0.5 mm. The largest displacements clearly occur in autumn and early winter with a stagnation or retreat phase in spring and summer. Thus, the movements are not increased during snowmelt which is a normal seasonal characteristic elsewhere. Although the temperature changes have a significant effect on the observed displacements, the seasonal variations could not fully be modelled with temperature terms in the regression models suggesting that there are other additional controlling factors. The rockslide is localized in arctic and periglacial conditions, and the documented seasonal variations are interpreted to be linked to effects of deformations caused by seasonal frost and permafrost.

Prediction intervals for future displacements were also derived from the current time series. These prediction intervals are considered useful for the evaluation of future measurements and may serve as basis for defining alert thresholds for possible future early warning systems.

© 2010 Elsevier B.V. All rights reserved.

1. Introduction

Forecasting of the failure of landslides is a difficult and complex task, but yet crucial due to the potentially serious consequences to the society (Crosta and Agliardi, 2003; Jaboyedoff et al., 2004). Special attention has been given to the use of 1/velocity relationship for the forecasting of accelerating landslide events, as exemplified by the Vaiont rockslide in Italy (Petley, 2006). The evaluation of the monitoring and deformation data is thus crucial for our ability to perform the best forecasting of landslide failures. It is particularly important to analyse data to establish the general trends as well as seasonal effects and erroneous observations. This in turn enables discrimination of expected variations in the rate of displacement from

the increased velocities and acceleration before the occurrence of a landslide collapse (see reviews by Crosta and Agliardi, 2003 and Jaboyedoff et al., 2004).

Several studies have analysed the seasonal movement characteristics in landslides, mainly controlled by rainfall (Crosta and Agliardi, 2003; Hong et al., 2005). The increased movement during rainfall is caused by increased water pressure, and is often superimposed on a linear trend (Crosta and Agliardi, 2003). However, snowmelt will also contribute to similar displacement patterns, as documented from the Åknes rockslide (Blikra, 2008; Grøneng et al., in press).

The Nordnes rockslide complex in northern Norway is located in arctic and periglacial conditions, and may pose serious consequences to inhabited areas due to its tsunamigenic potential. Analysis of displacement data in landslides located in the arctic and periglacial regions, with possible permafrost conditions, are not reported in the literature. To the authors' knowledge, this study is the first attempt to analyse the seasonal variations of deformation data in these special geological and climatic settings.

* Corresponding author. Division of Geomatics, Norwegian University of Science and Technology, N-7491 Trondheim, Norway. Tel.: +47 95 13 92 99; fax: +47 73 59 70 21.
E-mail address: trond.nordvik@ntnu.no (T. Nordvik).

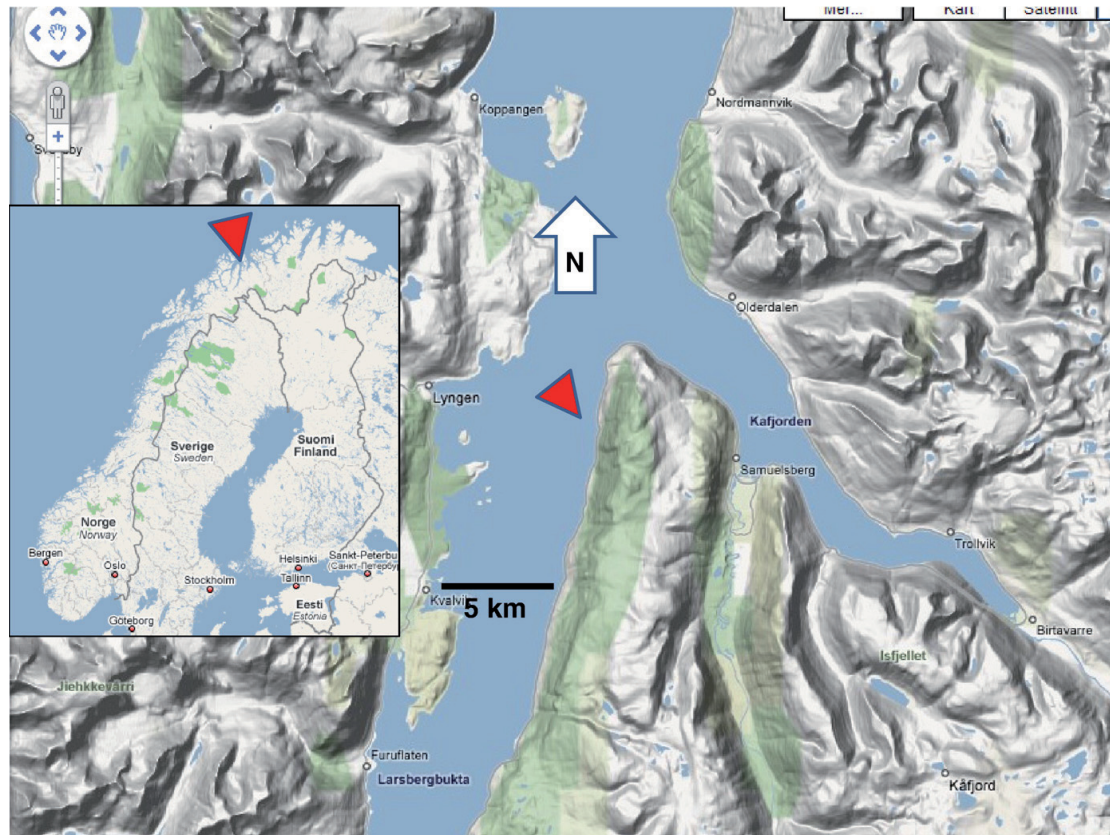


Fig. 1. Location of the Nordnes rockslide. (Annotation added to a hill shaded terrain from Google Maps, ©2009 Google – Kartdata © Tele Atlas.) An overview of the site is shown in Fig. 2.

The potential for catastrophic consequences in case of rock-slope failures calls for a careful understanding of the sliding processes. Evaluation of laser and crackmeter measurements is expected to provide important contributions to the understanding of the sliding mechanisms as well as serving as a basis for decisions regarding future investigations and instrumentation of the site. The main objective of this paper is thus to carefully analyse the deformation data to provide accurate estimates of the annual displacement rates and the pattern of seasonal fluctuations. This implies that autocorrelation between the observations needs to be taken into account.

It is also important to consider both controlling factors and nuisance factors that affect the measurements. Regression analysis based on the method of weighted least squares was used for evaluation of the monitoring data. The main advantage of this approach is that it provides optimal estimates of displacement rates and the uncertainties associated with these estimates. This is vital for obtaining correct conclusions of the deformation analyses. Some relevant examples of applications of statistical analysis to rockslide monitoring data are presented in Nordvik and Nyrnes (2009). The aforementioned article also contains relevant references to background theory of displacement analyses.

2. The Nordnes rockslide

The possible occurrence of a large rockslide at Nordnes in Northern Norway (Fig. 1), generating a catastrophic tsunami towards settle-

ments, has initiated geological investigations and continuous measurements of movements. The large unstable rock slope is located on the western margin of the mountain extending from about 900 m above sea level (asl) and downwards towards the fjord (Fig. 2). The specific area analysed in this paper is the northernmost part of a 4 km long and up to 1.2 km wide deformed area (Braathen et al., 2004; Blikra et al., 2009).

This area is established as an active rockslide with documented movements. Annual GPS measurements carried out since 2003 indicate annual displacement rates between 1 and 5 cm (Eiken, 2007; Blikra et al., 2009), see Fig. 2. The rock consists of different types of marble and schists (Andresen, 1988; Zwaan, 1988), with foliation dipping generally towards west (downslope). The unstable area is detached from the intact bedrock at its rear part by a well-defined back scarp with an up to 14 m deep cleft. Internally this area is characterized by a series of extensional fractures, and some can be traced as up to 250 m long surface depressions (Fig. 2). Closer to the steep cliff, the deformation of the surface is more chaotic and intense, and the direction of displacement has also changed (Fig. 2, left). The geometry and basal sliding plane(s) of the complex rockslide is not well understood due to limited depth data (Fig. 3). Geophysical measurements (electric and seismic) indicate fractured bedrock down to over 100 m (Rønning et al., 2008), but drilling, coring and deformation data is needed before any conclusions can be made. However, with an approximate depth of 50 to 100 m, the total volume of this area is estimated to be between 8 and 16 million m³ (Henderson et al., 2007).

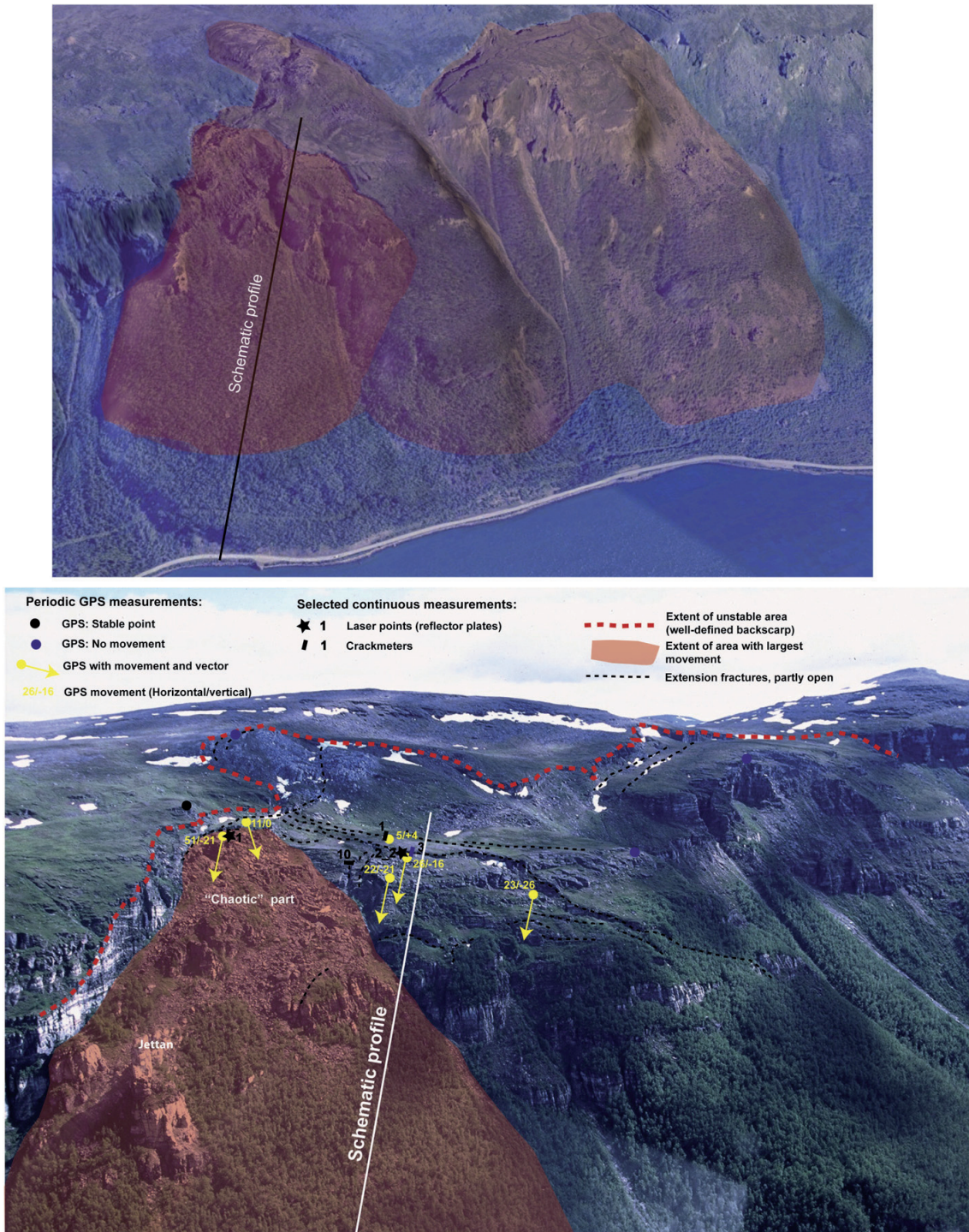


Fig. 2. Overview of the Nordnes site (from a North-westerly direction). Upper: the entire unstable area with red colour tone, the left-hand part is documented active with annual movements of 1 to 5 cm. The line indicates the position of the schematic profile shown in Fig. 3. Lower: photo showing the rockslide with the main geological features, the periodic GPS measurements and the position of some of the continuous displacement sensors. Note the chaotic left-hand part where the movements are largest.

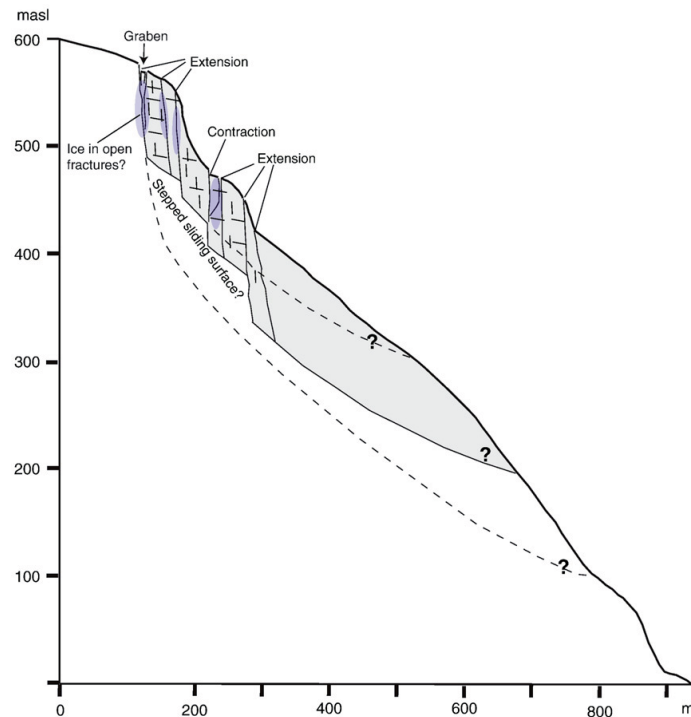


Fig. 3. Schematic profile indicating possible geometry and kinematics of part of the rockslide area. Note that both extension and contraction can be measured by displacement data across fractures simply due to the fracture development. Contraction will for example occur when a separated block moves inside a larger graben structure. It is also indicated that permanent ice can occur within parts of the fractures leading to an effect of both horizontal and vertical displacements.

There are ongoing studies on temperature regimes in this area, which will give more information about the seasonal frost and permafrost conditions (see Christiansen et al., 2010). The data so far indicate that there are frozen parts in the fractures, which will be important for the deformation processes (Fig. 3).

3. Methods

3.1. Instruments and displacement data

Measurements from three lasers, Dimetix DLS-BH 15 (Dimetix, 2009), and 10 crackmeters, Durham VW Crackmeter (Slope Indicator, 2003) are considered in this paper. Some technical data for the employed lasers and crackmeters are shown in Table 1 and Table 2, respectively.

Both laser and crackmeter datasets were collected during a period of nearly 16 months from October 2007 to March 2009. The nominal sampling interval was 6 min for the lasers and 2 min for the

crackmeters. The raw datasets were pre-processed (see Subsections 3.2 and 3.3) before the statistical analyses were carried out. Figs. 4 and 5 show some examples of the data, respectively from laser and crackmeter measurements. The air temperature (Fig. 5) was measured each hour at the upper part of the slope, near the laser emitters.

All statistical analyses reported in this paper were carried out using Matlab (see Matlab, 2009). However, these analyses could also be performed using other computing environments such as the R-software for instance (see R, 2009).

3.2. Analysis of laser measurements

The laser time series were analysed using linear regression (e.g. Koch, 1999; Montgomery et al., 2001); where the expectation values

Table 1
Technical specifications for Dimetix DLS-BH 15 laser.

Parameter/attribute	Value
Typical measuring accuracy	± 1.5 mm
Measuring range on reflecting target plate	0.05 to 500 m
Temperature range (continuous measurements)	− 40 °C to + 45 °C

Table 2
Technical specifications for Durham VW crackmeter.

Parameter/attribute	Value
Material	Stainless steel body and shaft, Neoprene O-rings, plated-steel swivels, mild-steel anchors.
Sensor type	Vibrating wire. A built-in thermistor or RTD provides temperature measurements
Resolution	The crackmeter can detect movements of 0.15 mm with a repeatability of ± 0.3 mm
Range	Available in 60 mm and 100 mm

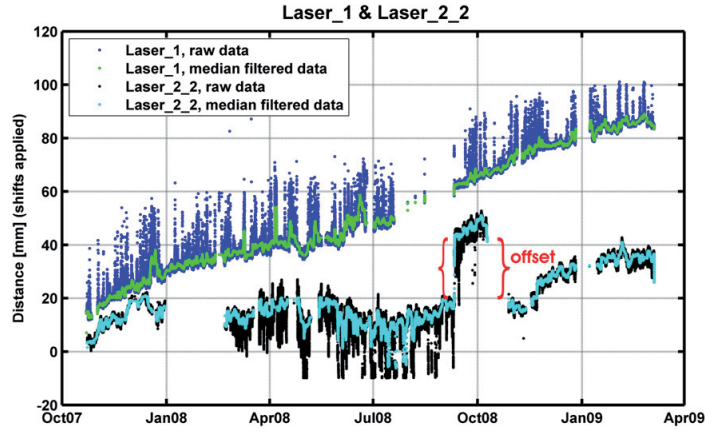


Fig. 4. Raw observations along with median filtered observations from laser 1 and laser 2.2. Median filtering was found to be useful in order to capture the “essence” of the time series in the presence of large numbers of erroneous observations. There were also periods with no observations due to malfunctioning instruments or maintenance. Some time series also contained temporal offsets (e.g. laser 2.2 around October 08) which did not reflect true displacements. Such offsets are due to the maintenance and adjustments of instrument settings.

$E(\mathbf{y})$ of the observed distances \mathbf{y} were assumed to be linear combinations of unknown parameters;

$$E(\mathbf{y}) = \mathbf{X}\boldsymbol{\beta} = \mathbf{y} - \mathbf{e} \text{ with } \text{Cov}(\mathbf{y}) = \text{Cov}(\mathbf{e}) = \mathbf{C}_{ee} = \sigma^2 \mathbf{Q}_{ee} \quad (1)$$

where \mathbf{X} is a known design matrix, $\boldsymbol{\beta}$ is a vector of unknown parameters and \mathbf{e} is a vector of errors. Eq. (1) shows that the error covariance matrix \mathbf{C}_{ee} can be expressed as the product of the variance σ^2 of unit weight and the cofactor matrix \mathbf{Q}_{ee} .

Due to the presence of strong positive autocorrelation (serial correlation), Weighted Least Squares (WLS) was used for parameter estimation. A WLS estimate of the unknown parameters is obtained from:

$$\hat{\boldsymbol{\beta}} = (\mathbf{X}^T \mathbf{P} \mathbf{X})^{-1} \mathbf{X}^T \mathbf{P} \mathbf{y} \text{ with } \text{Cov}(\hat{\boldsymbol{\beta}}) = \hat{\sigma}^2 (\mathbf{X}^T \mathbf{P} \mathbf{X})^{-1} = \hat{\sigma}^2 \mathbf{Q}_{\hat{\boldsymbol{\beta}} \hat{\boldsymbol{\beta}}} = \mathbf{C}_{\hat{\boldsymbol{\beta}} \hat{\boldsymbol{\beta}}} \quad (2)$$

where $\mathbf{P} = \mathbf{Q}_{ee}^{-1}$ is the weight matrix of the observations. Here, \mathbf{X}^T denotes the transpose of \mathbf{X} (the symbol T should not be confused with the temperature T_i in Eq. (6)) and the hat symbol $\hat{\cdot}$ is used to denote estimates of the corresponding true (but unknown) values. An unbiased estimate of the variance σ^2 of unit weight is obtained from:

$$\hat{\sigma}^2 = \frac{\hat{\mathbf{e}}^T \mathbf{P} \hat{\mathbf{e}}}{n-u} \quad (3)$$

where n is the number of observations and u is the number of unknown parameters. Thus, $n-u$ denotes the degrees of freedom. An estimate $\hat{\mathbf{e}}$ of the error vector \mathbf{e} is obtained from Eq. (4);

$$\hat{\mathbf{e}} = \mathbf{X} \hat{\boldsymbol{\beta}} - \mathbf{y} \quad (4)$$

and is referred to as residuals in the subsequent sections.

If the weight matrix in Eq. (2) is omitted, the resulting estimate is referred to as Ordinary Least Squares (OLS). Although OLS also provides unbiased estimators for the regression parameters in the presence of autocorrelation, OLS does not provide optimal (minimum variance) estimators. But more important; using OLS in the presence

of positive autocorrelation leads to the underestimation of the variance (e.g. Montgomery et al. 2001). This in turn leads to unrealistically optimistic (narrow) confidence- and prediction intervals. This may also lead to wrong conclusions with respect to hypothesis testing since the regression parameters may appear statistically significant even though they are truly non-significant. Weighted Least Squares was therefore used as a mean for coping with the aforementioned problems as this method accounts for the autocorrelation structure by introducing a weight matrix \mathbf{P} (Eq. (2)) containing off-diagonal elements.

The weight matrices (\mathbf{P} in Eq. (2)) needed for WLS estimation were obtained from the estimated autocorrelation of the residuals from corresponding initial OLS estimates. Autocorrelation values were calculated for lag 0, lag 1, ..., lag $n-1$, where n denotes the total number of time steps for the time series in question. These autocorrelation values were then used as elements in the weight matrix (\mathbf{P} in Eq. (2)).

As the laser time series contained a large number of erroneous observations, only the daily median values were used for the regression analysis. Assuming a normally distributed sample, both the median and the arithmetic average are unbiased estimators of the sample mean. Since daily median values are more robust with respect to gross errors than daily average values the median was used. Using aggregated data¹ instead of the full raw datasets is also favourable to avoid computational problems associated with large matrices. For our purpose; to analyse the long term displacements, daily median values were considered appropriate.

Plots of the different time series give strong indications of periodic (seasonal) variations. Based on the examination of the periodicity, using spectral analysis (see e.g. Shumway and Stoffer 2000), a sinusoidal component of the wavelength 365 days was included in the regression models as this gives a reasonable good approximation for all time series. Moreover, to account for offsets within the time series, the regression models were augmented with a set of offset parameters (commonly referred to as indicator variables in statistical literature). A method for modelling offset parameters in linear regression analysis is described in Nordvik and Nyrnes (2009). The offsets were mainly

¹ The term “aggregate data” here refers to some kind of extract of the data (e.g. daily median, daily average etc.) as opposed to the full datasets.

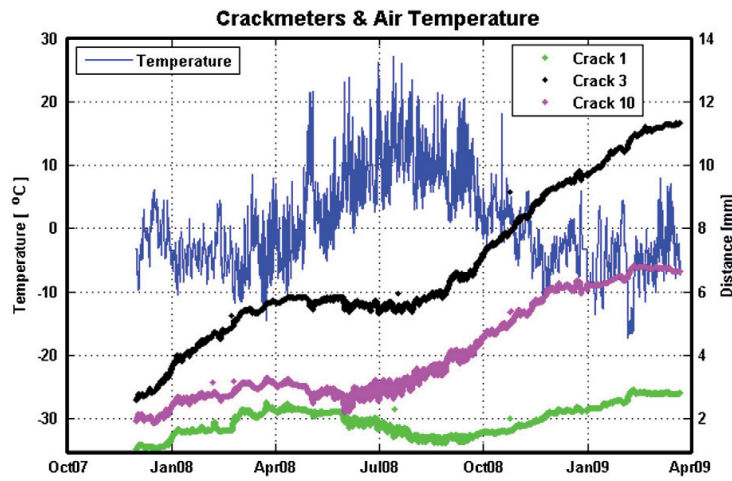


Fig. 5. Time series from crackmeter 1, 3 and 10 plotted with air temperature. The time series clearly indicate seasonal fluctuations. The most obvious blunders were removed before the plot was created.

caused by the maintenance and adjustment of the instruments. If Eq. (1) is rearranged as $y = X\beta + e$, the final regression model for a single displacement observation y_i [mm] for laser k is then given by;

$$y_{i,k} = \beta_{0,k} + \beta_{1,k} \cdot t_i + \beta_{2,k} \cdot \sin\left(\frac{2 \cdot \pi \cdot t_i}{365}\right) + \beta_{3,k} \cdot \cos\left(\frac{2 \cdot \pi \cdot t_i}{365}\right) + \sum_{j=0}^{n_{\text{offsets}}} \beta_{j+3,k} \cdot I_j + e_{i,k} \quad (5)$$

where t denotes time [days] and e is the residual [mm] for this particular observation. The sinusoidal terms correspond to a seasonal fluctuation and the indicator variables I_j correspond to offsets (cf. Fig. 3).

3.3. Analysis of crackmeter measurements

The same WLS approach used for the regression analysis of the laser time series was also used for the crackmeter time series. However, the regression analysis was carried out on a different type of aggregated data; average values were calculated based on every 180 consecutive raw observations, roughly corresponding to 4 “aggregated observations” per day. Moreover, the regression model was augmented with air temperature as regression variable. The final regression model, for a single observation y_i [mm] for crackmeter k , is then given by;

$$y_{i,k} = \beta_{0,k} + \beta_{1,k} \cdot t_i + \beta_{2,k} \cdot \sin\left(\frac{2 \cdot \pi \cdot t_i}{365}\right) + \beta_{3,k} \cdot \cos\left(\frac{2 \cdot \pi \cdot t_i}{365}\right) + \beta_{4,k} \cdot T_{t_i} + e_{i,k} \quad (6)$$

where T_t is the air temperature [Celsius] at time t [days] and e [mm] is the residual for this observation.

3.4. Prediction of future observations

The expected displacement value y_0 for time series k at time t_0 can be expressed as;

$$E(y_{0,k} | t_0) = \mathbf{x}_0 \cdot \beta_k \quad (7)$$

where \mathbf{x}_0 is the design matrix for t_0 , i.e. for the prediction point of time.

A corresponding least squares prediction estimate is obtained from:

$$\hat{y}_{0,k} = \mathbf{x}_0 \hat{\beta}_k \quad (8)$$

The vector $\hat{\beta}_k$ contains the estimated regression parameters (Eq. (2)) for time series k .

A $(1 - \alpha)$ percent Prediction Interval (PI) for a single observation y_i is obtained by:

$$\hat{y}_{0,k} \pm \tau_{n-p,\alpha/2} \cdot \sqrt{\hat{\sigma}_k^2 \cdot (1 + \mathbf{x}_0 \cdot (X^T \cdot P \cdot X)^{-1} \cdot \mathbf{x}_0^T)} \quad (9)$$

where $\tau_{n-p,\alpha/2}$ is a quantile from the Student's- t distribution with $n - p$ degrees of freedom.

4. Results

4.1. Laser measurements

Table 3 shows the estimated displacements for the three lasers. Annual displacement rates were obtained by multiplying the linear parameters $\beta_{1,k}$ from Eq. (5) by a factor of 365. The corresponding confidence intervals were scaled accordingly, i.e. the upper and lower confidence interval limits were also multiplied by 365.

Both laser 1 and laser 2_2 show significant linear trends. As suggested by the 95% CI, laser 2_1 shows no significant linear trend. Since the p -value² of β_1 for laser 2_1 (0.062) exceeds the chosen significance level of 0.05, this parameter is deemed non-significant. The seasonal amplitudes indicate the maximum seasonal deviations from the linear trends. Since the laser emitters are placed on stable areas, these measurements should take up a large part of the total movements down to the reflectors.

4.2. Crackmeter measurements

Results obtained from regression analysis of crackmeter time series are shown in Table 4. As for the lasers, annual displacement

² In hypothesis testing the term “ p -value” is commonly used to denote the probability of obtaining a test statistic that is at least as extreme as the one that was actually observed, assuming that the null hypothesis is true (Wikipedia, 2010).

Table 3
Results from regression analysis of time series for the three lasers.

Laser ID	Displacement rate [mm/year]		Seasonal amplitude [mm]	Approx. dist. to reflector [m]
	$365 \cdot \hat{\beta}_1$	95 % CI for $365 \cdot \hat{\beta}_1$	$\sqrt{\hat{\beta}_2 + \hat{\beta}_3}$	
1	51.7	[50.7, 52.6]	3.2	114
2_1	(0.9)	[−0.1, 1.7]	0.8	63
2_2	23.3	[19.1, 27.6]	10.5	258

rates were obtained by scaling the linear parameters $\beta_{1,k}$ from Eq. (6) by a factor of 365 and the corresponding confidence intervals were scaled accordingly.

All crackmeters show statistically significant displacements. Crackmeter 3 shows the largest displacement rate of 6.1 mm/year. Crackmeters 1, 3, 4, 5, 6, 7, and 10 show an extension whereas crackmeters 2, 8 and 9 show contraction (Fig. 6; Table 4). The estimated annual displacement for crackmeter 9 is somewhat uncertain as the chosen regression model does not give a satisfactory fit towards the end of this time series. The estimated air temperature parameters range from -0.017 to -0.002 mm/°C (Table 4). As all these estimates are negative, this means that the observed distances are expected to decrease with the increasing air temperature.

4.3. Prediction

In connection with real-time monitoring it is important to consider the expected development in order to detect and evaluate any important changes in the movement pattern. It was therefore made an effort to make prediction curves for future movements.

The initial regression models specified for the crackmeters (Eq. (6)) require future air temperature as input for the prediction of future observations. In order to give an idea of the expected progress one year ahead, the regression models used for the prediction in this paper were slightly modified such that the temperature parameters (i.e. the term $\beta_{4,k} \cdot T_i$ in Eq. (6)) were removed from the models. This only has a negligible effect on the long term predicted mean values. However, the variance of the estimates of the remaining regression parameters, including the linear trend parameter β_1 , increased as the effect of temperature changes was spread out on the other remaining parameters. Thus, the resulting prediction interval obtained from a model without the temperature parameter reflects a situation assuming the same temperature distribution in the future as for the past 16 months. However, if the prediction model is to be implemented in a real-time early warning system the actual, or possibly forecasted, temperature should be used.

Predicted “mean values” along with the corresponding 95% PIs (Eqs. (8) and (9)) for a period of 365 days into the future were calculated for all time series. Figs. 7 and 8 show predictions for laser 1 and crackmeter 3 respectively. It should be noted that the prediction intervals specified for the laser time series are valid for the median values of the raw observations during a full day. Thus, these prediction intervals will not cover 95% of the raw observations but 95% of the daily median values. Similarly, the prediction intervals specified for the crackmeter time series are valid for the average value obtained from 180 consecutive raw observations (corresponding to the observations made during a period of 6 h).

5. Discussion

5.1. Regression analysis

It is well known that high precision electronic distance measurements require corrections for atmospheric conditions that deviates from the standard condition defined for the specific instruments in question,

Table 4
Results from regression analysis of time series for the 10 crackmeters.

Crackmeter ID	Displacement rate [mm/year]		Air temperature parameter [mm/°C]	Seasonal amplitude [mm]
	$365 \cdot \hat{\beta}_1$	95 % CI for $365 \cdot \hat{\beta}_1$	$\hat{\beta}_2$	$\sqrt{\hat{\beta}_2 + \hat{\beta}_3}$
1	0.83	[0.77, 0.89]	−0.010	0.49
2	−0.13	[−0.16, −0.11]	−0.008	0.05
3	6.10	[6.02, 6.18]	−0.010	0.85
4	0.54	[0.51, 0.57]	−0.007	0.36
5	0.12	[0.11, 0.14]	−0.002	0.06
6	2.12	[2.06, 2.17]	−0.009	0.25
7	1.27	[1.21, 1.33]	−0.016	0.26
8	−0.07	[−0.10, −0.04]	−0.009	0.04
9	−1.21	[−1.16, −1.26]	−0.006	0.19
10	3.81	[3.76, 3.87]	−0.017	0.58

(e.g. Rütger, 1996). Such corrections require observations of air temperature, air pressure and partial water vapour pressure. Moreover, the magnitudes of the meteorological corrections are dependent on the distance from the emitter to the reflector. In this investigation, observations of air pressure and partial water vapour pressure were not available, and, since the measured distances were relatively short; from 63 to 258 m, the atmospheric corrections were neglected in this investigation. However, the distance dependent impact from varying atmospheric conditions is evident from the increased seasonal fluctuations with increased distance (Table 3). The confidence interval for the linear trend for laser 2_2, which has the largest distance to the reflector, is also clearly the largest.

Because the regression models for the crackmeters contain both a 365 day sinusoidal component and an air temperature parameter (which also models a seasonal fluctuation), the question arises whether these two components are highly correlated, meaning that they both account for similar effects. The correlation coefficients between these parameter estimates were approximately 0.6 but the estimated air temperature parameters remained virtually the same after the sinusoidal 365 days components were omitted from the models. This indicates the presence of separate seasonal fluctuations that cannot be explained by the seasonal air temperature change.

For some of the crackmeter time series, spectral analysis revealed other significant periodic components besides the dominating 365 days period. However, to keep the regression models as simple as possible, these shorter periodic components were not included in the models since they only had a negligible impact on the estimated long term displacements (linear trends). Thus, the movements were found to be adequately modelled with linear trends and sinusoidal components with a period of 365 days.

Generally, a longer total observation time span is preferable with respect to the determination of the seasonal variations in the displacement rate. The current total time span of 16 months only captures about one and a half full cycle of the 1 year sinusoidal component. Thus, a longer time span will provide more reliable estimates with respect to the long term seasonal variations.

The presence of strong autocorrelation, particularly for the crackmeter time series, suggests that there are other additional factors besides the current regression parameters, which also have an impact on the observed displacement. Such additional factors may be related to the rock temperature. Some limited testing using rock temperature, measured at a depth of 0.4 m at the central part of the sliding area, as regression variable, indicated that this variable provided a significant contribution to the regression model even when air temperature was already included as a regression variable. The estimates for the rock temperature regression parameters were similar to those obtained for

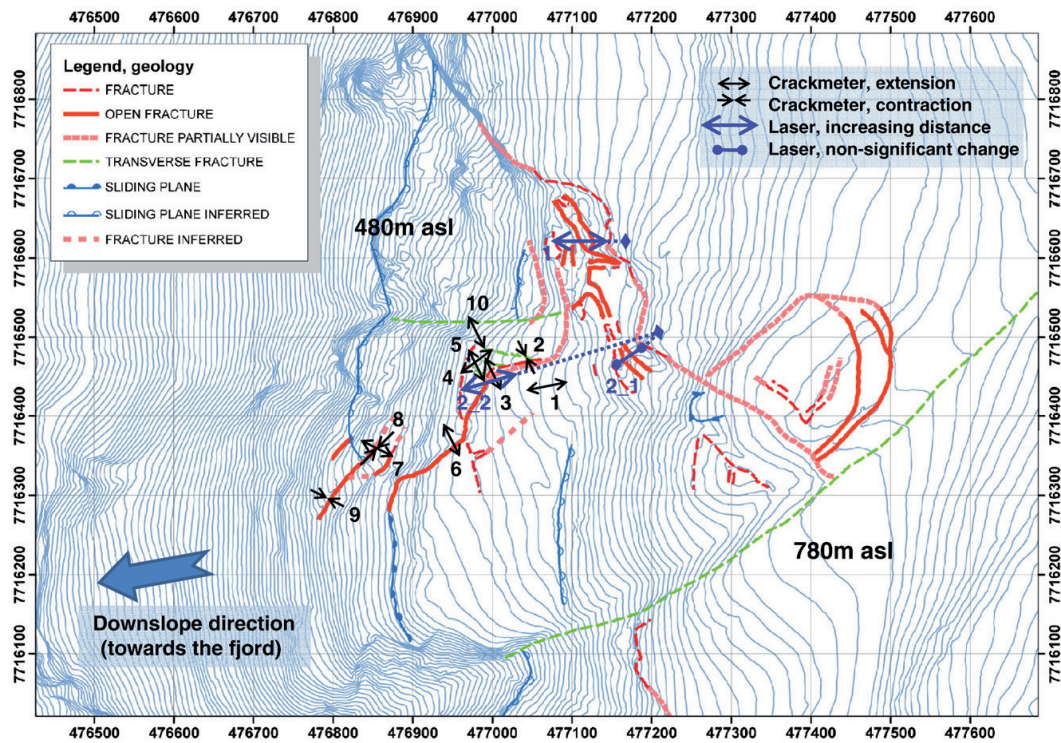


Fig. 6. Overview of lasers, crackmeters and geological structures. The coordinate system is UTM Zone 34N and the equidistance is 5m.

the air temperature. This means that the observed displacement is expected to decrease as the rock temperature increases. A physical explanation to this effect is that thermal expansion of the rock faces, on each side of the crack, causes compression of the crackmeters. However, as the rock temperature measurements were only available for a shorter period of time, not covering a full yearly cycle, this variable was not included in the final regression models. Despite the problems associated with omitted variables, such as rock temperature, the WLS approach

used in this paper enables realistic confidence intervals and significance levels, for the estimated regression parameters, to be obtained in the presence of strong autocorrelation.

5.2. Deformation, dynamics and seasonal changes

The continuous laser and crackmeter measurements provide important information in order to understand the deformation

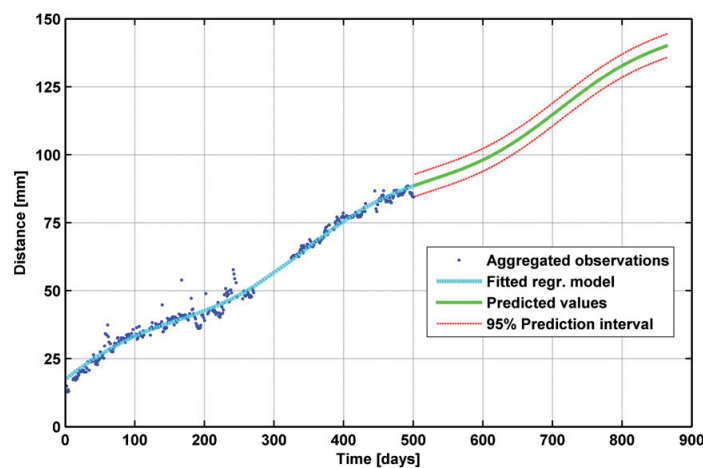


Fig. 7. Distance prediction curve for laser 1 together with the historical data. (Day 0 corresponds to 22 October 2007). The interval without observations, around day 300, is due to maintenance.

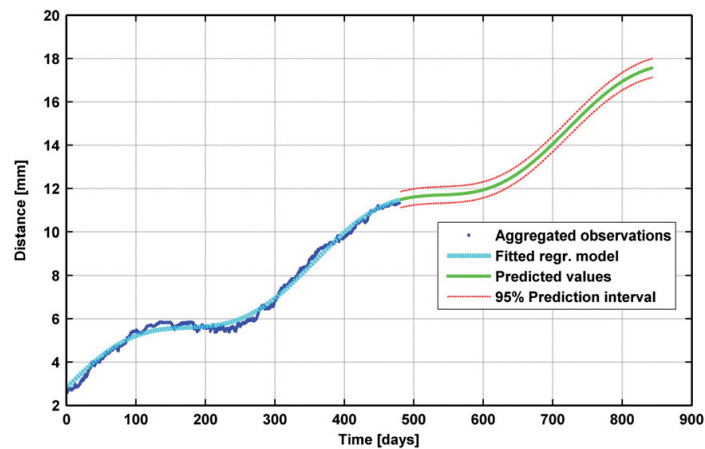


Fig. 8. Distance prediction curve for crackmeter 3 together with the historical data. (Day 0 corresponds to 30 November 2007).

pattern in the area, as well as a better basis for the evaluation of the controlling factors with respect to movement velocities and seasonal trends.

The fastest moving GPS control point which is located close to the reflector of laser 1 showed an annual displacement of 53 mm in both horizontal and vertical direction from 2006 to 2007 (Eiken, 2007). The laser data, which picks up the total movement in the area, indicates displacement values that are in the same order as those obtained from the annual GPS measurements. This confirms that the north-westernmost area (laser 1 and laser 2_2) is moving more rapidly than the other areas. It also clearly demonstrates that the fast-moving northernmost zone, with annual movement of more than 5 cm, is the most critical in terms of generation of a rapid rockslide. The crackmeter data give an informative picture of the deformation processes in terms of area of extension and contraction (Figs. 3, 6). In the lowermost part, several crackmeters indicate that opened fractures are presently closing. This indicates that locally the deformation has changed, passing from a stage of extension to a stage of compression. This is most probably an effect of local dynamics of fracture evolution, by the formation of internal graben structures where single blocks may back-rotate towards the main crack, see Fig. 3.

The crackmeter data gives also new information about the other area considered to be stable based on annual GPS measurements. Crackmeter 1 indicates a small deformation here, but these movements are too small to be detected by the GPS measurements.

The deformation data gives information about the seasonal fluctuations, and thus will be an important basis for evaluating controlling factors. It is quite clear that the deformations have a temperature effect (Fig. 5, Table 4). This can be both direct effects (e.g. on instruments or heating/cooling of bedrock), but also indirectly controlling the formation and melting of ice. Surprisingly, any increased deformation cannot be seen during snowmelt in the spring time, which is a normal characteristic elsewhere (e.g. at Åknes in western Norway, Blikra, 2008). Actually, the snowmelt season in May–June is characterized by the smallest deformation rate (Fig. 5). The largest movements are seen in autumn, in a period where the snowmelt season is finished, and with no specific precipitation events. We speculate that this strange pattern may be an effect of processes related to seasonal frost and permafrost conditions in parts of the unstable slope (Fig. 3). Such processes can affect the deformation pattern in a complex matter, including both horizontal pushing and detraction, in addition to vertical movements by either subsidence (melting) or vertical lifting by freezing of water. This link has not been evaluated in detail, as it will require a large amount of

temperature and deformation data in the fractures and in bedrock boreholes. However, we interpret the characteristic seasonal fluctuations, including the increased movement from autumn to mid winter, to be an effect of freezing of water.

6. Summary and conclusions

The main objective for this investigation was to determine the long term displacement pattern of the Nordnes rockslide in Northern Norway, situated in the arctic and periglacial conditions. Ten crackmeter time series and three laser time series were analysed using linear regression. Due to the presence of strong autocorrelations, a WLS approach was required to obtain optimal parameter estimates.

All crackmeters showed statistically significant displacements. The maximum crackmeter displacement was estimated to 6.1 mm/year (crackmeter 3). However, the estimated linear trends for 5 out of the 10 crackmeters were less than 1 mm/year. Thus, the crackmeter measurements revealed new unstable parts of the areas since these minor displacements were not previously detectable from annual GPS measurements. Results obtained from the crackmeter data provided an informative picture of areas showing extension and contraction (Fig. 6). The estimated amplitudes of seasonal displacement fluctuations range from about 0.04 to 0.85 mm. The temperature effects on the crackmeters seemed to be two-fold; i) change in air temperature probably affects the instruments directly such that the tension of the vibrating wire is affected by the instrument temperature, and ii) rock temperature changes causes thermal expansions of the rock faces. However, as the seasonal fluctuations could not be fully modelled with only temperature parameters, this suggests that there are other factors besides the temperature changes which contribute to the seasonal fluctuations. The largest displacements clearly occur in autumn and early winter with a stagnation or retreat phase in spring and summer.

The estimated displacements for laser 1 and laser 2_2 were 51.7 mm/year and 23.3 mm/year, respectively. No statistically significant displacement was established for laser 2_1. As with the crackmeter time series, the laser time series also show seasonal fluctuations. However, despite the short reflector ranges, the laser measurements should ideally be corrected for variable atmospheric conditions in order to reliably quantify the true displacements fluctuations. Also, the high noise level of the raw laser measurements is a limitation with respect to accurate determination of the magnitudes of the fluctuations.

From the analyses of the displacement data it is established that the north-westernmost part of the area has the largest movement of

more than 5 cm per year (laser 1) which makes this part the most critical in terms of generation of a rapid rockslide.

The seasonal displacements established at Nordnes are totally different from what has been documented from landslides controlled mainly by rainfall and snow melt leading to increased water pressure. The characteristic seasonal pattern, including the increased movement from autumn to mid winter, is interpreted to be an effect of the freezing of water.

Prediction intervals for future displacements were also established in this paper. These prediction intervals are intended as a reference for future analysis and can also be used as a basis for defining alert thresholds for early warning systems, possibly with a refinement of the models if other relevant data such as rock temperature become available in the future. Both the results and methodology reported here are expected to be useful for the evaluation of future displacement measurements.

Acknowledgements

We thank Professor Håvard Rue at the Norwegian University of Science and Technology for his useful comments on time series analysis, Professor Hanne Christiansen at the University Centre of Svalbard for discussions on the temperature regime in the area and Dr. Iain Henderson at the Geological Survey of Norway for discussions on the geological model. Mr Bernt Lyngstad and Mr Per Steinar Lyngstad, Kåfjord municipality, are acknowledged for their kind support with the monitoring data.

References

- Andresen, A., 1988. Caledonian terranes of Northern Norway and their characteristics. *Trabajos de Geologia* 17, 103–117.
- Blikra, L.H., 2008. The Åknes rockslide: monitoring, threshold values and early-warning. In: Chen, Z., Zhang, J., Li, Z., Wu, F., Ho, K. (Eds.), *Landslides and Engineered Slopes. Proceedings of the Tenth International Symposium on Landslides and Engineered Slopes*. CRC Press, Taylor & Francis Group, Xi'an, China, pp. 1089–1094.
- Blikra, L.H., Henderson, I. and Nordvik, T., 2009: Faren for fjellskred fra Nordnesfjellet i Lyngenfjorden, Troms (in Norwegian). Geological Survey of Norway Report 2009.026, pp 29.
- Braathen, A., Blikra, L.H., Berg, S.S., Karlsen, F., 2004. Rock-slope failures in Norway: type, geometry, deformation mechanisms and stability. *Norwegian Journal of Geology* 84, 67–88.
- Christiansen, H., et al., 2010. The thermal state of permafrost in the Nordic area during IPY 2007–2009, to appear in special issue 'Permafrost in the Polar Regions during the International Polar Year' of the *Journal Permafrost and Periglacial Processes Permafrost and Periglacial Processes* 21, 156–181.
- Crosta, G.C., Agliardi, F., 2003. Failure forecast for large rock slides by surface displacement measurements. *Can. Geotech. J.* 40, 176–191.
- DIMETIX, 2009. Distance Laser Sensor, Technical Reference Manual, V1.02. URL: <http://www.dimetix.com> URL accessed 14 April 2009.
- Eiken, T., 2007. Rapport om Deformasjonsmålinger i Troms 2003–2007, Department of Geosciences, University of Oslo (Technical Report 04.12.2007, in Norwegian), 1–14.
- Grøneng, G., Christiansen, H.H., Nilsen, B., Blikra, L.H., in press. "Meteorological Effects on Seasonal Rock Displacements of the Åknes Rockslide, Western Norway", *Landslides*, doi:10.1007/s10346-010-0224-x.
- Henderson, I.H.C., Saintot, A., Vennik-Ganerød, G., Blikra, L.H., 2007. Fjellskredkartlegging i Troms. NGU Rapport 2007.041, Norwegian Geological Survey (in Norwegian), pp. 1–37.
- Hong, Y., Hiura, H., Shino, K., Sassa, K., Fukuoka, H., 2005. Quantitative assessment on the influence of heavy rainfall on the crystalline schist landslide by monitoring system-case study Zentoku landslide, Japan. *Landslides* 2, 31–41.
- Jaboyedoff, M., Ornstein, P., Rouiller, J.-D., 2004. Design of a geodetic database and associated tools for monitoring rock-slope movements: the example of the top of Randa rockfall scar. *Natural Hazards and Earth System Sciences* 4, 187–196.
- Koch, K.-R., 1999. Parameter Estimation and Hypothesis Testing in Linear Models. Springer-Verlag, Germany.
- MATLAB, URL: <http://www.mathworks.com/>, URL accessed 13 December 2009.
- Montgomery, D.C., Peck, E.A., Vining, G.G., 2001. *Introduction to Linear Regression Analysis*. John Wiley & Sons, USA.
- Nordvik, T., Nyrnes, E., 2009. Statistical analysis of surface displacements – an example from the Åknes rockslide, western Norway. *Nat. Hazards Earth Syst. Sci* 9, 713–724.
- Petley, D., 2006. On the initiation of large rockslides: perspectives from a new analysis of the Vaiont movement record. In: Evans, S.G., et al. (Ed.), *Landslides from Massive Rock Slope Failure*. Springer, pp. 77–84.
- R, URL: <http://www.r-project.org/>, URL accessed 13 December 2009.
- Rüger, J.M., 1996. *Electronic Distance Measurement*, 4th Ed. Springer, Germany. ISBN 3-540-61159-2.
- Rønning, J.S., Dalsegg, E., Heincke, B.H., Juliusen, H., Tønnesen, J.F., 2008. Geofysiske målinger på Nordnesfjellet sommeren 2007. NGU Rapport 2008.024, Norwegian Geological Survey (in Norwegian), pp. 1–28.
- Shumway, R.H., Stoffer, D.S., 2000. *Time Series Analysis and Its Applications*. Springer, USA.
- Slope Indicator, 2003. Technical manual for Durham VW Crackmeters, Slope Indicator Company, <http://slopeindicator.com/pdf/manuals/vw-crackmeter.pdf> URL accessed 14 April 2009.
- Wikipedia. <http://en.wikipedia.org/wiki/P-value>, URL accessed 10 January 2010.
- Zwaan, K.B., 1988. *Bedrock Map Nordreisa, M 1:250,000*. Geological Survey of Norway.

